VERIFICATION OF A NUMERICAL MODEL FOR THERMAL PLUMES

SMHI

Dnr 610/131

VERIFICATION OF A NUMERICAL MODEL FOR THERMAL PLUMES

by B Vasseur, L Funkquist and J F Paul

SMHI Rapporter

HYDROLOGI OCH OCEANOGRAFI
Nr RHO 24 (1980)

ISSN 0347-7827

SVERIGES METEOROLOGISKA OCH HYDROLOGISKA INSTITUT

Norrköping 1980

TABLE OF CONTENTS

SUMMARY I

Initiation of the project III

TABLE OF CONTENTS

CONCLUSIONS AND RECOMMENDATIONS 1

INTRODUCTION

A general description of the behaviour of discharged cooling water 3
Integral models 10
Numerical models 13
Problems to be addressed 27

MATHEMATICAL MODEL

Development of the model equations 28
Boundary conditions 36
Numerical procedure 39

PHYSICAL BACKGROUND

Karlshamn 56
Barsebäck 63

RESULTS

Karlshamn 71
Barsebäck 98

DISCUSSION

Ways to improve the model 110
Applicability of the model 114

REFERENCES 116

SUMMARY

As a part of a research project, financially supported by the CDL, to study the thermal effects of waste heat discharged into natural water recipients, this report describes a numerical model for this purpose and a number of verifications against real data.

The model is based on the conservation laws for mass, momentum and energy. It is time-dependent, three-dimensional and has the possibility of using a varying horizontal resolution depending on the nature of the problem.

A coordinate transformation in the vertical direction gives the model the same number of calculating points in the vertical all over the modelled area, which increases the confidence in the vertical description considerably. This is of great value, as most of the discharges and the pollution problems are in shallow areas, where other models in general will have a poor resolution.

Applications of the model to different types of recipients are presented and the effects of important mixing mechanisms are illustrated. The model results have been verified against field measurements, and important plume characteristics like area of heated surface water, vertical extent of the plume, and centerline temperature decay have all been successfully simulated. The verification study demonstrates in addition that recirculation of cooling water is well described by the model.

The verification studies suggest enlarged use of this type of model studies both in the planning of new locations for power plants and in the monitoring of the environmental effects of the discharged heat.

This model can be used both to predict thermal effects in the immediate neighbourhood of the power plant and to predict distribution and long term variations in wider surroundings. Of special interest is the use of the model when locations of the inlet and outlet are to be considered.

INITIATION OF THE PROJECT

In 1975 the Central Operating Management (CDL) - a joint organization of major Swedish power producers - initiated a project extending over the physical, chemical, and biological effects of the excess temperature caused by the discharge of heated cooling water into coastal water.

A necessity for these studies is a good description of the distribution of the excess temperature both in the vicinity of the outlet and further out. However, the integral model developed by Prych (1972), and frequently used in plume predictions in Sweden as being the best available model, in general describes the thermal spreading satisfactory only up to about one kilometer from the outlet. Therefore, the main purpose of this project was to find another kind of model with the ability to describe the further spreading of the plume, where the initial jet characteristics no longer are important.

CONCLUSIONS AND RECOMMENDATIONS

A numerical model has been used to calculate the distribution of excess temperature resulting from the discharge of cooling water with a special address to the far-field, and the results have been verified against field measurements from two different types of recipients. The main conclusions and recommendations are as follows:

(i) The model has been verified against real data, and important plume characteristics like area of heated surface water, vertical extent of the plume, and centerline temperature decay have been successfully predicted.

(ii) The verifications indicated that recirculation of cooling water was well described.

(iii) In a far-field description it is important to model the transient response of the plume accurately both to changing wind-conditions and to changes in the main current in the area. These processes have been successfully simulated by the model.

(iv) Experiences from the verifications show that the vertical mixing is the most difficult element to model. So, an important matter to improve is the description of turbulence in the vertical direction.

(v) If possible, the description of the horizontal turbulence should be given a more physical dependence. For example, there ought to be a relation to the variable gridsize.

(vi) The rather divergent nature of the wind field in limited coastal areas needs a good description in

the model, specially where the local wind is the main determining factor. This can be achieved by more representative field data or by a more sophisticated wind model.

(vii) Further improvements in modelling the wind-forcing can be made by adding a dependence on the wind speed, duration, fetch and the air stability in the formula describing the stress on the water surface.

(viii) The near-field should be calculated as a separate part, and the results should be used as input data for the far-field model.

(ix) An additional equation for the conservation of salinity should be introduced in the model, if the model is to be applied to coastal areas with varying salinity.

(x) One should aim at a more interactive relationship between the model work and the design of the field program. In that way both the performance of the model and the value of the field data would increase.

INTRODUCTION

A GENERAL DESCRIPTION OF THE BEHAVIOUR OF DISCHARGED COOLING-WATER

In a discharge tunnel from a power plant, a typical Reynolds number is in the range of 30,000 - 150,000. So the turbulence is high in the tunnel and, therefore, the temperature is homogeneous and the velocity profile rather flat and not parabolic.

Since a typical discharge velocity is about 1 m/s, the velocity difference between the cooling water and the receiving water creates a very strong shear-induced turbulence. In the zone where the transition from a channel flow to a free-jet flow occurs, the free-shear layer grows towards the center of the jet. In the end of this zone, the well mixed core has disappeared and a more or less Gaussian distribution for temperature and velocity field is produced (see Figure 1).

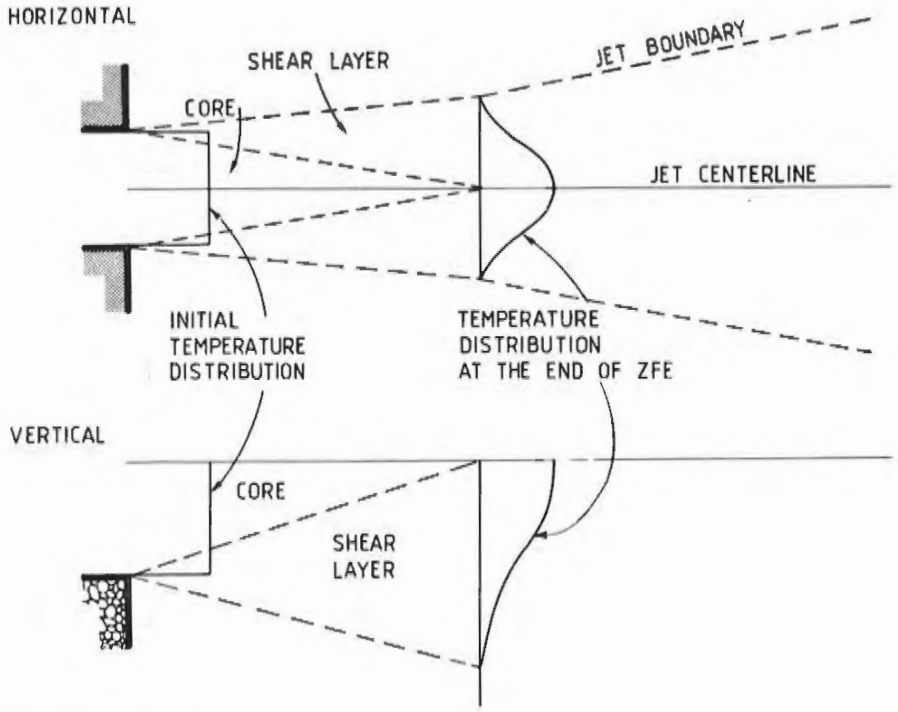

FIGURE 1 Schematic temperature distributions at the beginning and end of the zone of flow establishment (ZFE)

The length of this zone of flow establishment will depend on the outlet dimensions and velocity and density differences between the cooling water and the receiving water. For a more detailed description see, e.g., Stefan, Bergstedt and Mrosla (1975) and Vasseur (1979).

The shear created turbulence mixes ambient water into the jet. This is called the jet entrainment. For a nonbuoyant jet, Taylor (1945) suggested a simple transfer assumption. A detailed understanding of the turbulent structure was not necessary. He related the local entrainment velocity to the jet centerline velocity simply by

$$V_e = e \cdot u$$

where V_e = local entrainment velocity,

e = entrainment coefficient, and

u = jet centerline velocity.

Several laboratory experiments have shown the success of this simple relationship. This has therefore been commonly used even if it says very little about the physics of the mixing processes involved.

The jet will entrain ambient water both horizontally and vertically if there is water available for the dilution. If, e.g., it is shallow outside the outlet, vertical entrainment will be reduced or even vanish so the jet will reach the bottom. Due to the decreased entrainment the dilution will then be less and the temperature in the jet will consequently be higher.

For a cooling water discharge there exists a density difference between the jet and the ambient water which will decrease the vertical mixing. Laboratory experiments by Ellison and Turner (1959) indicate that the vertical entrainment as a function of the buoyancy can be well approximated, as Figure 2 shows, by

$$e = e_o \cdot \exp(-5Ri)$$

where e_o = entrainment coefficient for the nonbuoyant case,

$Ri = g \frac{\Delta\rho}{\rho} \frac{h}{u^2}$ is the local Richardson number,

g = gravitational acceleration,

$\Delta\rho$ = density difference between the water masses,

ρ = ambient water density,

h = local thickness of the jet, and

u = local jet velocity.

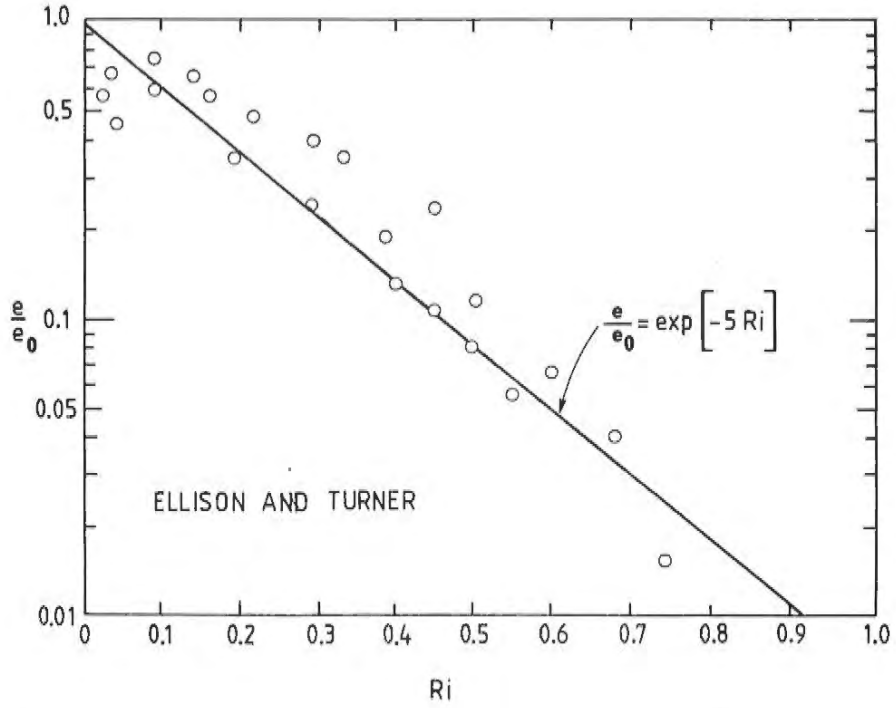

FIGURE 2 Entrainment coefficient e as a function of Richardson number Ri. (Dunn, Policastro and Paddock, 1975)

Stolzenbach and Harleman (1971) and Koh and Fan (1970), among others, have used similar expressions.

As mentioned above, the entrainment coefficient depends on the buoyancy. This dependence is used just in vertical direction. In horizontal direction, one neglects the small dependence, and it is most common to use a constant (see, e.g., Prych, 1972).

A pressure gradient is generated by the density difference and is, in addition to the initial momentum and interfacial shear, the most important factor for the jet behaviour in the beginning. The shear and therefore the entrainment increases with the jet velocity, as indicated in Taylor's relation.

If the outlet velocity were small and the buoyancy high, then the jet would act as a plume. The spreading would be dominated by the excess pressure caused by the density difference and would be more or less concentrical from the outlet. The densimetric Froude number for the outlet gives the proportion between the initial momentum and the density difference induced pressure,

$$F_o = \frac{u_o}{\sqrt{g \frac{\Delta\rho_o}{\rho} H}}$$

where u_o = discharge velocity,

$\Delta\rho_o$ = the density difference between the discharge water and the ambient water, and

H = water depth of the outlet.

A typical value of the densimetric Froude number for a power plant outlet is in the range 2 - 10.

Spreading of cooling water can schematically be divided into three phases.

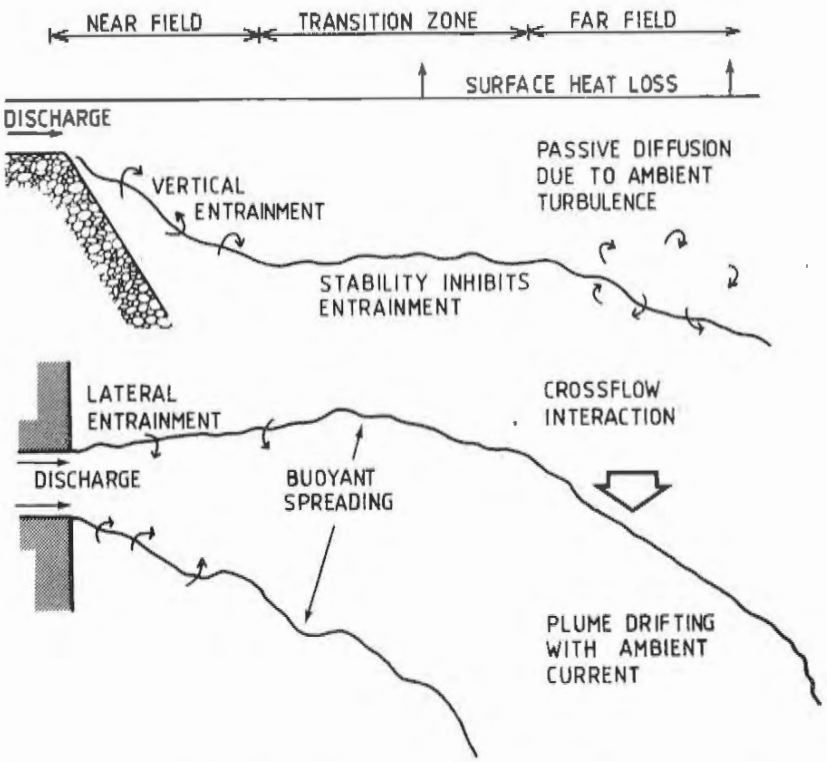

FIGURE 3 Definition sketch of the different phases for a thermal plume (adapted from Dunn, Policastro and Paddock, 1975)

Near-field, where the hydrodynamics of the jet are important. The outlet structure must be considered and the initial momentum will mainly determine the entrainment. The temperature and velocity excesses are great. Surface heat loss is minimal.

A transition zone, where both the initial momentum and the ambient turbulence in the receiving water are of great importance to the mixing.

Far-field, where the excess velocity and temperature are small in the jet and, consequently, ambient conditions are predominant. Diffusion is mainly caused by ambient turbulence. As large areas are involved, surface heat loss will be significant.

In the transition zone and the far-field, the ambient current will be of importance. An ambient crosscurrent will bend the jet in downstream direction. If the bottom is shallow, then the vertical entrainment is reduced. Consequently the water on the downstream side of the jet will be isolated. This water will be gradually entrained. In order to compensate, a large eddy is created which will partly recycle the cooling water. If this recirculation is great enough the jet will reach the coast, see Figure 4 A. For a deep basin water can pass by underneath and vertical entrainment can occur. Therefore, the jet will not bend as much unless the crosscurrents are extremely strong compared to the jet velocity, see Figure 4 B.

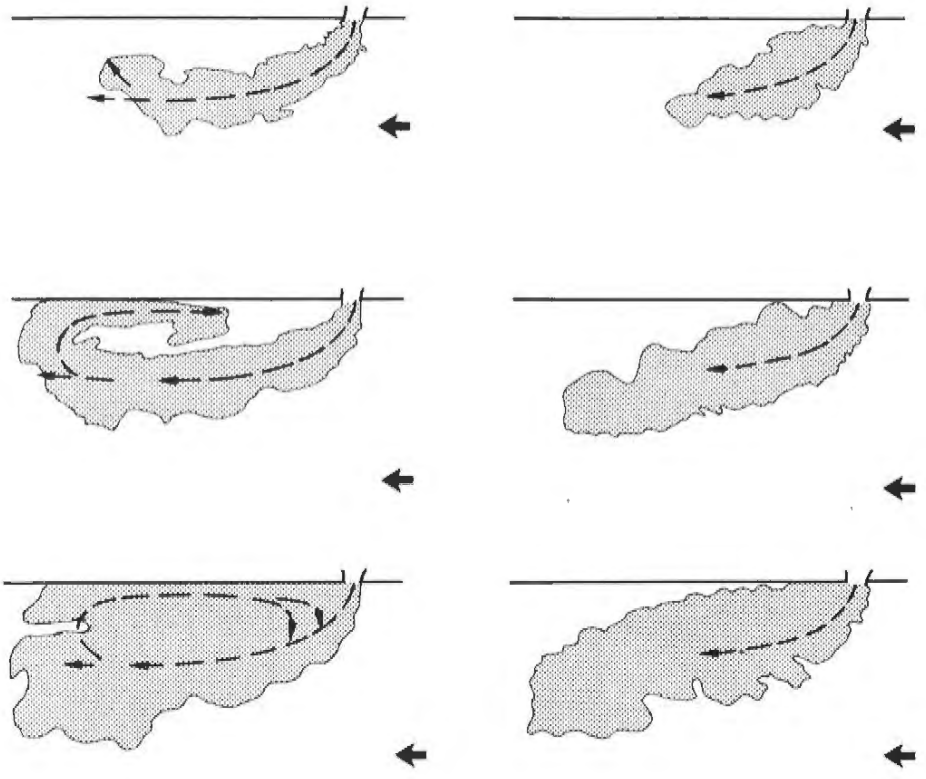

A. Shallow basin B. Deep basin

FIGURE 4 Laboratory experiments on surface jets discharged into a flowing receiving water. In case A the jet reaches the bottom and recirculation occurs. But in case B, the basin is deeper and the jet is not influenced by the bottom. (Cederwall and Sjöberg, 1969).

The reduced turbulence in the boundary between the jet and the ambient water will reduce the momentum transfer from the jet and thus most of the wind-induced momentum in the jet is retained. The wind-driven current will therefore be greater in the jet than in the surrounding water and the sensitivity by the wind will accordingly be pronounced and the jet propagation will most often be in the wind direction.

When wind or a crosscurrent deflects the plume, a strong temperature gradient is formed upstream because the spreading due to the excess buoyancy is opposed by the windstress or the form drag of the current. If the plume is not influenced by the shore on the downstream side, then the gradients are weaker as the stress acts in the same direction as the buoyancy. Furthermore, if the wind forces the jet towards the coast, the warm water layer will thicken until it is large enough to balance the windforce with the increased buoyancy in that region. The thickness of the jet can thus be 3 - 4 times the normal value.

Heat exchange between the water surface and the atmosphere through evaporation, conduction and radiation goes on continuously. As this heat exchange depends strongly on the water temperature, there will be a relatively greater heat loss from the jet than from the ambient water. Thus the temperature difference between the two masses will decrease. This is, however, a very slow process. Compared with the intense mixing caused by shear, the heat loss to the atmosphere can be disregarded just outside the outlet. Further out the heat loss is even smaller per area. However, very large areas are involved and the mixing processes are much smaller, so the heat loss to the atmosphere will be more important.

INTEGRAL MODELS

Early jet models have only been able to calculate the spreading in the near-field. This is because they have been mainly based upon laboratory experiments which discharge into a quiescent surrounding and have a very weak turbulence in the receiving water.

In these experiments (Schmidt, 1941, Albertson, Dai, Jensen and Rouse, 1950, Rouse, Yih and Hympreys, 1952) one found that the excess velocity and temperature of the jet were transformed very fast into a more or less Gaussian distribution both laterally and vertically, see Figure 5. This distribution is expected as the mixing is created by the jet-induced shear and no deflecting forces are participating. The zone of flow establishment was found to be at most six times the outlet diameter (e.g. Albertson, Dai, Jensen and Rouse, 1950, Gordier, 1959, Pratte and Baines, 1967).

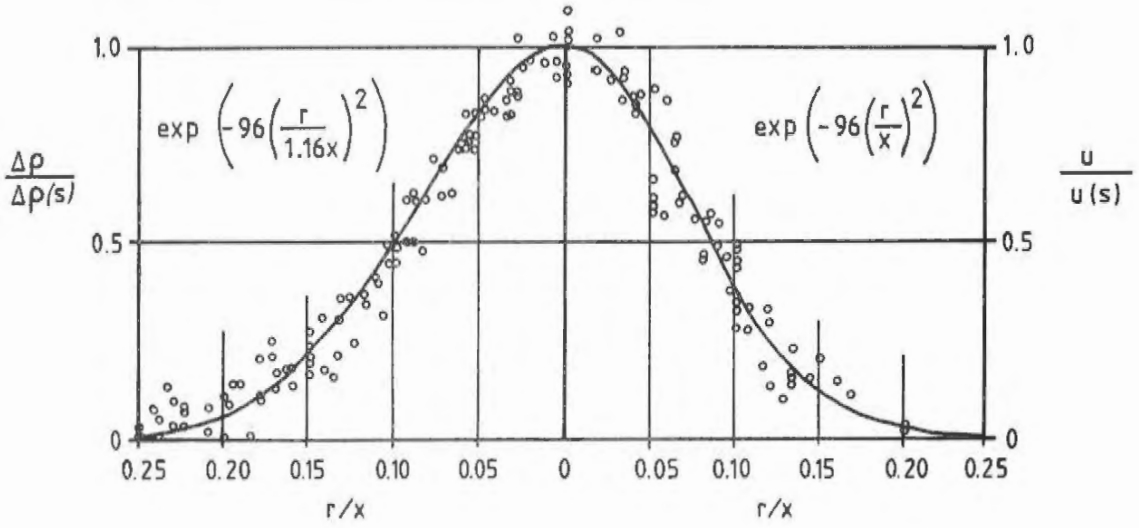

FIGURE 5 Distribution of density and velocity in a round jet, after Rouse, Yih and Humpreys (1952)

Models were simplified to one dimension by integration and by assuming that the jet always is Gaussian distributed, laterally and vertically, after this zone. This integration method is used by, among others, Motz and Benedict (1970), Stolzenbach and Harleman (1971) and Prych (1972).

Several investigators tried with different methods to get the models to work satisfactory in the transition zone and even in the far-field and thus get a more universal application. Prych (1972), consequently, tried to describe the entrainment due to turbulence in the ambient water in a similar manner as the shear-induced entrainment in order to keep the one-dimensional form of his model.

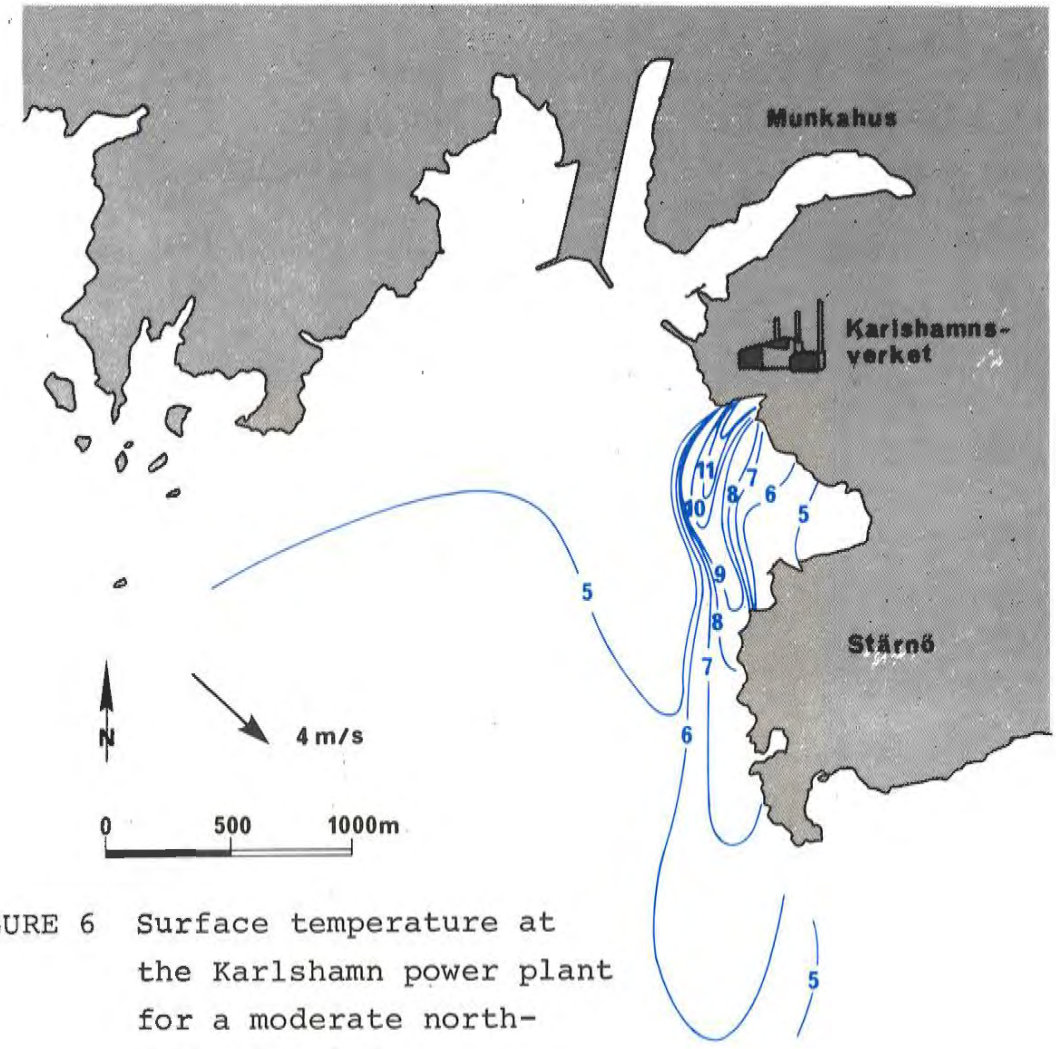

FIGURE 6 Surface temperature at the Karlshamn power plant for a moderate north-westerly wind

Unfortunately the plume will only keep its Gaussian-shaped form if it moves straight out from the coast into deep receiving waters without currents and with no wind effect. The plume will otherwise be deformed due to limited entrainment from one side or from below by respectively, the form drag caused by the ambient current or the wind-stress. Figure 6 shows an example from Karlshamn where the moderate wind deflects the plume towards Stärnö. The temperature is far from being Gaussian distributed. It is not even equally distributed on both sides of the jet axis. This is particularly seen at the level of Sandvik. As a consequence, such a model can only be used when wind and current effects are relatively unimportant, i.e., generally only in the near-field. To be able to describe the unequal distributions that frequently occur in both horizontal and vertical directions, three dimensional models are required. Also, it is of great value to be able to simulate real situations. So the models should be time dependent.

NUMERICAL MODELS

In integral models several rules of thumb observed in laboratory studies are necessary. A more general physical description of jet behaviour is to use the Navier-Stokes and heat-energy equations and solve them, for example, by finite-difference techniques for a number of discrete points in a grid. This technique needs, however, more computational resources than the integral technique and is therefore more expensive. However, the expense should not necessarily be a limitation if a better description of the physical behaviour can be obtained.

Even in a numerical model some simplifications of the physical description must be made or can be done due to the nature of the problems solved.

The hydrostatic approximation

Variations in the vertical velocity are most often small enough so that the acceleration and viscosity terms in the vertical momentum equation are negligible compared to the gravitational acceleration term. These terms can then be removed in order to arrive at a simpler system of equations. The horizontal momentum equations will remain unchanged. The hydrostatic approximation has been used extensively in the modelling of oceanic basins and lakes (Crowley, 1968, Bryan, 1969, Simons, 1971, 1972, Haq, Lick and Sheng, 1974) and it has been shown to be valid in the modelling of river discharges (Paul and Lick, 1973) and for most surface thermal-plume problems (Dunn, Policastro and Paddock, 1975, Waldrop and Farmer, 1974).

Table 1 indicates approximate values for the neglected terms in the vertical momentum equation for different types of thermal discharge problems one might apply the

model to. For comparison, the gravitational acceleration term is about 10^3 cm/sec^2. This table indicates that the hydrostatic assumption is valid except for certain types of submerged discharges when the discharge is directed vertically upward.

	u (cm/sec)	w (cm/sec)	Δz (cm)	Δx (cm)	h (cm)	ΔT ($^\circ$C)	A_H (cm^2/sec)	A_V (cm^2/sec)
Surface thermal plume	10^2	1	25	10^3	10^3	10	10^3	2
Horizontally discharged submerged plume	10^2	3	25	10^3	10^3	10	10^3	2
Vertically discharged submerged plume	1	10^2	2×10^2	5×10^2	2×10^3	10	10^3	10^2

TABLE 1 A Representative physical parameters for typical thermal discharge applications

	Horizontal convection $\frac{uw}{\Delta x}$ (cm/sec^2)	Vertical convection $\frac{w^2}{\Delta z}$ (cm/sec^2)	Horizontal diffusion $A_H \frac{w}{(\Delta x^2)}$ (cm/sec^2)	Vertical diffusion $A_V \frac{w}{(\Delta z^2)}$ (cm/sec^2)
Surface thermal plume	10^{-1}	4×10^{-2}	10^{-3}	3.2×10^{-3}
Horizontally discharged submerged plume	.3	.36	3×10^{-3}	9.6×10^{-3}
Vertically discharged submerged plume	.2	50	.4	.25

TABLE 1 B Values for neglected terms in vertical momentum equation for typical thermal discharge applications

Rigid-lid approximation

The rigid-lid approximation is used to damp out the surface gravity waves that would otherwise be present. The time scales associated with the surface gravity waves are small compared with other relevant time scales in calculations of a plume behaviour. Accordingly the elimination of surface gravity waves allows the use of greater time steps and will greatly reduce the computation time. An additional relief is that the rigid-lid approximation allows the use of a fixed grid because the surface does not move. The rigid-lid condition does not, however, eliminate the internal waves. Table 2 lists the time scales associated with the gravitational surface waves and the other relevant physical phenomena in some possible thermal discharge applications. These time scales are calculated from the one-dimensional numerical stability limit for each of the phenomena. In all circumstances the surface gravity waves are associated with small time scales compared to the others. In practical computational terms, this means that extremely small numerical time

	$\frac{\Delta x}{u}$	$\frac{\Delta z}{w}$	$\frac{\Delta x}{\sqrt{gh}}$	$\frac{\Delta x}{\sqrt{\frac{\Delta\rho}{\rho}gh}}$	$\frac{(\Delta x)^2}{2A_H}$	$\frac{(\Delta z)^2}{2A_V}$	$\frac{1}{f_0}$
Surface thermal plume	10	25	1	22	5×10^2	156	10^4
Horizontally discharged submerged plume	10	8.3	1	22	5×10^2	156	10^4
Vertically discharged submerged plume	5×10^2	2	.35	7.7	125	200	10^4

Note all times in seconds

TABLE 2 Time scales associated with typical thermal discharge applications

steps would be required for solutions containing the surface gravity waves, and this would result in large computer calculation times. However, if one is interested in a particular application where surface gravity waves are of interest, then the free surface variations must be included. Note that recent work has been done which indicates that implicit free-surface calculations can be made as efficient as rigid-lid calculations (Paul and Lick, 1979).

The Boussinesq approximation

The density variations are always small both in the fluctuations and in the mean values. In the Baltic Sea the variations are at most 1 % and, furthermore, the density difference between discharged cooling water and the ambient water will never exceed this value. A good approximation is thus to neglect the effect of the density variations on the mass in the inertia terms but keep their effect on the weight term. The water is thus treated as incompressible. As a consequence of the Boussinesq approximation, the energy equation reduces to a balance between convection and diffusion. The coupling between the momentum and energy equations is, however, retained.

The simulation of turbulence

A good definition of turbulence that will satisfy everyone, does not exist. One tries instead to describe the characteristics of turbulent flows (see, e.g., Tennekes and Lumley, 1972, Bradshaw, 1971, Hinze, 1959). The most common and obvious characteristic is the randomness, but there is no sharp dividing-line between pure random and entirely regulated motions.

The most common way to treat turbulence is to use Reynold's decomposition of velocity into mean and fluctuating components and to call the mean velocity advection and the fluc-

tuating velocity turbulence. This decomposition can be done with respect to time or space and will, of course, be highly arbitrary.

In a numerical model the resolutions in time and space are limited. This limitation not only forces you to use Reynold's decomposition technique, it also gives you the minimum scale for advection, since this cannot be smaller than the grid size. There is, however, a troublesome circumstance - the fact that the time and space resolutions used in models will give quite different answers on what is turbulence and what is not. The relation between the length and time scale is according to Kolmogorov's theory (Nihoul, 1975):

$$\ell \approx \varepsilon^{1/2} \tau^{3/2}.$$

Nihoul takes a tidal model of the North Sea as an example. The grid size was 5 km, and the time step 5 min. In this case the rate of energy transfer, ε, is about 10^{-8} m^2/sec^3. The time step gives consequently a typical length scale in the order of 5 m, which is 1/1000 of the turbulent length scale given by the grid. Furthermore, it is unnecessarily small for a tidal model. However, a time step that will give the same length scale of 5 km will be in the order of one day and will thus be meaningless in such a model. The numerical stability also requires time steps of the order of some minutes.

The decomposition technique will have Reynold's stress terms as an unknown part in the momentum equations. One way to handle them is to form equations for the turbulent kinetic energy, k, and its rate of dissipation, ε, and thus use a so-called k-ε model. We still will have a closure problem, but with some assumptions about the turbulent behaviour some investigators claim that the constants one uses in the end are more or less universal (Launder and Spalding, 1974, Mc Guirck and Rodi, 1976). This method has its advantages

particularly for free-shear layer calculations, but it also introduces extra equations into the model, that will demand much additional computation capacity. Yet higher order closure models have been developed, but they have so far not been used for practical purposes.

Another and the most common way is to use the analogy in laminar flow with molecular viscosity and introduce so-called turbulent or eddy viscosity and diffusivity coefficients.

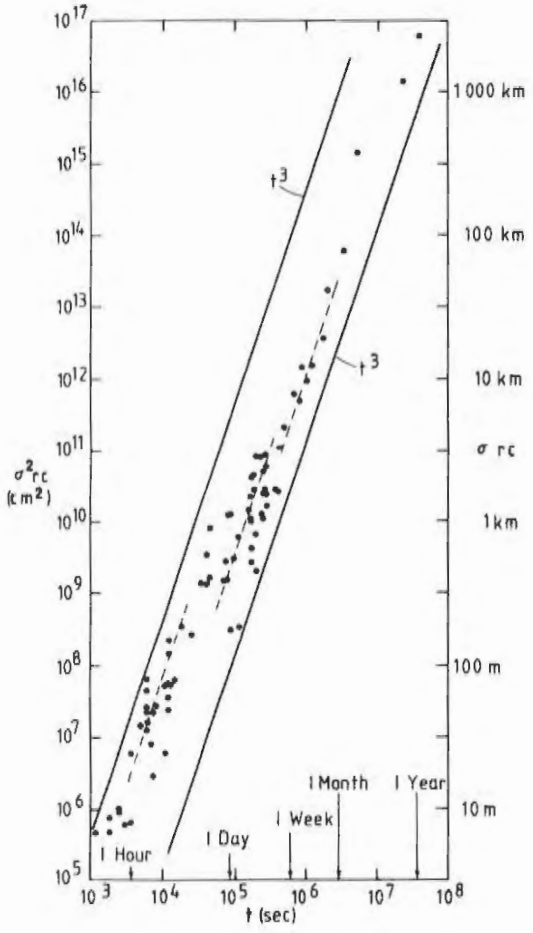

FIGURE 7 Variance versus time fit of the third power law locally (Okubo, 1971)

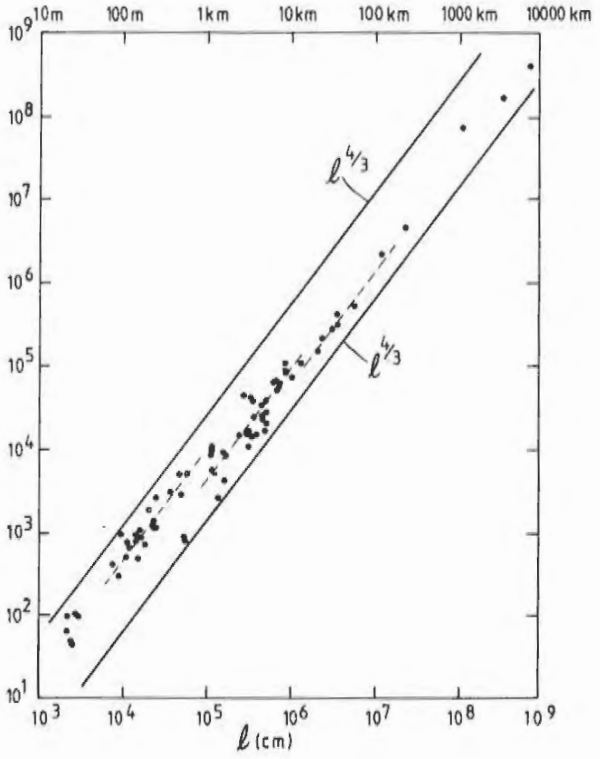

FIGURE 8 Apparent diffusivity versus scale of diffusion. Fit of the 4/3 power law locally (Okubo, 1971)

Several experimental studies on diffusion in oceans and lakes have been made. Figures 7 and 8 show data of patch diffusion from oceanic experiments. The relative diffusion in a patch should, according to dimensional arguments, depend on the time as

$$\sigma^2 \sim \epsilon \tau^3,$$

where σ^2 is the variance of the tracer in the patch. The diffusivity, K, is related to the variance and time by

$$K \sim \frac{\sigma^2}{\tau}.$$

Using the relation between the length and time scale mentioned above, one gets the 4/3 power law

$$K \sim \epsilon^{1/3} \ell^{4/3}.$$

Okubo's diagrams show that experimental data can support this theory, if on varies ϵ with the time and length scales. He also concludes (Okubo, 1974) that the clear jumps in the line fitting coincides almost with gaps in the energy spectrum of oceanic turbulence proposed by Ozmidov (1965), see Figure 9.

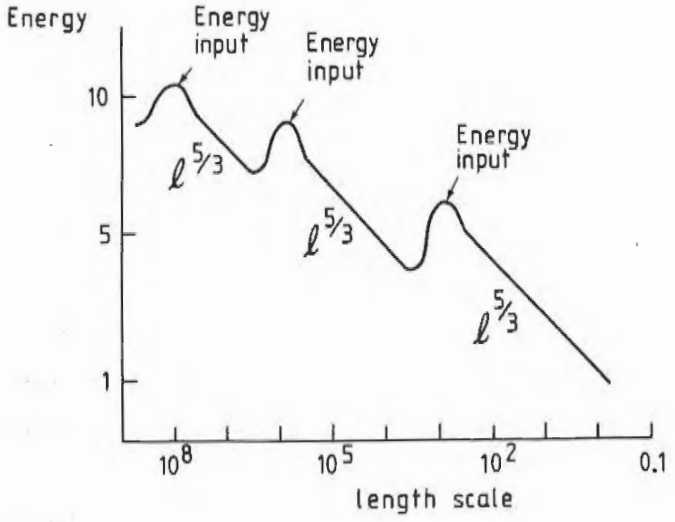

FIGURE 9 Ozmidov spectrum for oceanic turbulence

In spite of the strong dependence of diffusivity on the time and length scales, the most frequently used form is constant eddy diffusivity and eddy viscosity coefficients in the horizontal directions (Simons, 1971, 1972, Bryan, 1969, Haq, Sheng and Lick, 1974, Paul and Lick, 1974). The smallest scale possible to describe advection in a numerical model is equal to the grid spacing. Everything smaller must be parametrized and considered as turbulence. This fact must be considered when the values are to be chosen.

From the related experiments above and an assumption that the horizontal diffusion is isotropic, Okubo (1976) found the following relation:

$$K = 0.0680 \quad r^{1.15},$$

where r = the grid size.

If the intention is to use Okubo's relation, then one must be aware of the restriction that it puts on the model. The one dimension stability criterium is

$$K > \frac{1}{2} r q$$

where q = horizontal current. Together with Okubo's relation this will give

$$q < 0.136 \; r^{0.15}.$$

So, Okubo's relation will only permit very weak currents - 10 km grid size or less will require smaller velocities than 1 cm/sec - and so numerical stability requires greater eddy coefficients than this relation will give. Even the use of a multi-dimensional stability criterium only relaxes the restriction with a factor of 2 - 4.

Modellers have also used the k-ε model in the vertical direction (Spalding and Svensson, 1976), but the most common way to solve the closure problem is to use an eddy coefficient in the same way as in the horizontal directions. The use of a constant eddy coefficient has to be considered carefully since experiments have shown a strong dependence upon the vertical density and velocity gradients. Modelling lake circulation with a constant coefficient can sometimes be successful (Sheng, Lick, Gedney and Molls, 1978).

Rossby and Montgomery (1935) proposed following relation based upon energy conservation aspects

$$A_v = A_o \ (1 + cRi)^{-1},$$

where

A_v = vertical eddy viscosity coefficient,
A_o = vertical eddy viscosity coefficient of homogeneous water,
c = empirical constant, and

$$Ri = \frac{\frac{g}{\rho}\frac{\partial \rho}{\partial z}}{(\frac{\partial q}{\partial z})^2} = \text{Richardson number.}$$

This formula satisfies the condition that the turbulence will vanish for high Richardson numbers. Holzman (1942) proposed

$$A_v = A_o \ (1 - cRi)$$

to meet the condition that the turbulence is suppressed for a certain critical value of Ri. This formula has, however no theoretical basis.

Munk and Anderson (1948) generalized the above relations into

$$A_v = A_o \, (1 + cRi)^{-\alpha_v},$$

where

α_v = constant,

and proposed a similar formulation for the eddy diffusivity

$$K_v = A_o \, (1 + c_1 Ri)^{-\alpha_k},$$

where

c_1 and α_k are constants.

By doing so, these relations are made essentially empirical. They determined the empirical constants as $c = 10$, $\alpha_v = 0.5$, $c_1 = 3.33$ and $\alpha_k = 1.5$. Those expressions have been commonly used (Bennett, 1977, Svensson, 1980).

Mamayev (1958) on the other hand argued for exponential relations:

$$A_v = A_o \, e^{-cRi}$$

and

$$K_v = A_o \, e^{-c_1 Ri}.$$

His intention was not only to satisfy the condition that for very high stability the flux of momentum and heat will be pure molecular, but also to be able to use the formulas for unstable stratification. In this latter case the mixing will - according to his formulas - be more intense.

In a classical work Ellison (1957) proposed the following relation based on laboratory experiments:

$$\frac{K_v}{A_v} = \frac{b(1-Rf/Rf_c)}{(1-Rf)^2},$$

where

$b = K_v/A_v$ in neutral conditions,

$Rf = \frac{K_v}{A_v} Ri$ = flux Richardson number, and

Rf_c = the critical value of Rf at which K_v vanishes.

Ellison found $Rf_c = 0.15$. Kullenberg (1974) used the same relation but with $Rf_c = 0.05$ (see Figure 10).

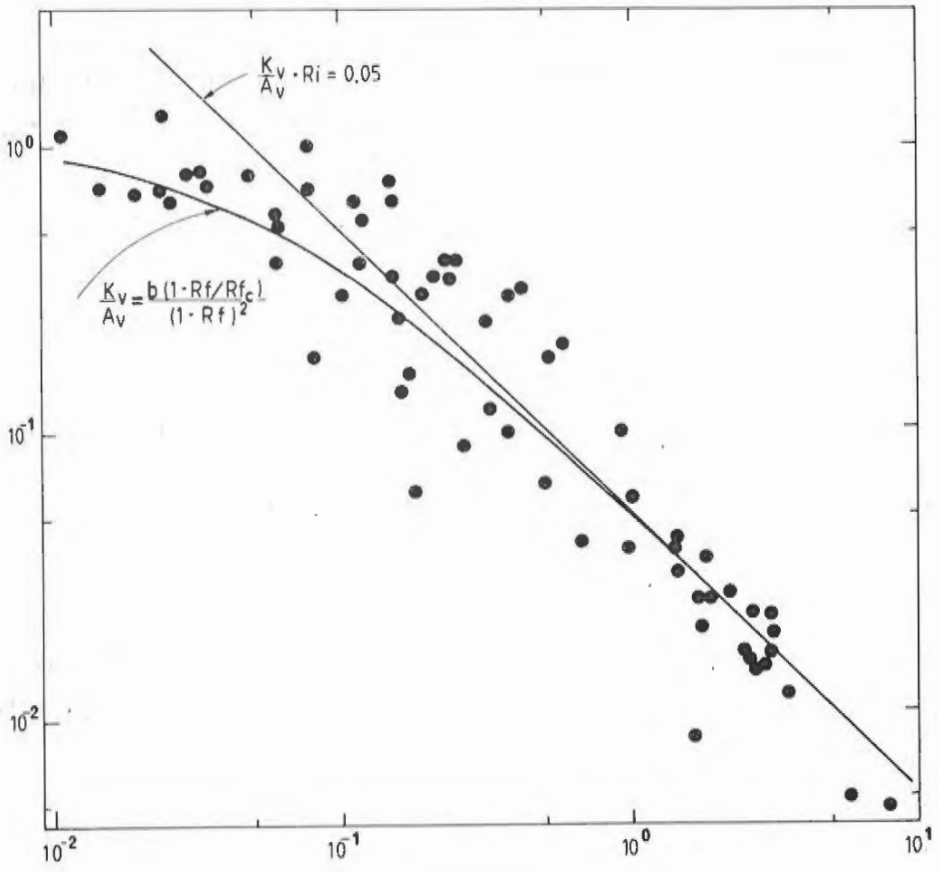

FIGURE 10 Relation K_v/A_v vs. Richardson number Ri.
Line indicates $\frac{K}{K_m} \cdot Ri = 0.05$.
Curve indicates Ellison's (1957) equation with $Rf_c = 0.05$. (Kullenberg, 1974)

Kullenberg (1969, 1971) and Kullenberg, Murthy and Westerberg (1973, 1974) studied the diffusion in the thermocline and the upper layers in coastal water and in Lake Ontario. In the upper parts of the water mass the turbulence will be created mainly by the wind-driven shear. Accordingly, the turbulence can be related to the wind speed and current shear and the stratification of the water, when the wind speed exceeds 4 - 5 m/sec. He proposed a relation that can be rewritten in this manner:

$$K_v = \frac{c \cdot W^2}{Ri \cdot |\frac{dq}{dz}|}$$

where

W = wind velocity.

Kullenberg suggested that the shear was wind-induced. This relation between the wind and the shear would therefore be possible to include in the formula.

For lighter winds Kullenberg suggested

$$K_v = \frac{c \cdot q'^2}{Ri \cdot |\frac{dq}{dz}|}$$

where

q' = horizontal current fluctuations.

Noticeable is that the scale of diffusion is not so important for the vertical diffusion as for the horizontal diffusion. The vertical diffusion is instead limited by the vertical stability.

Approximation of the equation of state

The water density depends on the salinity, temperature and the pressure. As we only are concerned about areas

one hundred meters deep at the most, the pressure dependence can be neglected. In fresh water modelling it is common to simplify to a linear relationship between temperature and density anomalies (see e.g. Waldrop and Farmer, 1973, and Paul and Lick, 1974) or a second order relation (see e.g. Simons, 1974). For the more complex situation with salinity, investigators have proposed several empirical relations. One very useful for the Baltic Sea was adapted from Fredrich and Levitus (1972) and modified by Wilmot (1976):

$$\rho = -0.09895 + T(0.06505 + T(-0.007697 + 0.00003519\,T)) + S(0.8071 + T(-0.003081 + 0.00003730\,T)).$$

The f-plane approximation

When circulation in lakes and dispersion of pollutants are to be modelled, areas are on the order of a few 10 km at the most. The geographical variations will therefore not be of any significance to the Coriolis terms, and the f-plane approximation can be used. This has been used even in the Great Lakes (Simons, 1971, and Bennett, 1977).

The resulting equations

With the approximations mentioned above, one gets the following equations:

$$\frac{\partial u}{\partial x} + \frac{\partial v}{\partial y} + \frac{\partial w}{\partial z} = 0,$$

$$\frac{\partial u}{\partial t} + \frac{\partial u^2}{\partial x} + \frac{\partial uv}{\partial y} + \frac{\partial uw}{\partial y} + f_o v = -\frac{1}{\rho_o}\frac{\partial P}{\partial x} + \frac{\partial}{\partial x}\left(A_H \frac{\partial u}{\partial x}\right) + \frac{\partial}{\partial y}\left(A_H \frac{\partial u}{\partial y}\right) + \frac{\partial}{\partial z}\left(A_V \frac{\partial u}{\partial z}\right),$$

$$\frac{\partial v}{\partial t} + \frac{\partial uv}{\partial x} + \frac{\partial v^2}{\partial y} + \frac{\partial vw}{\partial z} - f_o u = -\frac{1}{\rho_o}\frac{\partial P}{\partial y} + \frac{\partial}{\partial x}\left(A_H \frac{\partial v}{\partial x}\right)$$

$$+ \frac{\partial}{\partial y}\left(A_H \frac{\partial v}{\partial y}\right) + \frac{\partial}{\partial z}\left(A_H \frac{\partial w}{\partial z}\right)$$

$$\frac{1}{\rho}\frac{\partial P}{\partial z} = g,$$

$$\frac{\partial T}{\partial t} + \frac{\partial uT}{\partial x} + \frac{\partial vT}{\partial y} + \frac{\partial wT}{\partial z} = \frac{\partial}{\partial x}\left(K_H \frac{\partial T}{\partial x}\right) + \frac{\partial}{\partial y}\left(K_H \frac{\partial T}{\partial y}\right)$$

$$+ \frac{\partial}{\partial z}\left(K_V \frac{\partial T}{\partial z}\right)$$

$$\frac{\partial S}{\partial t} + \frac{\partial uS}{\partial x} + \frac{\partial vS}{\partial y} + \frac{\partial wS}{\partial z} = \frac{\partial}{\partial x}\left(K'_H \frac{\partial S}{\partial x}\right) + \frac{\partial}{\partial y}\left(K'_H \frac{\partial S}{\partial y}\right)$$

$$+ \frac{\partial}{\partial z}\left(K'_V \frac{\partial T}{\partial z}\right),$$

$$\rho = f(T,S),$$

where

x,y = horizontal coordinates,
z = vertical coordinate,
u,w = fluid velocities in x and y directions,
w = fluid velocity in z-direction,
t = time,
P = pressure,
T = temperature,
S = salinity,
ρ = density,
f_o = Coriolis parameter,
A_H = horizontal eddy viscosity,
A_V = vertical eddy viscosity,
ρ_o = density at reference conditions,
K_H = horizontal eddy conductivity,
K_V = vertical eddy conductivity,
K'_H = horizontal eddy diffusivity for salinity,
K'_V = vertical eddy diffusivity for salinity,
g = gravitational acceleration, and
$f(T,S)$ = equation-of-state.

PROBLEMS TO BE ADRESSED

A recipient where the excess heat caused by the discharged cooling water is effectively reduced by mixing and advection is a major concern when locating power plants. However, other environmental and economical factors are important as well and the recipients therefore can exhibit quite different ventilation characteristics.

The recipients outside the Barsebäck and the Karlshamn power plants are each representative for two rather extreme conditions. This is the primary reason why choosing to make plume predictions were made in these recipients. Moreover, experiences from these areas ought to be of value when discussing conditions in other recipients and locations of new plants.

The flow characteristics in the recipient outside Barsebäck are dominated by the general current in Öresund. This current is rather strong and goes either to the north or to the south, and so the advective transport is effective. Furthermore, the great velocity gradients caused by this current create a strong turbulence that effectively mixes the cooling water with the ambient water.

At the Karlshamn power plant the cooling water is discharged into a rather small bay. Here the cooling water sometimes can extend over the whole bay. This is because the currents in that area are highly wind-dependent, and so unfavourable winds often reduce both the advective transport and the mixing.

Therefore, the problems which principally will be adressed here, are to predict a cooling water plume in a clearly wind-dependent recipient and in a recipient that is dominated by a strong current.

MATHEMATICAL MODEL

DEVELOPMENT OF THE MODEL EQUATIONS

The basic equations for the numerical model are derived from the time-dependent, three-dimensional equations of motion for a viscous, heat-conducting fluid. The geometry for the problem is shown in Figure 11.

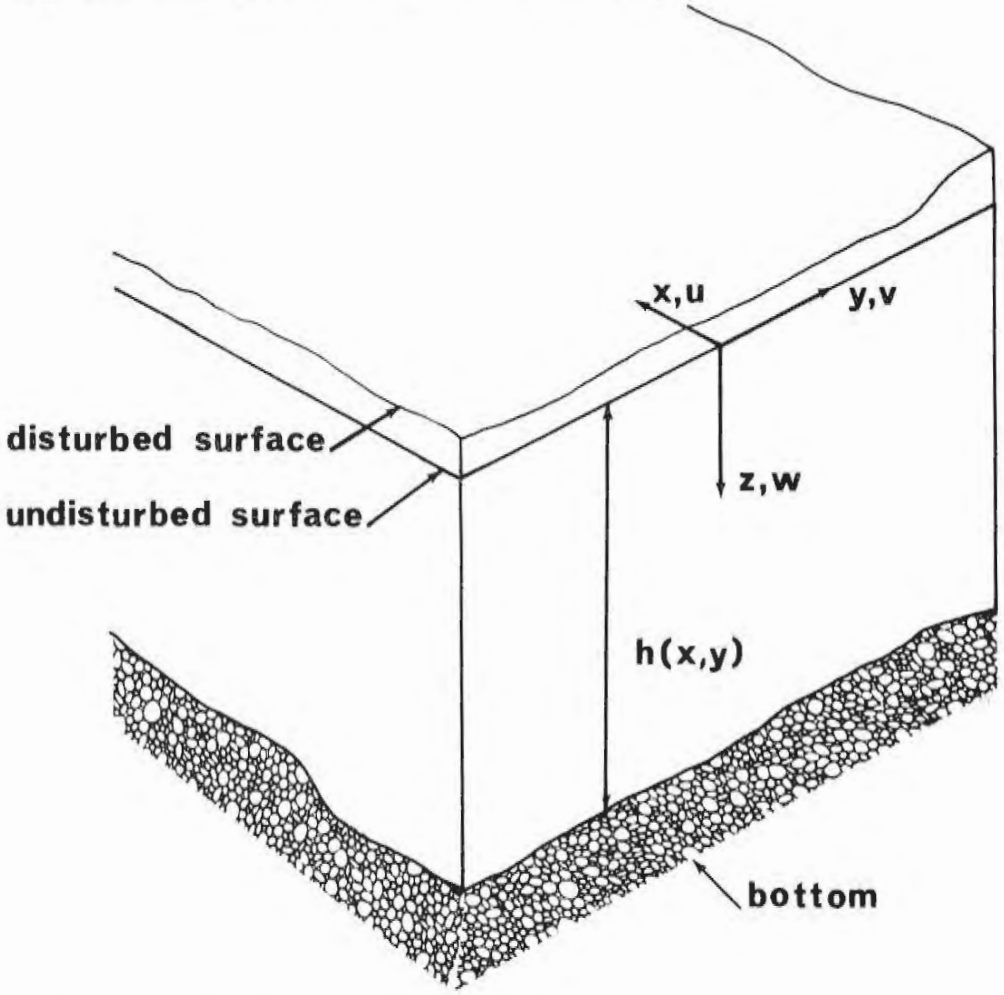

FIGURE 11 Geometry for the problem

The horizontal coordinates are x and y, the vertical coordinate is z and is positive downward from the undisturbed free surface, and the velocities are, respectively, u, v, and w. The following simplifications are made:

The hydrostatic approximation

For the cases on which the model is used, variations in the vertical velocity are small enough so that the neglected terms in the vertical momentum equation are small compared to the gravitational acceleration term. A consequence of this approximation is that the order of the system of equations is reduced, and thus the computational effort required for a solution is reduced. In particular, the elliptic equation that is solved for the pressure is reduced from three dimensions to two dimensions.

The rigid-lid approximation

With the rigid-lid approximation, only surface variations associated with the gravity waves are neglected. Pressure variations along the undisturbed free surface, $z = 0$, and internal gravity waves associated with vertical density variations are permitted. In the steady-state limit, the rigid-lid model will give identical results as the comparable free surface model, if the steady-state limit exists.

The Boussinesq approximation

This allows the water to be treated as incompressible. The density differences that are encountered in our applications of the model are small, and therefore this approximation is valid.

Heat sources and/or sinks in the water are neglected

All heat inputs and outputs to the model are assumed to occur at the boundaries of the model. As a consequence of this, heat transfer by radiation to the water is treated as a surface heat flux.

Eddy coefficients are used to account for the turbulent effects

As mentioned previously, the horizontal eddy diffusivity depends on the length scale. Yet, even if the model makes it possible to use a varying grid in the horizontal, constant horizontal eddy coefficients are used. Experience has shown that usually the results don't suffer to much by this shortcoming.

The vertical eddy coefficient is taken as dependent on the local vertical temperature gradient. This is similar to the form suggested by Sundaram et al (1969, 1970). The expressions for the vertical eddy coefficients are:

$$A_v = A_o + \beta_A \frac{\partial T}{\partial z}$$

$$K_v = K_o + \beta_K \frac{\partial T}{\partial z}$$

where β_A and β_K are constants dependent on the local conditions. Thus, no true Richardson number dependence exists in the model. The vertical velocity gradient, i.e., the turbulence creating part, is disregarded and only the damping effect by the density gradient is considered. These formulas are in principal the same as Holzman (1942) proposed if one regards the velocity gradient as rather constant. As the vertical diffusion is more sensitive to the stability than the momentum exchange, $\beta_A < \beta_K$.

The variations in the bottom topography are assumed to be gradual

The present model allows for variations in topography of the system modelled. A standard numerical procedure to fit the variable topography into a model is to vary the number of vertical grid points in the computational mesh according to the local depth (Bennett, 1971, Simons, 1971,

Huang, 1977). A problem with this procedure is that vertical resolution is lost in shallow areas, and this happens to be where some of the most interesting phenomena can be occurring. A seemingly more complicated procedure, although a lot simpler in many aspects, is to stretch the vertical coordinate with respect to the local depth. The equations are transformed according to

$$x \mapsto x$$

$$y \mapsto y$$

$$\sigma \mapsto z/h(x,y).$$

The equations to be solved are more complicated looking because of the appearance of the depth in the equations, but they are solved for a basin of constant depth in the transformed system. Also, as Figure 12 indicates, there is no loss of resolution in the shallow areas because the same number of vertical points is used at every horizontal location. The coordinate transformation greatly reduces the programming complexities associated with the model and makes the inclusion of topographic variations quite straight forward.

The assumption of gradual variations in the depth allows a reduced form for the transformeddiffusion terms to be used. The transformation is not conformal and so the transformed diffusion terms involve cross-derivatives of the spatial coordinates. The transformed diffusion terms containing derivatives of the depth are neglected with respect to those terms containing only the depth. This approximation has been used in meteorological problems when topographic variations are included (Philips, 1957, Smagorinsky, et al., 1965), and has been used in modelling lakes (Paul and Lick, 1976, Sheng, 1975, Freeman, Hale and Danard, 1972).

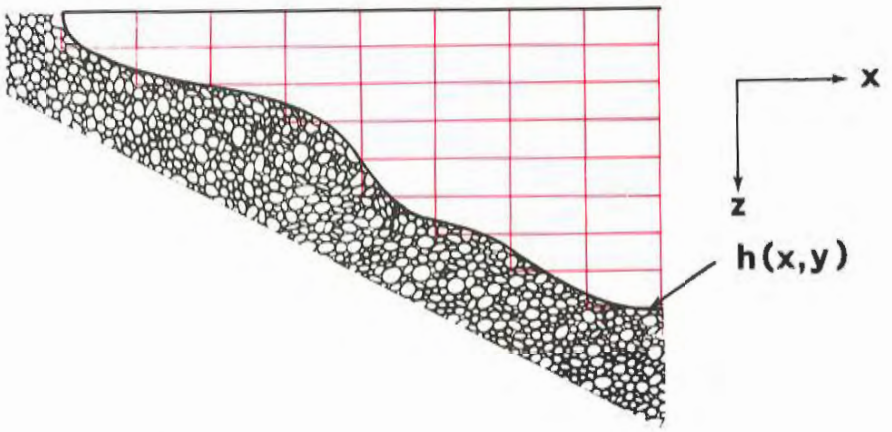

Standard grid

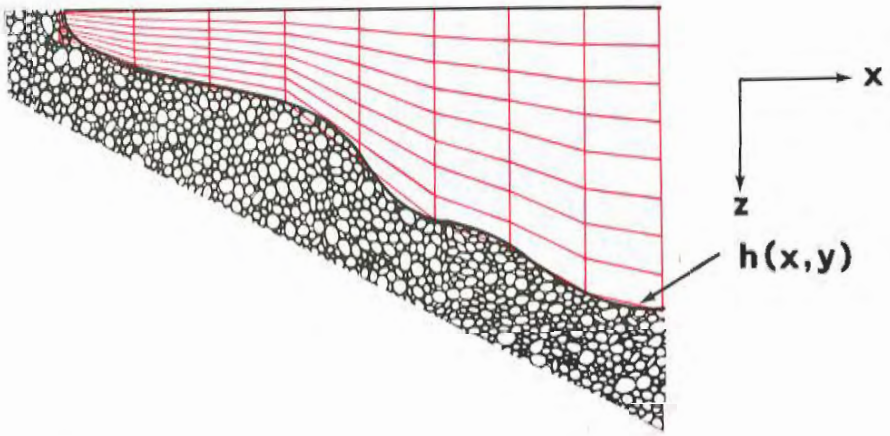

Grid in Pauls model

FIGURE 12 Vertical resolution for a standard grid and the one used in Paul's model (schematic)

Density is assumed to be a function of temperature and salinity only

In our model applications, pressure variations have a negligible influence on the density. In these tests Wilmots empirical relation is used (Wilmot, 1976). The measured salinity variations were negligible during the verificated days at both Barsebäck and Karlshamn, and so the salinity were held constant in the calculations.

The resulting equations

The equations, in non-dimensional form, which form the basic model, are the following:

$$\frac{1}{h}\frac{\partial hu}{\partial x} + \frac{1}{h}\frac{\partial hv}{\partial y} + \frac{\partial \Omega}{\partial \sigma} = 0,$$

$$\frac{\partial u}{\partial t} + Re\left[\frac{1}{h}\frac{\partial hu^2}{\partial x} + \frac{1}{h}\frac{\partial huv}{\partial y} + \frac{\partial \Omega u}{\partial \sigma}\right] + Rov = -\frac{\partial Ps}{\partial x}$$

$$- \frac{Re}{Fr^2}\left[\frac{\partial}{\partial x}\left(h\int_0^\sigma \rho\, d\sigma\right) - \sigma\frac{\partial h}{\partial x}\rho\right]$$

$$+ \frac{1}{h}\frac{\partial}{\partial x} h \frac{\partial u}{\partial x} + \frac{1}{h}\frac{\partial}{\partial y} h \frac{\partial u}{\partial y} + \left(\frac{b_o}{h_o}\right)^2 \frac{1}{h^2}\frac{\partial}{\partial \sigma}\gamma\frac{\partial u}{\partial \sigma},$$

$$\frac{\partial v}{\partial t} + Re\left[\frac{1}{h}\frac{\partial huv}{\partial x} + \frac{1}{h}\frac{\partial hv^2}{\partial y} + \frac{\partial \Omega v}{\partial \sigma}\right] - Rou = -\frac{\partial Ps}{\partial y}$$

$$- \frac{Re}{Fr^2}\left[\frac{\partial}{\partial y}\left(h\int_0^\sigma \rho\, d\sigma\right) - \sigma\frac{\partial h}{\partial y}\rho\right]$$

$$+ \frac{1}{h}\frac{\partial}{\partial x} h \frac{\partial v}{\partial x} + \frac{1}{h}\frac{\partial}{\partial y} h \frac{\partial v}{\partial y} + \left(\frac{b_o}{h_o}\right)^2 \frac{1}{h^2}\frac{\partial}{\partial \sigma}\gamma\frac{\partial v}{\partial \sigma},$$

$$Pr\left[\frac{\partial T}{\partial t} + Re\left[\frac{1}{h}\frac{\partial huT}{\partial x} + \frac{1}{h}\frac{\partial hvT}{\partial y} + \frac{\partial \Omega T}{\partial \sigma}\right]\right] =$$

$$\frac{1}{h}\frac{\partial}{\partial x} h \frac{\partial T}{\partial x} + \frac{1}{h}\frac{\partial}{\partial y} h \frac{\partial T}{\partial y} + \left(\frac{b_o}{h_o}\right)^2 \frac{1}{h^2}\frac{\partial}{\partial \sigma}\beta\frac{\partial T}{\partial \sigma},$$

$$\rho = f(T,S)$$

where

$$Re = \frac{u_o b_o}{A_H},$$

$$Ro = \frac{f_o b_o^2}{A_H},$$

$$Fr^2 = \frac{u_o^2}{g h_o},$$

$$Pr = \frac{A_H}{K_H},$$

$$\gamma = \frac{A_V}{A_H},$$

$$\beta = \frac{K_V}{K_H},$$

x,y = transformed horizontal coordinates,

σ = transformed vertical coordinate,

u,v = fluid velocities in x and y-directions,

Ω = fluid velocity in σ-direction,

$$= \frac{d\sigma}{dt} = \frac{1}{h}\left(w - \sigma\left(u\frac{\partial h}{\partial x} + v\frac{\partial h}{\partial y}\right)\right),$$

h = local depth,

P_s = surface pressure, integration constant resulting from vertical integration of hydrostatic pressure equation, function of only x and y,

$$= P - gh\int_0^\sigma \rho d\sigma,$$

b_o = reference horizontal dimension,

h_o = reference depth,

ρ_o = reference density, and

u_o = reference horizontal velocity.

Note that the reference time is b_o^2/A_H, reference vertical velocity is $u_o h_o/b_o$, and the reference pressure is $\rho_o gh\ Fr^2/Re$.

It should be noted that all of the derivative terms are written in conservative form. This is done to ensure that when the equations are discretized appropriately, the resultant difference equations will satisfy many of the basic conservation laws that the differential equations do. This is a point that is easily overlooked when one develops a numerical model. It is easy to derive difference equations that are approximations to a set of differential equations but do not satisfy certain basic conservation laws, which result in the solutions being not too meaningful. More on this topic will be presented when the differential equations are discretized.

BOUNDARY CONDITIONS

The actual boundary conditions used for a particular application of the model depends in part on the system being modelled. However, certain conditions must always be specified and the types of boundary conditions allowable can be discussed. In Paul's model there is consequently a possibility to make a wide range of choices. In this section we merely discuss the boundary conditions used in our applications for Barsebäck and Karlshamn.

The bottom of the water body is treated as an impermeable, no-slip, insulated surface, and the water surface has the rigid-lid condition specified.

A stress is applied at the water surface. This stress is a specified function of the wind condition over the water. In these applications we have used the well-known formula

$$\tau = C_D \rho_a W^2,$$

where C_D is a dimensionless drag coefficient, ρ_a is the mass density of the air, W is the wind velocity measured at some specified height, usually 10 m. The value on the drag coefficient varies depending on primarily the wind velocity and the stability of the atmosphere. Here we have used the value 1.5 for light winds (< 4 m/s) and 2.4 for stronger winds, as recommended by Wilson (1960).

The temperature condition at the water surface is a heat flux condition, where the flux is proportional to the difference between the temperature of the surface and a specified equilibrium temperature. This is a form of the Newton law of cooling condition. The equilibrium temperature is defined as that temperature at the water surface for which there would be no net flux through the surface;

it is a function of the meteorological conditions above the water surface and can vary with time.

The model has been applied to sections of a water body such that some of the boundaries of the system are actually open water conditions. In this situation, it is either possible to specify the velocities and temperature on these boundaries completely (from a model of the whole water body or from interpolation of field data), or to treat these as open water boundaries. This latter method is to let the velocities and temperature vary smoothly as the boundary is approached. This is accomplished by specifying the first normal derivatives of the variables to be zero at these boundaries.

Roache (1972) has considered the question of what kind of conditions to specify at open boundaries and comes up with the suggestion that the actual condition is not so important as long as the condition that you specify does not restrict the flow or cause unusual things to occur near these boundaries. The procedure mentioned above has been successfully applied and it was found that this procedure behaved as Roache suggests it should (Paul and Lick, 1973). The obvious problem with this type of open boundary specification is that the water on the other side of these boundaries appears to approach infinity. In other words, no effects such as reflections or disturbances from outside the region can be felt inside the region modelled. The only proper way to handle a situation like this is to do two simultaneous calculations: one on the whole basin and another on the particular part of the basin desired. A fine grid can be used in the smaller open-boundary part and a coarse grid could be used for the whole basin calculation. Sheng (1975) has successfully applied such a procedure to storm surge calculations in Lake Erie.

When specifying the data at the open boundaries by interpolation of field data, it is essential that the data do not exhibit any drastic changes neither in space nor in time and the variations should be rather smooth. The boundary values are kept constant during the run of the model, but by splitting the total real time into shorter periods, where the boundary values are held constant, it is possible to allow a step by step variation in time. Between the shorter periods it is possible to vary the functional dependence in space. The location of the open boundaries is naturally governed by physical (and computational) considerations and it may arise a conflict when the available field data at the open boundaries are too irregular. Then it is necessary to locate the boundary where the variations in the field data are more homogeneous and easier to handle.

At the boundaries representing the shore the conditions are no-slip, impermeability, and insulation, except where inflows and outflows occur. Then the horizontal velocities and the temperatures are specified.

NUMERICAL PROCEDURE

Finite-differencing

The basic procedure used to discretize the differential equations is the following: the dependent variables are defined in a grid lattice to fit in the geometry of the particular system modelled; grid cells are defined around each variable in the grid lattice; the differential equation for a particular variable is integrated over the volume of its respective grid cell; and the resulting integrals are evaluated and/or approximated as required to give the difference equations.

This particular procedure for discretization is one of several methods discussed by Varga (1962) and has the advantage that irregular boundaries and non-uniform grids can be easily treated. Another advantage is that if the differential equations to be discretized are written in conservative form, the discretization process preserves the basic conservation properties of the differential equations. For example, by this procedure it is straightforward to derive difference equations that satisfy continuity of mass between cells, even in cases of irregular geometry and non-uniform grids.

It is not always so straightforward to derive the comparable difference equations by the Taylor series method, especially in multi-dimensional problems and for differential equations in fairly complicated form. The rationale for the placement of particular variables in the grid lattice with respect to the other variables depends in part on one's preference but more in part on which arrangement lends itself to better use of the integral evaluations.

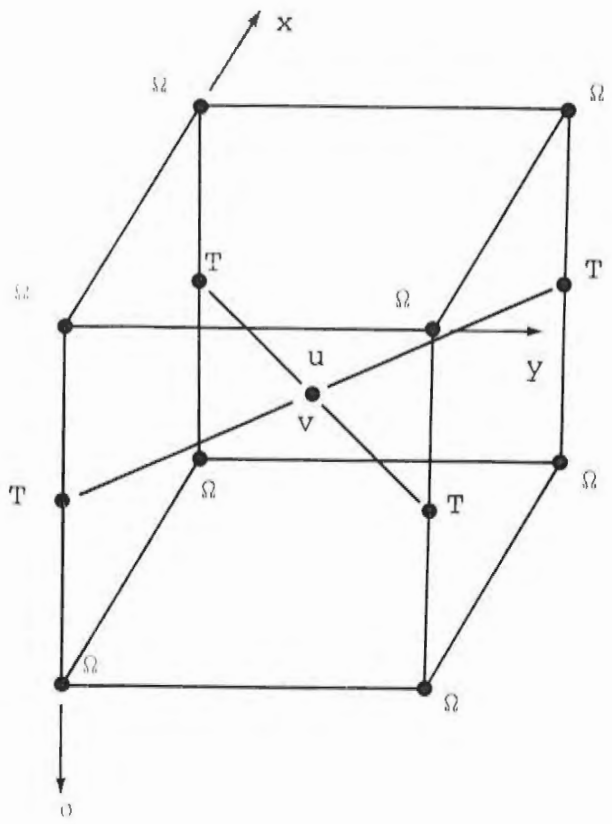

FIGURE 13 Typical nodal cell for u and v in the grid system

A typical grid cell is shown in Figure 13 and it indicates the relative arrangement of the variables in three dimensions.

Once the volume integration has been performed over a particular grid cell and the integrals have been evaluated where possible, the only thing left is the approximation of the remaining terms. Generally, a midpoint integral approximation is used, i.e., for a particular quantity A,

$$\int_{x_o}^{x_o + \Delta x} A dx \simeq \Delta x A(x_o + \frac{\Delta x}{2}). \qquad (6)$$

As often happens, a quantity is evaluated at a particular location where it is not defined. In such a circumstance, a simple average is taken of the neighbouring values. For example, if $A(x_o + \frac{\Delta x}{2})$ is not defined, then the following substituation is used, assuming $A(x_o)$ and $A(x_o + \Delta x)$ are defined:

$$A(x_o + \frac{\Delta x}{2}) = \frac{1}{2} (A(x_o) + A(x_o + \Delta x)).$$

The only problem that one would encounter if the above procedure were carried through is when the grid cell at a boundary is integrated over, for example, in the vicinity of the water surface. Since the surface stress boundary condition is specified, the differential equation has to be approximated at the boundary (the velocity is not specified there). The problem comes up when the midpoint rule is used to evaluate things. A simplified form of the equation that results looks like:

$$\frac{\partial u}{\partial t})_{\sigma = \frac{\Delta\sigma}{4}} - F)_{\sigma = \frac{\Delta\sigma}{4}} = G(\sigma = \frac{\Delta\sigma}{2}) - G(\sigma = 0), \tag{7}$$

where

$$\frac{\partial u}{\partial t} = F + \frac{\partial G}{\partial \sigma}. \tag{8}$$

Note that the terms are located at $\sigma = \frac{\Delta\sigma}{4}$ and are not defined there. Two different procedures could be used to put this equation in terms of only defined locations. They are:

1. Assume the values in the center of the cell are the values at the boundary of the cell, for example,

$$F)_{\sigma = \frac{\Delta\sigma}{4}} = F)_{\sigma=0}.$$

The equation becomes:

$$\frac{\partial u}{\partial t})_{\sigma = 0} - F)_{\sigma = 0} = G(\sigma = \frac{\Delta\sigma}{2}) - G(\sigma = 0). \qquad (9)$$

2. Assume that the values in the center of the cell are obtained from a linear interpolation of the two neighboring values, for example,

$$F)_{\sigma = \frac{\Delta\sigma}{4}} = \left\{\frac{1}{2}\,(F)_{\sigma = 0} + F)_{\sigma = \frac{\Delta\sigma}{2}}\right\}$$

$$= \frac{1}{4}\left\{(3\,F)_{\sigma = 0} + F)_{\sigma = \Delta\sigma}\right\}.$$

The equation reduces to, after manipulation:

$$\frac{\partial u}{\partial t})_{\sigma=0} - F)_{\sigma=0} = \frac{4}{3}\,\frac{G(\sigma = \frac{\Delta\sigma}{2}) - G(\sigma=0)}{\Delta\sigma/2} - \frac{1}{3}\,\frac{G(\sigma = \frac{3\Delta\sigma}{2}) - G(\sigma = \frac{\Delta\sigma}{2})}{\Delta\sigma}. \qquad (10)$$

The first method has the advantage that the resultant matrix equation for the difference equations in the vertical direction is tridiagonal, while the second method gives a matrix which is quidiagonal (two non-zero off-diagonal lines on each side of the diagonal). This point is important because the numerical procedure for the solution of the difference equations involves making the vertical diffusion terms implicit in time, and the additional off-diagonal lines greatly increase the computational time

required for solutions. As a result, the first method has been only employed so far in the model. Some experimentation has been performed with a two-dimensional (one horizontal and one vertical dimension) version of the present model with both methods employed. The differences noted in solutions by the two methods have not been found to be of significance. Strictly speaking, the first method is first-order in the vertical grid spacing while the second method is second-order accurate. One interpretation of the first method could be that the variables solved for in the boundary grid cells are not really located at the boundary, but really one-fourth of the distance between the boundary and the next grid point. This is just a matter of interpretation of where you might say the value is calculated at.

Details of the spatial discretization are presented in Paul and Lick (1980). The expressions have been derived for non-uniform grids in the horizontal directions.

Once the spatial discretizing has been accomplished, the equations have to be discretized with respect to time. Simple procedures have been used for the most part because of the complexities associated with using sophisticated time integration schemes in multi-dimensional problems and because of the enormous computer resources that would be required. A forward time difference is used on the time derivative with most of the remaining terms in the equation evaluated at the previous time. The vertical diffusion terms have been evaluated implicitly and the Coriolis terms have been evaluated both explicitly and implicitly. The reason for the use of implicitness in the diffusion terms is because of the small time step restrictions that

can result when solving the model on a water body that has shallow depths. For example, if the minimum depth is 2 m, and seven grid points are used in the vertical direction, the one-dimensional vertical diffusion time step restriction for a vertical diffusivity of 20 cm^2/sec would be:

$$\Delta t \leq \frac{1}{2} \frac{(\Delta z)^2}{A_V} = 28 \text{ seconds.}$$

This is extremely small time step restriction and severely limits application of the model. By writing these terms implicitly, this time step restriction is completely eliminated from the model. The reason for writing the Coriolis terms the two possible ways is because, in some circumstances, the explicit formulation will lead to numerical instability in the solution. This is because the explicit form of the Coriolis terms is generally unstable (Crowley, 1968). The problem with using the implicit formulation exclusively is that it requires considerable more computational time for a solution compared to when the explicit form can be used. The explicit form is suitable generally when there is sufficient natural damping in the model to overcome the instability associated with the Coriolis terms. This generally occurs when the basin is relatively shallow. If the explicit Coriolis formulation is suitable, then the implicit formulation will only provide insignificant differences in the solution.

Modified SMAC method

The equations as they exist at this point are not in a form that lead to a solution procedure if the rigid-lid condition is to be satisfied. Previous versions of this rigid-lid model used a solution scheme similar to what is called the

marker and cell method (MAC) (Paul and Lick 1973, 1974, 1976). The basics of this method are to take the divergence of the horizontal momentum equations and use the vertically integrated continuity equation and hydrostatic equation. This resulted in a Poisson equation for the surface pressure with a forcing term involving derivatives of the terms in the momentum equations. Included in the forcing term was a correction term (Hirt and Harlow, 1967) to account for the fact that the calculated values for the surface pressure at the previous time step were not necessarily an exact solution to the numerical pressure equation. This condition could result because an iterative scheme had to be used to solve the pressure equation. The previous versions of the model derived the Poisson equation from the differential momentum equations and differenced this resulting equation. Several difficulties resulted from this procedure. First, it was noted that the difference equation for the pressure was not necessarily directly deriveable from the difference equations for the momentum equations. Of course, this is only a numerical error associated with the discretization process; however, it was noted that the error associated itself with the inability of the numerical solution to satisfy the rigid-lid condition to an acceptable degree. In some circumstances, this error was tolerable but in others it led to meaningless solutions. This error had nothing to do with the inability to solve the numerical Poisson equation exactly. In fact, some direct methods were tried and iterative procedures with extremely stringent convergence criteria were used. Neither of these could reduce the vertical velocities at the rigid-lid to sufficiently small values. The values at the rigid-lid could only be reduced by decreasing the time step used in the numerical solution. But by decreasing the numerical time step, the computational time required for a solution became unreasonable. The second difficulty with this method was that the for-

cing term for the Poisson equation was quite complicated and required a lot of computational time just to evaluate it. The third difficulty was that a consistent way to implement time-implicitness on the diffusion terms in the momentum equations was not available. This would have been desireable because of stringent numerical time step restrictions for certain problems. Even if the difference equation for the pressure could be made directly deriveable from the difference equations for the momentum equations in the completely explicit case, there was no reasonable way to do this when the diffusion terms were made implicit. The only way would have been to simultaneously solve the momentum equations and the Poisson equation at each time step, not an efficient procedure.

A procedure is now used to alleviate the difficulties mentioned above. This procedure is a modification to the simplified marker and cell method (SMAC) of Amsden and Harlow (1970). The idea is to separate the velocities into two components: one component satisfies the momentum equations with some prescribed pressure field and the second component is the gradient of some scalar field which when added to first component satisfies the full equations. Amsden and Harlow (1970) developed the method for explicit-time, free-surface, moving boundary problems; the procedure to be described here deals with rigidlid problems with some terms treated implicitly. Work is presently in the process of using the procedure on implicit-time, free-surface problems (Paul and Lick, 1979). Both the vertical terms and the Coriolis terms are treated implicitly. However, the discussion which follows only treats the vertical diffusion terms implicitly. The procedure for treating the Coriolis terms impli-

citly are straightforward and are presented in Paul and Lick (1980). It should be noted that the procedure of Amsden and Harlow (1970) dealt with the differential equations before discretizing them, while the present one deals with the discretized equations directly. This eliminates the difficulties associated with the boundary conditions for the pressure.

Consider the following system of equations:

$$\frac{1}{h}\frac{\partial hu}{\partial x} + \frac{1}{h}\frac{\partial hv}{\partial y} + \frac{\partial \Omega}{\partial \sigma} = 0, \tag{11}$$

$$\frac{\partial u}{\partial t} - \left(\frac{b_o}{h_o}\right)^2 \frac{1}{h^2}\frac{\partial}{\partial \sigma}\gamma\frac{\partial u}{\partial \sigma} = g(u,v,\Omega) - \frac{\partial P_s}{\partial x}, \tag{12}$$

$$\frac{\partial v}{\partial t} - \left(\frac{b_o}{h_o}\right)^2 \frac{1}{h^2}\frac{\partial}{\partial \sigma}\gamma\frac{\partial v}{\partial \sigma} = f(u,v,\Omega) - \frac{\partial P_s}{\partial y}, \tag{13}$$

where

P_s = surface pressure (function of x and y only),

$g(u,v,\Omega)$ = rest of terms in x-equation,

$f(u,v,\Omega)$ = rest of terms in y-equation.

The vertical boundary conditions are:

$$\frac{1}{h}\frac{\partial u}{\partial \sigma}\Big)_{\sigma=0} = \tau_{wx}, \quad \frac{1}{h}\frac{\partial v}{\partial \sigma}\Big)_{\sigma=0} = \tau_{wy}, \text{ at } \sigma=0$$

$$u = v = 0, \text{ at } \sigma=1 .$$

Using the finite-differencing described in the previous section, these equations become in matrix form:

$$\vec{A}\vec{J} = \vec{G} + \vec{U} - \frac{\partial P_s}{\partial x}\vec{I}, \tag{14}$$

$$\vec{A}\vec{v} = \vec{F} + \vec{V} - \frac{\partial Ps}{\partial y}\vec{I}, \qquad (15)$$

where,

$$\vec{u} = \begin{bmatrix} u_1^{L+1} \\ u_2^{L+1} \\ \cdot \\ \cdot \\ \cdot \\ u_J^{L+1} \end{bmatrix} \qquad \vec{v} = \begin{bmatrix} v_1^{L+1} \\ v_2^{L+1} \\ \cdot \\ \cdot \\ \cdot \\ v_J^{L+1} \end{bmatrix}$$

$$\vec{G} = \begin{bmatrix} g_1^{L} - \tau_x \\ g_2^{L} \\ \cdot \\ \cdot \\ \cdot \\ g_J^{L} \end{bmatrix} \qquad \vec{F} = \begin{bmatrix} f_1^{L} - \tau_y \\ f_2^{L} \\ \cdot \\ \cdot \\ \cdot \\ f_J^{L} \end{bmatrix}$$

$$\vec{U} = \frac{1}{\Delta t}\begin{bmatrix} u_1^{L} \\ u_2^{L} \\ \cdot \\ \cdot \\ \cdot \\ u_J^{L} \end{bmatrix} \qquad \vec{V} = \frac{1}{\Delta t}\begin{bmatrix} v_1^{L} \\ v_2^{L} \\ \cdot \\ \cdot \\ \cdot \\ v_J^{L} \end{bmatrix}$$

$$\vec{I} = \begin{bmatrix} 1 \\ 1 \\ \cdot \\ \cdot \\ \cdot \\ 1 \end{bmatrix}$$

$$A = \begin{bmatrix} \alpha_1 - \beta_1 & & & & \\ -\xi_2 & \alpha_2 - \beta_2 & & & \\ & \ddots & \ddots & \ddots & \\ & & -\xi_{J-1} & \alpha_{J-1} & -\beta_{J-1} \\ & & & -\xi_J & \alpha_J \end{bmatrix}$$

and

α_i, β_i, ξ_i = coefficients dependent of differencing and equations at vertical grid i,

u_i^L = u-velocity at time step L and vertical grid i,

g_i^L, f_i^L = discretizations of $g(u,v,\Omega)$ and (u,v,Ω) at time step L and vertical grid i,

τ_x, τ_y = discretized surface boundary conditions at time step L+1,

Δt = time step.

Note that these equations are written for every horizontal grid location (M,N).

Because these equations are linear in $\vec{u}$ and $\vec{v}$, it is possible to do a velocity splitting like

$$\vec{u} = \vec{u}^* + \vec{u}' \tag{16}$$

$$\vec{v} = \vec{v}^* + \vec{v}' \tag{17}$$

where the individual components satisfy

$$A\vec{u}^* = \vec{G} + \vec{V}, \tag{18}$$

$$A\vec{u}' = -\frac{\partial Ps}{\partial x}\vec{I}, \tag{19}$$

$$A\vec{v}^* = \vec{F} + \vec{V}, \tag{20}$$

$$A\vec{v}' = -\frac{\partial Ps}{\partial y}\vec{I}. \tag{21}$$

Formally, the solutions for $\vec{u}'$ and $\vec{v}'$ can be written as:

$$\vec{u}' = -\frac{\partial Ps}{\partial x}\vec{\lambda}, \tag{22}$$

$$\vec{v} = -\frac{\partial Ps}{\partial y}\vec{\lambda}, \tag{23}$$

where $\vec{\lambda}$ satisfies

$$A\vec{\lambda} = \vec{I}. \tag{24}$$

Now, "integrate" the equations for $\vec{u}$ and $\vec{v}$ over the vertical coordinate, i.e., sum them up vertically using the following summation scheme:

$$\sum_{i=1}^{J} \psi_i A_i, \tag{25}$$

where

A_i is the appropriate equation,

and

$$\psi_i = \begin{cases} \frac{\Delta\sigma}{2}, & i = 1. \\ \Delta\sigma, & 1 < i \leq J. \end{cases}$$

The result is

$$\frac{1}{\Delta t}\sum_i \psi_i (u_i^{L+1} - u_i^L) + \phi u_J^{L+1} = -\chi\frac{\partial Ps}{\partial x} + \sum_i \psi_i G_i^L, \tag{26}$$

$$\frac{1}{\Delta t}\sum_i \psi_i (v_i^{L+1} - v_i^L) + \phi v_J^{L+1} = -\chi\frac{\partial Ps}{\partial y} + \sum_i \psi_i F_i^L, \tag{27}$$

where

$$\chi = \frac{J-1/2}{J} = (J-1/2)\cdot\Delta\sigma,$$

$$\phi = \left(\frac{b_o}{h_o}\right)^2 \frac{1}{h^2}\frac{1}{(\Delta\sigma)^2}\gamma_J + 1/2.$$

The above equations are evaluated at each horizontal location (M,N). Next, take the numerical divergence of the above two equations multiplied by the local depth. Using the vertically summed continuity equation and the rigid-lid condition

$$h_{M+1/2,N+1/2}\Omega_{1,M+1/2,N+1/2} = \sum_i \psi_i \frac{hu_{i,M+1,N+1} + hu_{i,M,N+1} - hu_{i,M+1,N} - hu_{i,M,N}}{2\,\Delta x(N+1)}$$

$$+ \sum_i \psi_i \frac{hv_{i,M+1,N+1} + hv_{i,M+1,N} - hv_{i,M,N+1} - hv_{i,M,N}}{2\,\Delta y(M+1)}$$

$$= 0,$$

the result is

$$\tau_{Bx}^{L+1} + \tau_{By}^{L+1} = -\chi \nabla^2 P + \bar{G} + \bar{F}, \tag{29}$$

where

$$\tau_{Bx}^{L+1} = \frac{1}{\Delta x(N+1)} \left[h\phi u_{J-1,M+1,N+1}^{L+1} + h\phi u_{J-1,M,N+1}^{L+1} - h\phi u_{J-1,M+1,N}^{L+1} - h\phi u_{J-1,M,N}^{L+1} \right],$$

$$\tau_{By}^{L+1} = \frac{1}{\Delta y(N+1)} \left[h\phi v_{J-1,M+1,N+1}^{L+1} + h\phi v_{J-1,M+1,N}^{L+1} - h\phi v_{J-1,M,N+1}^{L+1} - h\phi v_{J-1,M,N}^{L+1} \right],$$

$$\nabla^2 P = \frac{1}{\Delta x(N+1)} \left[h \frac{\partial Ps}{\partial x})_{M+1,N+1} + h \frac{\partial Ps}{\partial x})_{M,N+1} - h \frac{\partial Ps}{\partial x})_{M+1,N} - h \frac{\partial Ps}{\partial x})_{M,N} \right] - \frac{1}{\Delta y(M+1)} \left[h \frac{\partial Ps}{\partial y})_{M+1,N+1} + h \frac{\partial Ps}{\partial y})_{M+1,N} - h \frac{\partial Ps}{\partial y})_{M,N+1} - h \frac{\partial Ps}{\partial y})_{M,N} \right],$$

$$\bar{G} = \sum_i \psi_i \frac{hG_{i,M+1,N+1}^{L} + hG_{i,M,N+1}^{L} - hG_{i,M+1,N}^{L} - hG_{i,M,N}^{L}}{\Delta x(N+1)}, \text{ and}$$

$$\bar{F} = \Sigma \psi_i \frac{hF_{i,M+1,N+1}^{L} + hF_{i,M+1,N}^{L} - hF_{i,M,N+1}^{L} - hF_{i,M,N}^{L}}{\Delta y(M+1)}.$$

The corresponding equation in terms of $\vec{u}^*$ and $\vec{v}^*$ can similarly be derived and the result is:

$$-\frac{2}{\Delta t} h\Omega^*_{1,M+1/2,N+1/2} + \tau'_{Bx} + \tau'_{By} = \bar{G} + \bar{F}. \qquad (30)$$

The final equation for the pressure is obtained by subtracting equation (30) from equation (29) and using the solutions for $\vec{u}'$ and $\vec{v}'$ (equations (22) and (23). It is:

$$\frac{2}{\Delta t} h\Omega^*_{1,M+1/2,N+1/2} = \frac{1}{\Delta x(N+1)} \left[(\chi - \phi\lambda_{J-1}) h \frac{\partial Ps}{\partial x})_{M+1,N+1} \right.$$

$$+ (\chi - \phi\lambda_{J-1}) h \frac{\partial Ps}{\partial x})_{M,N+1} - (\chi - \phi\lambda_{J-1}) h \frac{\partial Ps}{\partial x})_{M+1,N}$$

$$\left. - (\chi - \phi\lambda_{J-1}) h \frac{\partial Ps}{\partial x})_{M,N} \right] + \frac{1}{\Delta y(M+1)} \left[(\chi - \phi\lambda_{J-1}) h \frac{\partial Ps}{\partial y})_{M+1,N+1} \right.$$

$$+ (\chi - \phi\lambda_{J-1}) h \frac{\partial Ps}{\partial y})_{M+1,N} - (\chi - \phi\lambda_{J-1}) h \frac{\partial Ps}{\partial y})_{M,N+1}$$

$$\left. - (\chi - \phi\lambda_{J-1}) h \frac{\partial Ps}{\partial y})_{M,N} \right] \qquad (31)$$

The final difference form for this equation is obtained by central differencing the pressure gradients, i.e.,

$$\frac{\partial Ps}{\partial x})_{M,N} = \frac{Ps)_{M+1/2,N+1/2} + Ps)_{M-1/2,N+1/2} - Ps)_{M+1/2,N-1/2} - Ps)_{M-1/2,N-1/2}}{\Delta x(N+1) + \Delta x(N)}$$

and

$$\frac{\partial Ps}{\partial y})_{M,N} = \frac{Ps)_{M+1/2,N+1/2} + Ps)_{M+1/2,N-1/2} - Ps)_{M-1/2,N+1/2} - Ps)_{M-1/2,N-1/2}}{\Delta y(M+1) + \Delta y(M)}.$$

It should be noted that in general the difference equation relates the pressure at one grid location to the eight neighbouring values. Simplifications do result for constant and equal horizontal grid spacings.

The above equation is for the interior region, away from any boundaries. Similar equations can be obtained near boundaries. Paul and Lick (1980) discuss the procedures for this and show how to handle different types of boundary conditions on the velocities.

The modified SMAC solution scheme for the horizontal velocities is the following:

1. Solve for $\vec{u}^*$ and $\vec{v}^*$ from equations (18) and (20).
2. Solve for $\vec{\lambda}$ from equation (24).
3. Calculate Ω^* from the vertically summed continuity equation.
4. Calculate the pressure from equation (31).
5. Calculate $\vec{u}'$ and $\vec{v}'$ from equations (22) and (23).
6. Calculate the new velocities from equations (16) and (17).

The SMAC procedure, as discussed here, has the following advantages over the MAC procedure:

1. It is straight forward to treat terms in the momentum equations as implicit in time.
2. The forcing term for the pressure equation involves only a factor associated with the correction needed for the solution to satisfy the rigid-lid condition.
3. The pressure equation is derived such that the solution at any particular time step is required to satisfy the rigid-lid condition. This is because the pressure is solved for simultaneously with the velocities at each time step. With the MAC procedure, the pressure and velocities are solved independently. As a result, errors in satisfying the rigid-lid condition at a particular time step are not corrected until the next time step.

Solution scheme

The scheme to solve the difference equations through time is as follows:

1. Assume that values for all the variables are available for the previous time.
2. Calculate the temperature.
3. Calculate the density.
4. Calculate the horizontal velocities by the modified SMAC method.
5. Calculate the vertical velocities.
6. The present time step is complete.

The above procedure is repeated until either a steady-state is reached or until the appropriate time is reached. In the modified SMAC method a modified Poisson equation for the pressure has to be solved. Because it was desirable to apply the model to many different kinds of problems, a solution technique that would be generally applicable was used. The successive-over-relaxation (SOR) method is used. Since the solution procedure for the pressure is a separate element in the model, more efficient procedures could be used depending on their availability and applicability to a particular problem.

Infinite mixing of unstable water columns

When the temperatures are calculated, it is sometimes found that heavier water is above lighter water for a particular water column. This situation is handled by checking for static stability over the vertical columns after the temperature is calculated. If static instability is encountered, the unstable column is uniformly mixed. This procedure has been used by Bryan (1969) and in previous

versions of the model. Physically, the length scales associated with the convection cells initiated by vertical instability are much smaller than the grid cells used in the numerical computations. The uniform mixing procedure accounts for this small length scale motion that is not otherwise representable in the model. The static stability check can be modified to a dynamic stability criterion.

PHYSICAL BACKGROUND

KARLSHAMN

Background of the area outside the Karlshamn power plant

The Karlshamn power plant is situated on the south-east coast of Sweden on the peninsula Stärnö in the northern part of the Pukavik Bay (Figure 14). The operation started in 1969 and includes since 1973 three aggregates with totally 1020 MWE. They operate at a constant flow rate of 10.5 m^3/s each and give a temperature increase of 8 - 9°C to the cooling water.

FIGURE 14 Site of the investigated area

The locations of the intake and discharge and the topography of the surrounding area are shown in Figure 15.

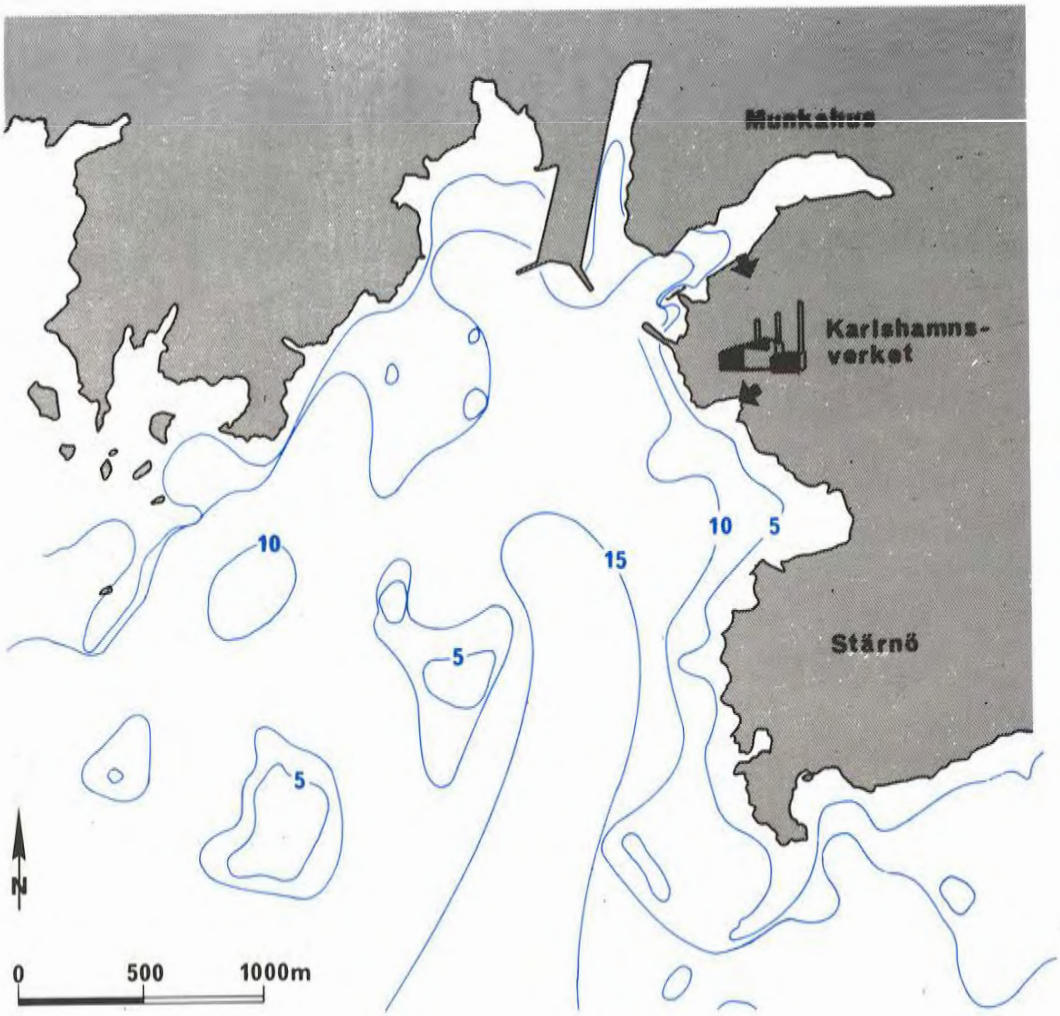

FIGURE 15 Topography

The receiving water is the Baltic Sea, which has a typical salinity of 7.5 - 8.0 °/oo in this area. Due to the absence of important rivers in the neighbourhood neither the horizontal nor the vertical salinity gradients are of importance except in spring when the Mörrum River can produce very weak gradients.

Experimental data

Oceanographical measurements in the area have been made by the SMHI during 1965 - 1976. Figure 16 gives a description

of the main measurements.

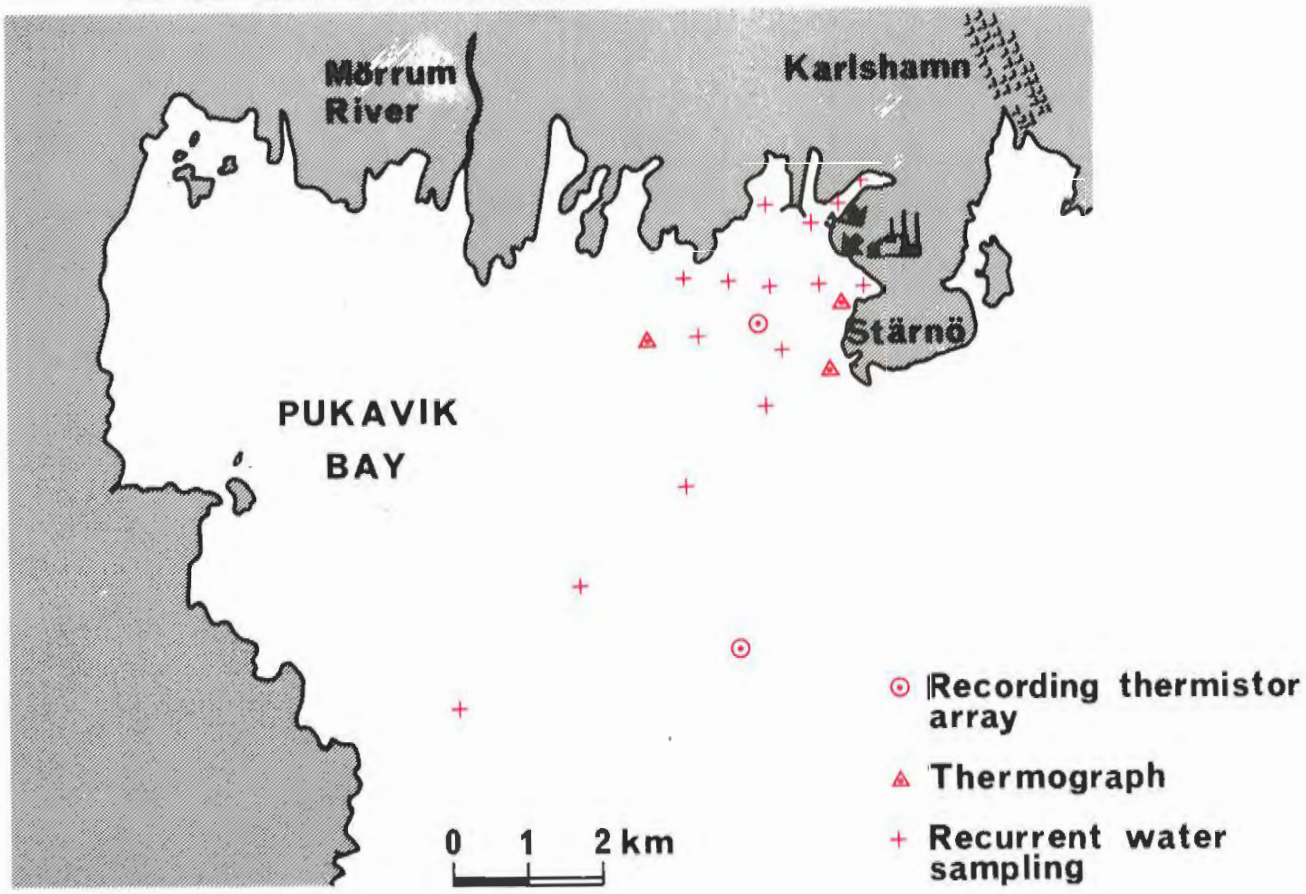

FIGURE 16 Measurements

The main purpose was to give a description of the temperature distribution and variation. The program contained measurements at several stations once a week, thermographs, two automatic termistorchains, type Aanderaa, and several temperature mappings at different depths by automatic registrations from a boat. In order to get an indication of the ventilation and circulation in the area, some additional current measurements were made. Besides that, salinity and turbidity were measured. For a complete description of all the data, see SMHI (1965, 1967, 1968, 1969 a, 1971, 1972, 1974 a, 1977 a, and 1977 b). At the power plant wind was recorded at 25 meter above sea level every half hour.

Circulation patterns

Since the river inflows are small in the Pukavik Bay, the salinity gradient is not strong enough to create a pronounced so called estuarie circulation driven by the density gradient alone. Instead the current is driven mainly by the local wind. This is even more pronounced for the natural conditions in the area outside the power plant. As this bay is only about 2 km times 2 km, the wind fetch is too small to create a fully developed wavefield for wind forces greater than 2 - 3 m/sec except when the wind comes from the south. Therefore, the bay will generally not have as big turbulence as in open sea for a certain wind, and, furthermore, the shores will shelter so that the average stress will be less. The currents are thus rather small. A typical value is 0.8 % of the wind speed, which can be compared to a typical value of 1.5 % when the wind blows from the south.

The wind-driven transport in the surface layer will naturally change the water level some, but will mainly be compensated by a current of opposite direction in the deeper layer.

When the power plant discharges warm-water into the bay, the momentum input will dominate the current field up to some hundreds of meters from the outlet. But even further out where the mixing has decreased the over-temperature to just a few degrees, the plume will modify the currents to a great extent. The created vertical density gradient will damp the vertical momentum exchange, and so more of the energy input by the windstress will stay in the upper layer and therefore give stronger surface currents in the wind direction.

Measured plume behaviour

Without exception all the measured plumes have been strongly wind-dependent. The mapped plumes may be divided into three classes:

1. Wind from SE - SW (Figure 17 a)

   The plume is pressed into the bay, and this creates a recirculation. As the entrainment of pure ambient water is heavily reduced, this recirculation can give an increase of the intake temperature with several degrees.

2. Wind from WSW - N (Figure 17 b)

   The plume is now pressed towards Stärnö. As in the preceding class, the vertical extension may be several meters. The entrainment in the far-field - i.e. from Sandvik and further south - is strongly reduced along Stärnö.

3. Wind from NE - E and weak winds (Figure 17 c)

   The wind is neither deflecting the plume nor reducing the lateral spreading induced by the buoyancy. The plumes are thus wider and shallower.

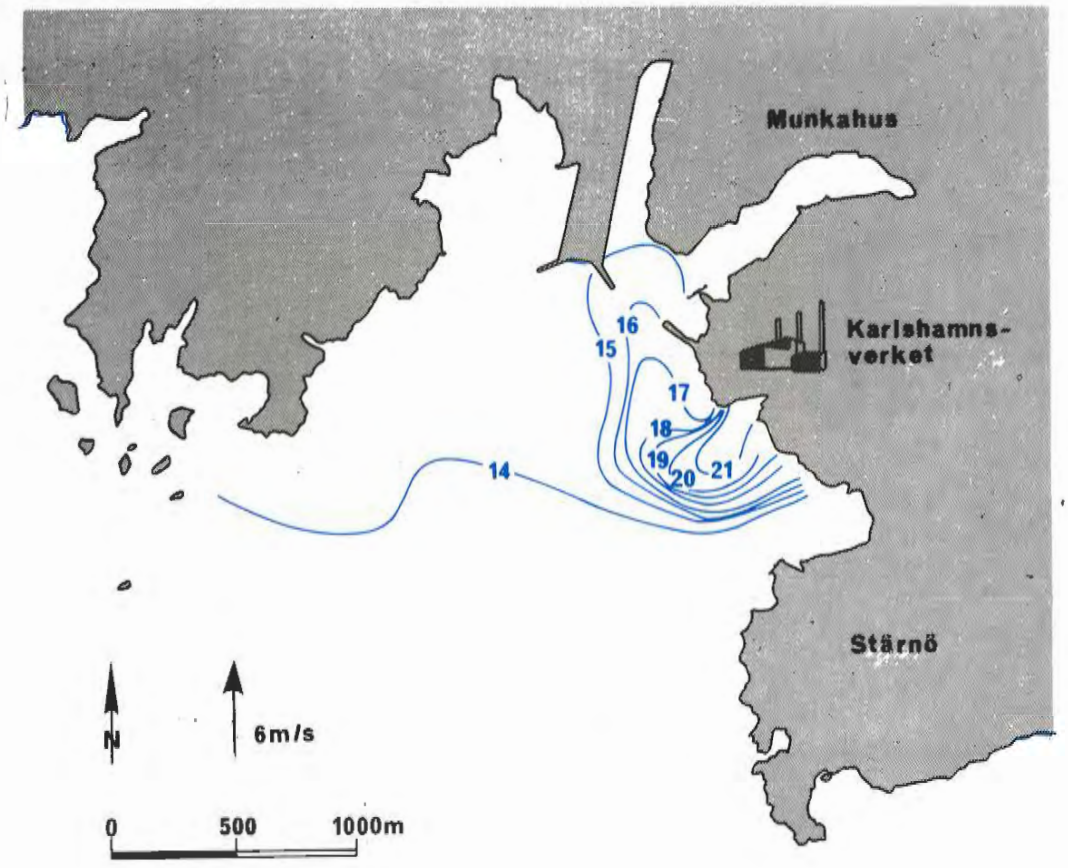

a) Class 1

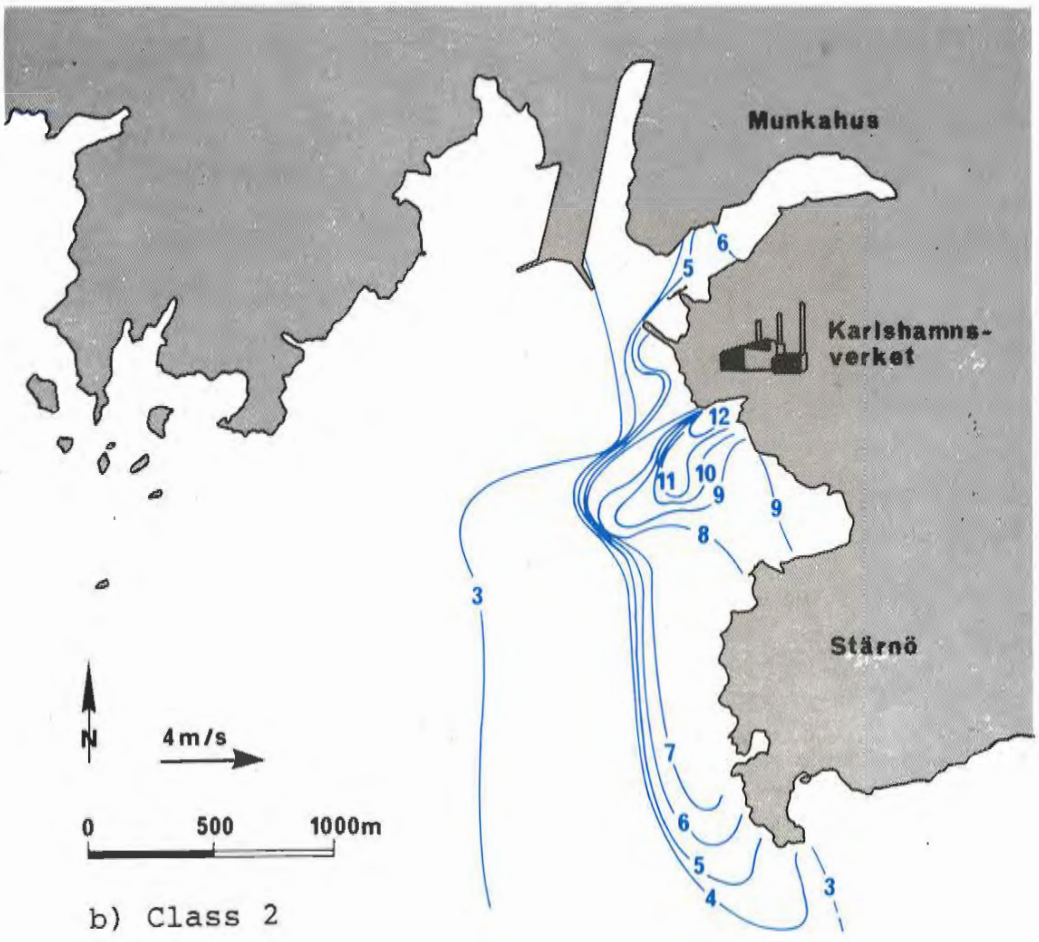

b) Class 2

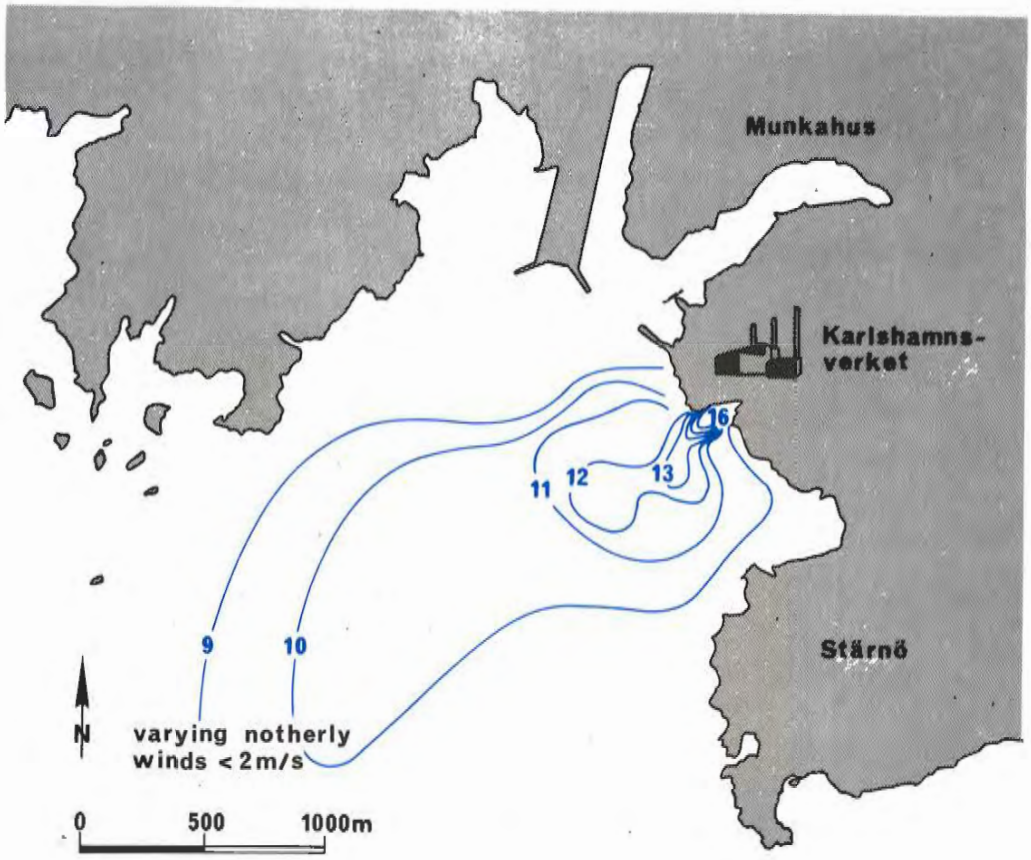

c) Class 3

FIGURE 17 Measured plumes representative for classes 1 - 3 (Figures a - c)

BACKGROUND OF THE RECIPIENT AREA OUTSIDE THE BARSEBÄCK POWER PLANT

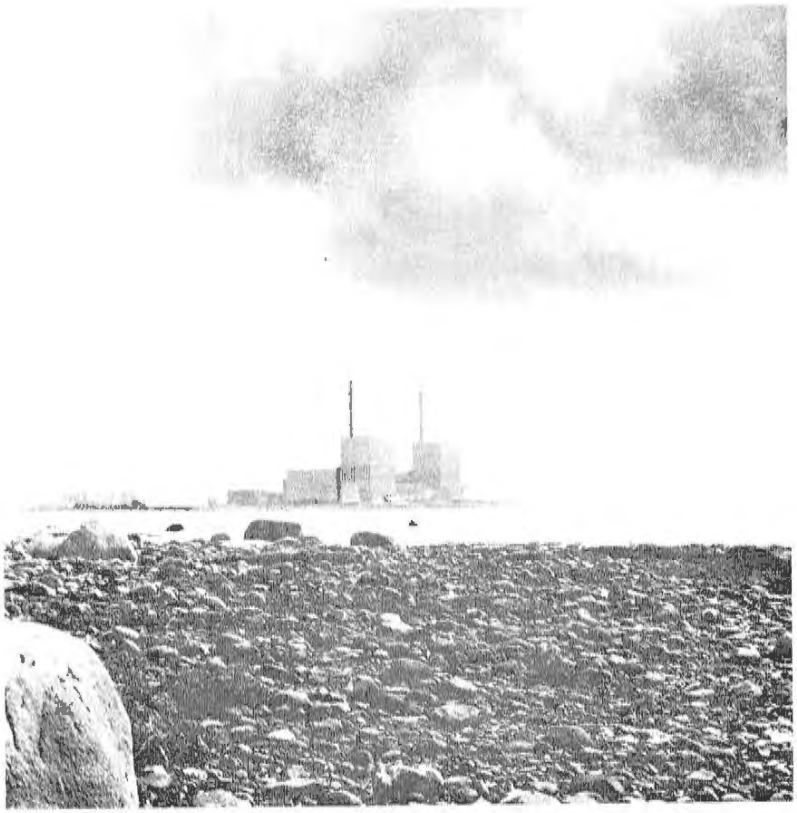

Barsebäck power plant is situated at the eastern side of Öresund, which is one of the major sounds between the Baltic Sea and Kattegat (Figure 18). The two reactors at the plant produce approximately 45 m^3 of heated water per second. The outlet velocity is about 2 m/sec and the inlet water is heated 12 ^{o}C before it enters the recipient.

FIGURE 18 Site of the investigated area

Experimental data

Automatic registration of current and temperature has been performed since 1976. Figure 19 gives a short description of the measurements. Manual observations of salinity and temperature have been made three times a week. Various chemical parameters such as nitrogen, phosphorus, and oxygen plus turbidity have been measured every fortnight.

Detailed mappings of the area exposed by the cooling-water have been made several times every year together with additional measurements of current and salinity. The plume mappings were made with a temperature profiling instrument. At some of these events supporting registrations of the surface temperature have been made with an IR-scanner.

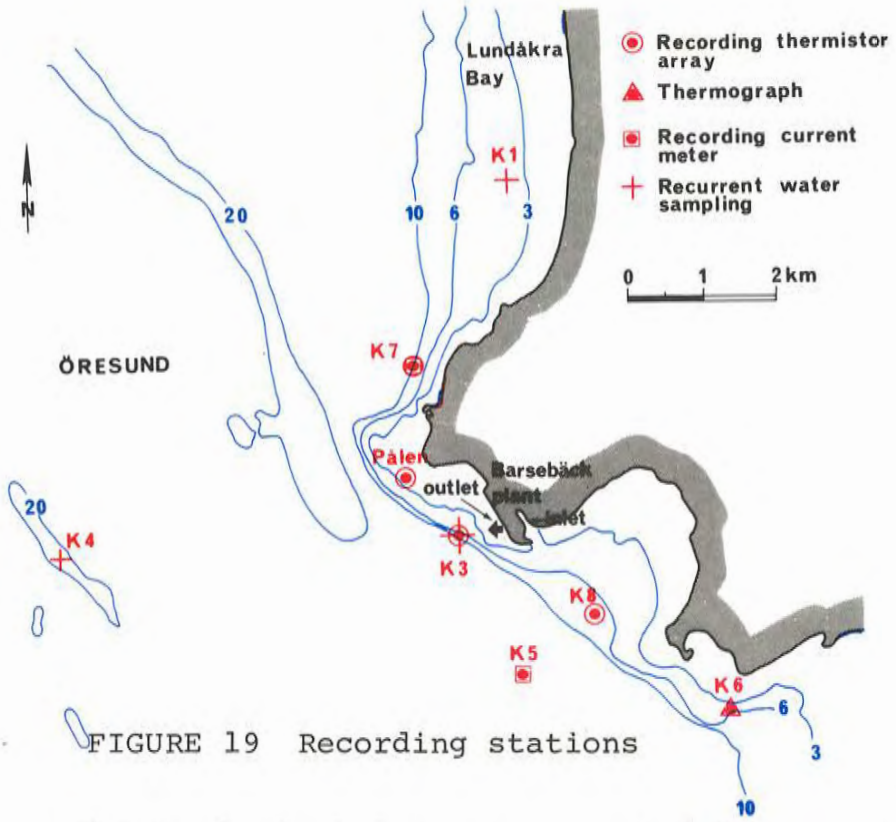

FIGURE 19 Recording stations

Meteorological data were sampled from a mast close to the plant. Wind data from ordinary meteorological stations in the vicinity of the plant have also been used. For a complete description of all the data, see SMHI (1969 b, 1969 c, 1974 b, 1977, 1978, 1979).

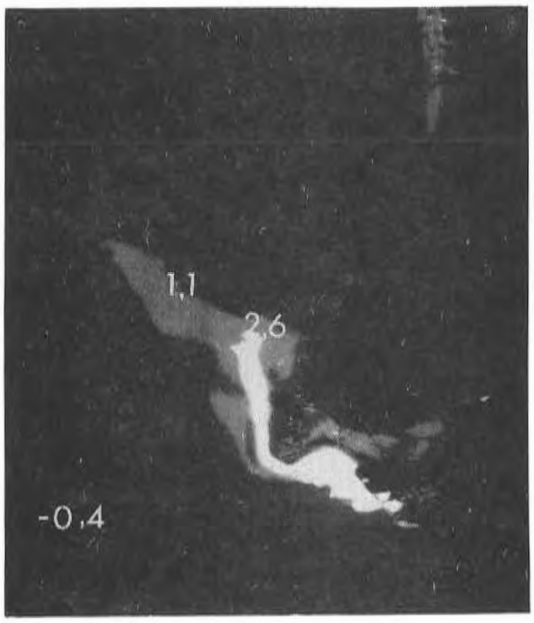

FIGURE 20 Plume mapped with an IR-scanner

Circulation patterns

There is a net outflow of less saltier water from the Baltic Sea through Öresund and further out into the Skagerrak. Baltic water with a salinity of 8 °/oo is then mixed during the outflow with saltier water, gradually increasing the salinity to 20 - 35 °/oo. Except near the southern sill with a maximum depth of 8 m, the currents in Öresund often form a two-layer system with the brackish water floating out above the incoming salty water. This is the dominant current pattern, but during strong westerly winds the whole sound can be filled with a salty south-going water mass. The water level is then raised in Kattegat while it is lowered in the Baltic Sea, thus producing a pressure fall towards south.

The tidal range in the southern Cattegat is only 12 - 15 cm while it is negligible in the Baltic Sea. Tidal currents then seem to have no influence in Öresund. A more detailed description of the flow in Öresund can be found in Dietrich (1951). Model studies have been performed by, e.g., Svensson and Wilmot (1978) and DHI (1977).

As can be seen from Figure 21a, the direction of the current outside the plant lies almost entirely in the interval 270 - 360°. The weakest currents are observed during summer. When averaging over the whole year, the intervals 0 - 20 cm/sec and 20 - 40 cm/sec each accounts for about 45 %.

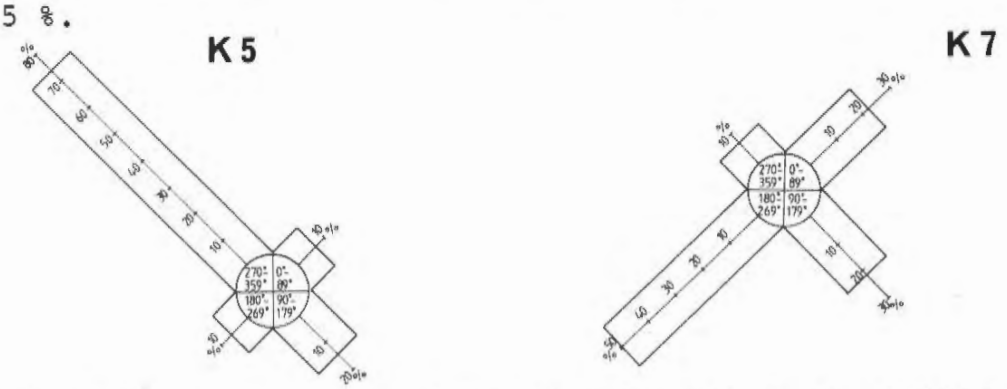

FIGURE 21 Percentage of current direction at stations K 5 and K 7 computed from 1978 data

The continuous recordings of current at the mooring K 7 started in 1978. Here the characteristic direction is south-west, which accounts for 50 % of the registrations (Figure 21 b). The velocity is lower than at K 5, e.g., during July - August almost 80 % can be assigned to the interval 0 - 20 cm/sec. When the general current in Öresund is southwards, the current at both the stations K 5 and K 7 is towards the south. It is more complicated during periods with a north-going current in Öresund. While the direction of the current at K 5 is very stable around 325°, the current at K 7 changes its direction rapidly depending on the extension of the eddy in the Lundåkra Bay. The development and behaviour of this eddy can't be predicted, primarily because the existing hydrographic measurements in the bay are too few. It is, however, believed that even small changes in the direction of the main current in Öresund can radically change the shape of the eddy.

Also the local wind-stress can be important and determine whether the eddy reaches the area influenced by the cooling water or not. It should be noted that it is the most sensitive features of the eddy that have the greatest influence on the plume behaviour. While the north-going current in Öresund can be very steady, the related north-going plumes appear as either a shore-attached type, a clearly eddy-influenced type, or an oscillating type (see Figure 22 a - c). A thorough understanding of the mechanisms which determine the behaviour of the eddy in the Lundåkra Bay therefore seems essential in predicting the north-going plumes.

Measured plume behaviour

The behaviour of the cooling water plume has shown to belong to either five classes (SMHI, 1978). Representative measured plumes are shown in Figure 22 a - e. The first three classes are reserved for different types of north-going plumes. Due to the higher magnitude of the north-going current compared to the south-going one, the north-going plumes are transported a longer distance and cover a larger area.

The behaviour of the plumes is partly determinated by the existence and extension of the eddy in the Lundåkra Bay. The eddy bends the plume offshore (class 2), and when it disappears or is restricted to the northern part of the bay, the plume attaches to the shore (class 1). The north-going plumes have a very unstationary character in contrast to the relative stability of the north-going current. In 94 - 100 % the plumes belong to class 1 or 2 less than 6 hours (SMHI, 1979). Plumes which oscillate between shore and open sea are therefore commonly observed and have been assigned to class 3.

A turning current is connected to a plume which is restricted to an area right west of the outlet (class 4). The mixing is then effective, resulting in a relatively small heated area.

A south-going plume (class 5) also mixes rather effectively, but during strong wersterly winds the plume can be confined in the bay south-east of the plant, resulting in recirculation problems.

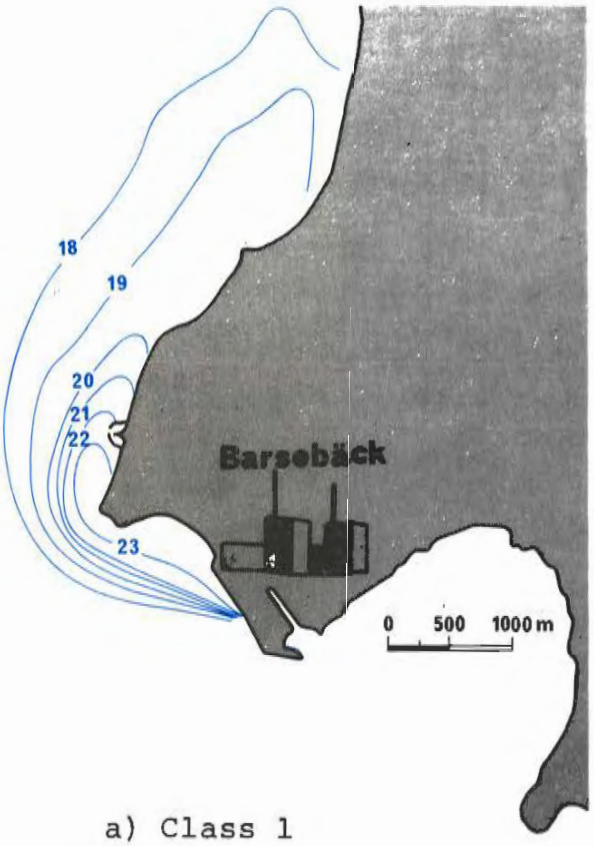

a) Class 1

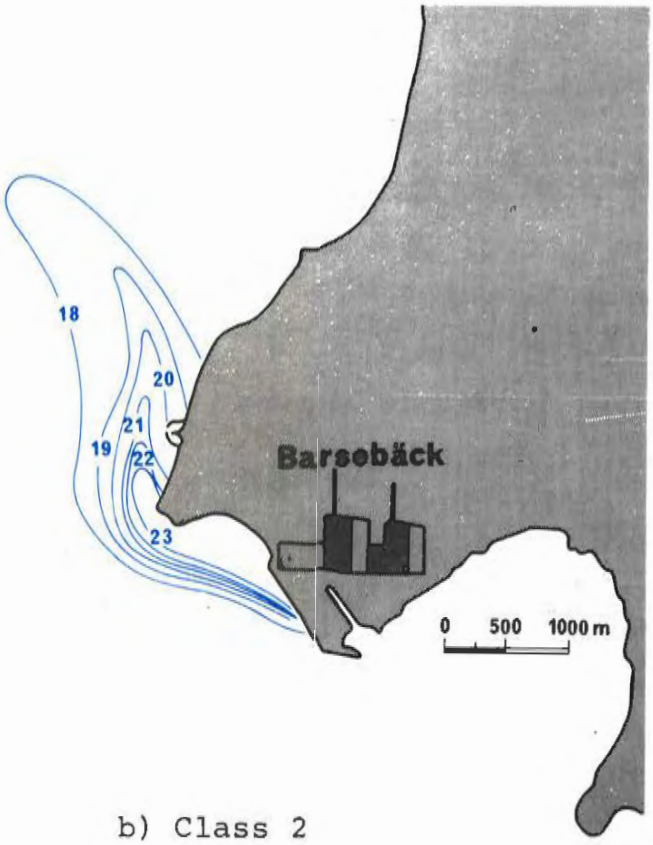

b) Class 2

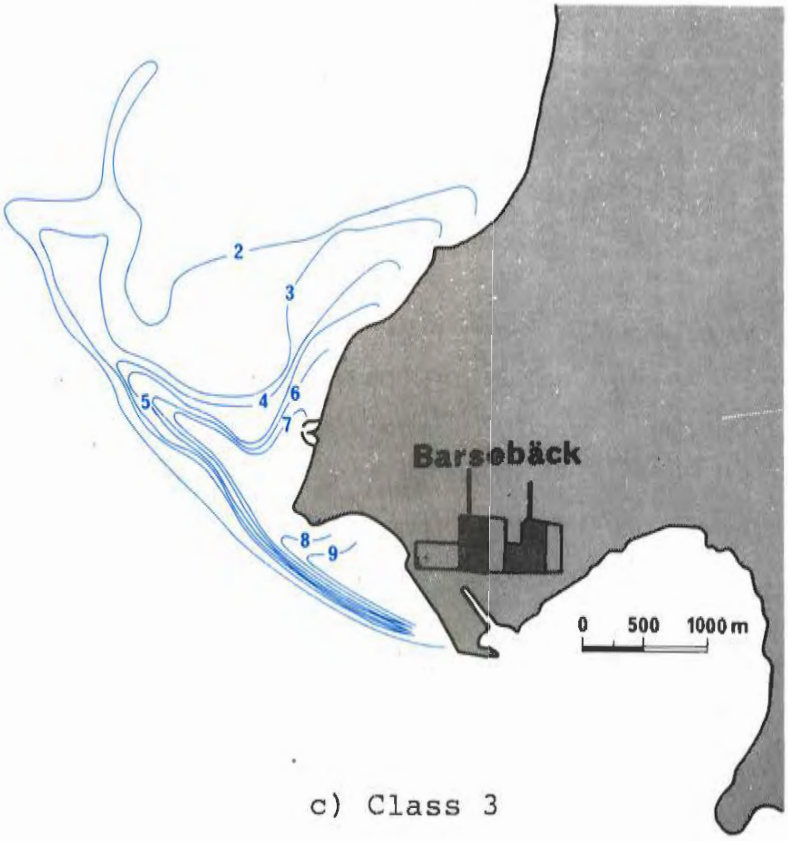

c) Class 3

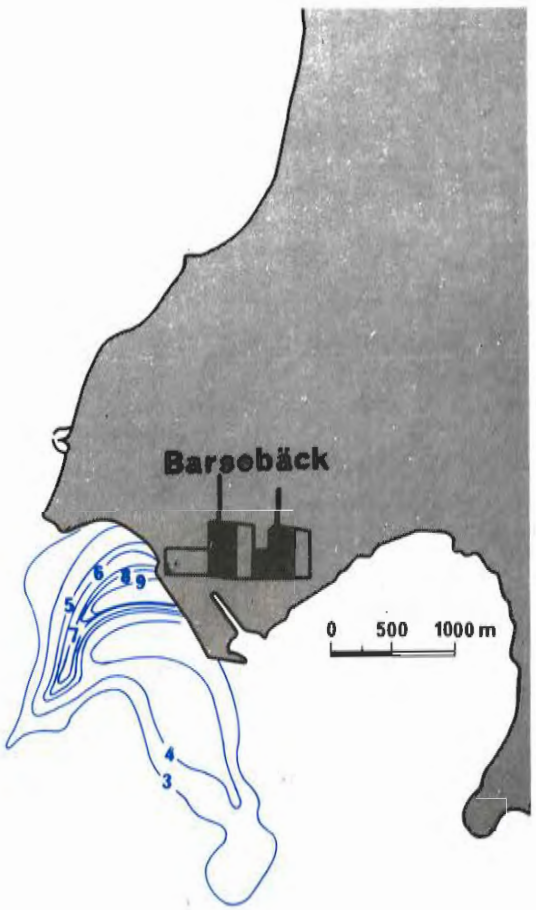

d) Class 4

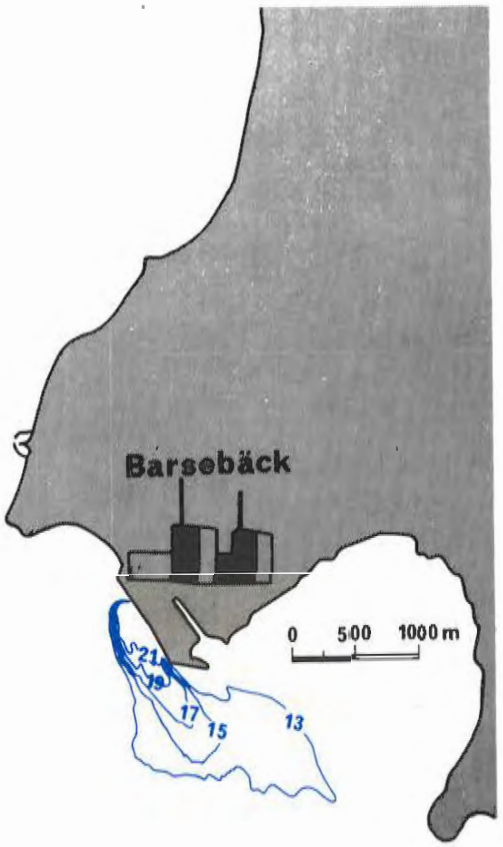

e) Class 5

FIGURE 22 Measured plumes representative for classes 1 - 5 (Figures a - e)

On the average, the area where the temperature of the surface water has been raised at least 0.5 ^{o}C, lies around 3 km^2 for south-going plumes and between 4 and 6 km^2 for north-going plumes. The areas are usually larger during periods with stronger stratification. Usually the plumes do not reach deeper than 2,5 m. It is only during spring and autumn, when the stratification is weaker, that plumes have been observed below 2.5 m.

RESULTS

KARLSHAMN

Introduction

The aim for the calculations of thermal plumes from the Karlshamn power plant was to simulate the dependency of wind on the plume. Data from 2 - 3 September, 1974 were used for comparison. Temperature mappings at the surface and at 1.5 m and 3 m depth were made during those days. An Aanderaa temperature recorder registrated the temperature profile every half hour at station T 2 and a termograph gave a continuous description of the temperature at 4 m depth at station "Fisket" and measurements at the intake were made, see Figure 23.

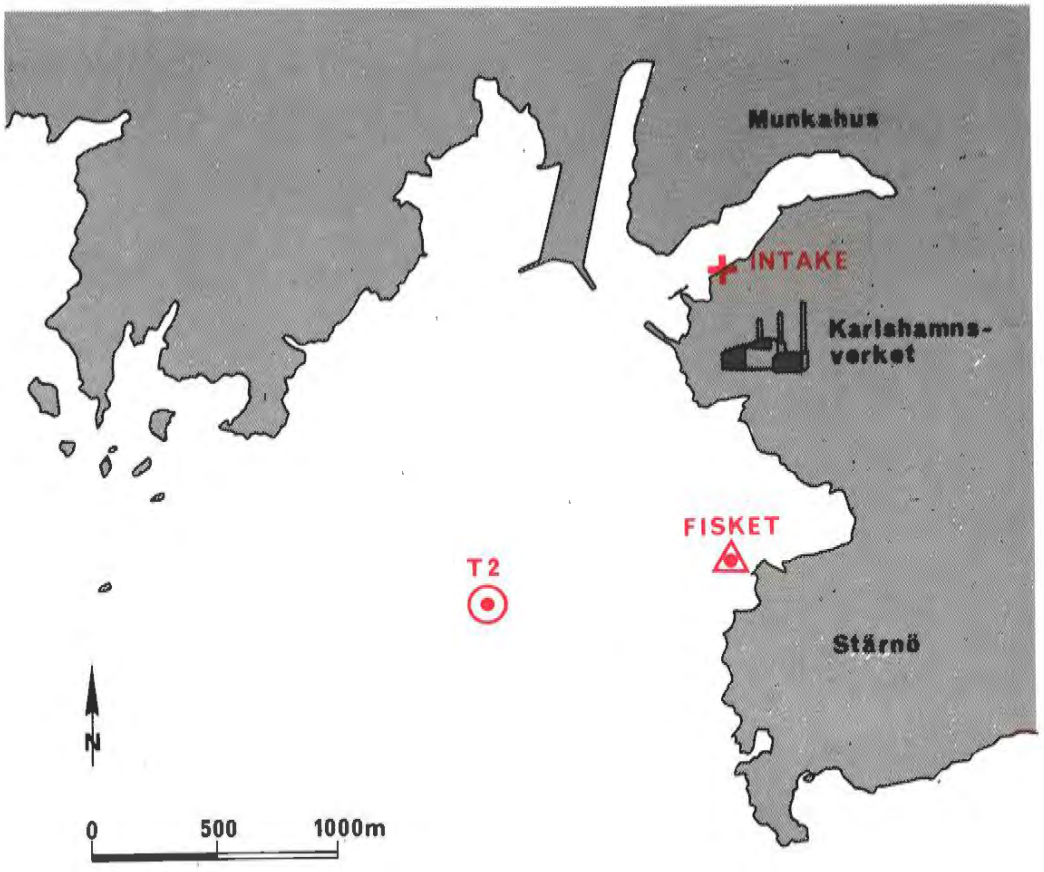

FIGURE 23 Measurements used in the verification study

Modelled area and grid construction

One of the first questions to be answered was how large area must be modelled. The bay, where the warm water is discharged, is extremely dependent on the local wind but not so much influenced by the main circulation in the Pukavik Bay. During the topical days the water level varied only about 10 cm, so disturbances from the main part of the Pukavik Bay could be disregarded. The major mechanisms that creates the circulation in the bay at the power plant will thus be included even if only this bay is modelled and simple boundary conditions, as putting the first normal derivatives of the variables equal to zero, are used. For a given number of grid points this will also give the best resolution in the bay where the most interesting things will occure.

Measurements have shown that the bay sometimes will be almost covered by the plume and somtimes the plume will extend south of Stärnö. In the latter case the greater turbulence in the main part of the Pukavik bay will rapidly mix it into the ambient water, and so the plume just reaches some hundred meters south of the cape. Nevertheless, it may be doubtful if the use of a zero normal derivative is a satisfactory condition for temperature at the open boundary. In our application, however, the plume is mostly pressed into the bay, and so the gradients ought to be rather weak and this boundary condition could be used.

The grid applied to the verification study is shown in Figure 24. A varying grid was used. The shortest distance between two grid points was 50 m and the longest was 250 m. The small grid size was used just outside the outlet where both the temperature and velocity gradients are greatest.

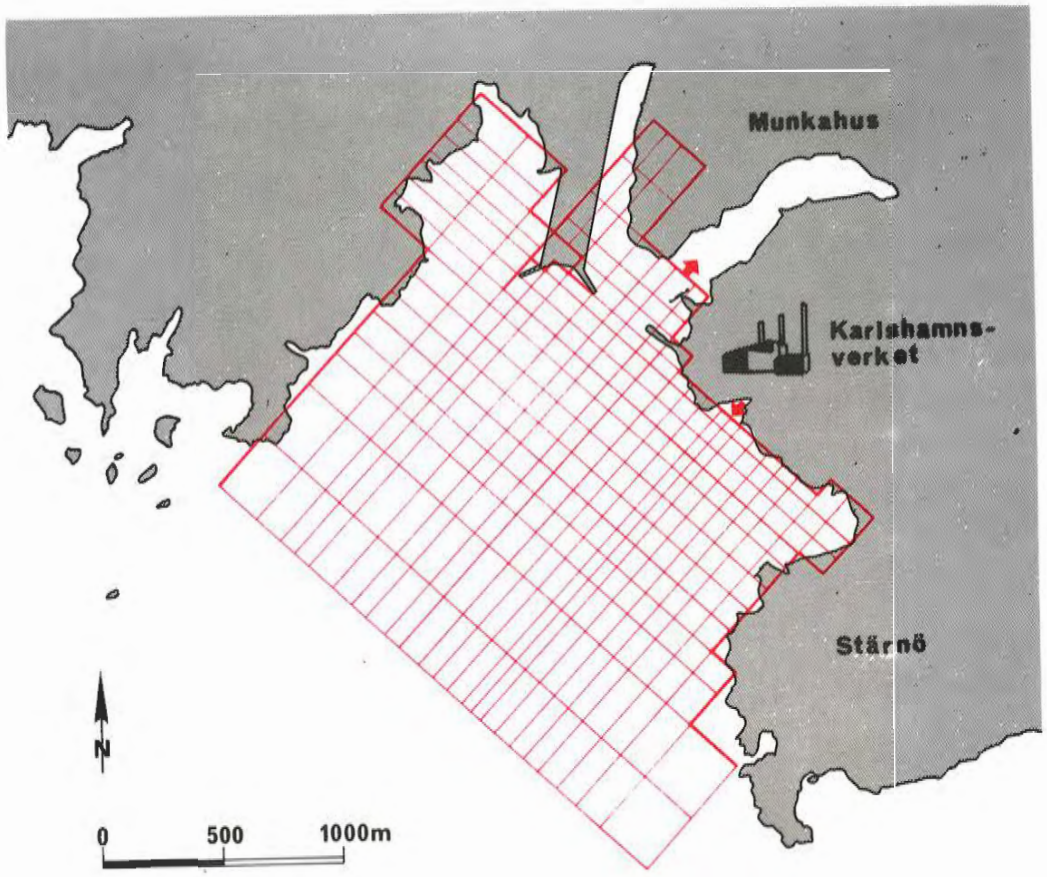

FIGURE 24 The grid applied in the verification study

Yet, this is far from the resolution necessary to get a good description of the near-field and will only give a very crude picture of it. An incorporation of a near-field model from which input data could be taken was planned from the beginning but was not included owing to lack of time.

The outlet is in reality situated in a small bay but has in the calculations been located to the mouth of the bay. The intake is situated in a narrow bay without any rivers entering it. The circulation in this bay is therefore very much influenced by the withdrawal of the cooling-water and will thus not mean anything for the predicitons, neither of the plume outside the bay nor of the recircu-

lation. In the model the intake is then located to the mouth of this bay and the bay is excluded.

None of the bays around the pier were believed to have any influence of importance to the main circulation of the modelled area and this particularly for the narrow bay towards the power plant. On the other hand their volumes and areas could be important for the heat budget. Of computational reasons then, has the bay between the pier and the intake been provided with a schematic structure.

Horizontal extents	2.05 km	x-direction
	2.50 km	y-direction
Minimum depth	1 m	
Maximum depth	19 m	
Number of grid points	18	x-direction
	25	y-direction
	8	z-direction

TABLE 3 Dimensions of the Karlshamn model

Boundary values and input parameters

At the open boundary towards the Pukavik Bay the normal derivatives of current and temperature were assumed to be very small and were set to zero. As mentioned above, it could be argued whether this is a good description of the situation at the boundary, particularly at northerly winds when the plume spreads across it. However, if that is the case, this condition will assure that influenced water reenters the modelled area for some time as the plume is forced inwards the bey again. To allow for unheated water to enter the area underneath the surface layer the temperature below 4 m was set equal to the background value if the current was inwards at that place.

The temperature and current were specified at the outlet, as Figure 25 shows. The temperature profile shown is only an example, as the outlet temperature was changed at each run in order to get a mean value 8.5 ^{o}C above the temperature at the inlet. The profiles have been adjusted so that the heat transport is equal to the actual discharged transport. Only the current was specified at the inlet, as the temperature has to be equal to the calculated temperature just in front of the inlet.

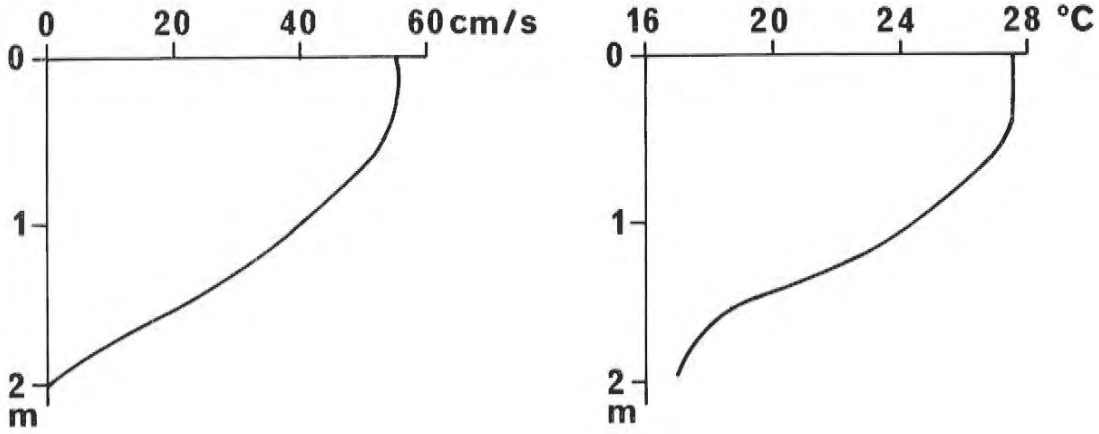

FIGURE 25 Vertical profiles of current and temperature at the outlet

The heat loss to the atmosphere was accounted for in this study. The surface transfer coefficient varies with the wind speed and the values were chosen according to Milanov (1969), see Table 4.

Table 4 shows the used eddy coefficients. As it is a very intricate task to try to simulate both the jet-driven and the wind-driven turbulence, the intention was mainly to give a fairly good description of the turbulence outside the near-field. The values for AVO and BVO represents the conditions in a homogeneous water mass and were put equal.

Equilibrium temperature	17.5 ^{o}C
Salinity	7.5 $^{o}/oo$
Maximum velocity	60 cm/sec
Coriolis parameter	$1.21 \cdot 10^{-4}$ sec^{-1}
Surface heat transfer coefficient	30 - 60 $W/m^2 \cdot {}^{o}C$
Horizontal eddy viscosity	50 000 cm^2/sec
Vertical eddy viscosity	AVO $(1 + 0.5 \frac{\partial \Delta T}{\partial z})$ cm^2/sec
with AVO = 10 - 50 depending on the wind speed	
Horizontal eddy diffusivity	40 000 cm^2/sec
Vertical eddy diffusivity	BVO $(1 + 4 \frac{\partial \Delta T}{\partial z})$ cm^2/sec
with BVO = 10 - 50 depending on the wind speed	

TABLE 4 Input parameter

The observations presented by Sverdrup et al. (1942) were used for the guidance of picking these values. However, at high wind speed AVO and BVO were never set above 50 cm^2/sec as the area is a rather closed bay and the related observations are representative for open oceans. When the wind dies out, earlier created turbulence will still remain to some extent and in order to account for this "old" turbulence values below 10 cm^2/sec were not used.

Computed plumes

At the beginning of the simulation the temperature in the area was set equal to the background temperature, see Figure 26, and the velocity was set to zero. An easterly wind, 4 m/sec, represented the wind conditions on 1 September. This was used during 12 hours model simulations in order to get a plume to start with for the verification study. The achieved plume is shown in Figure 27.

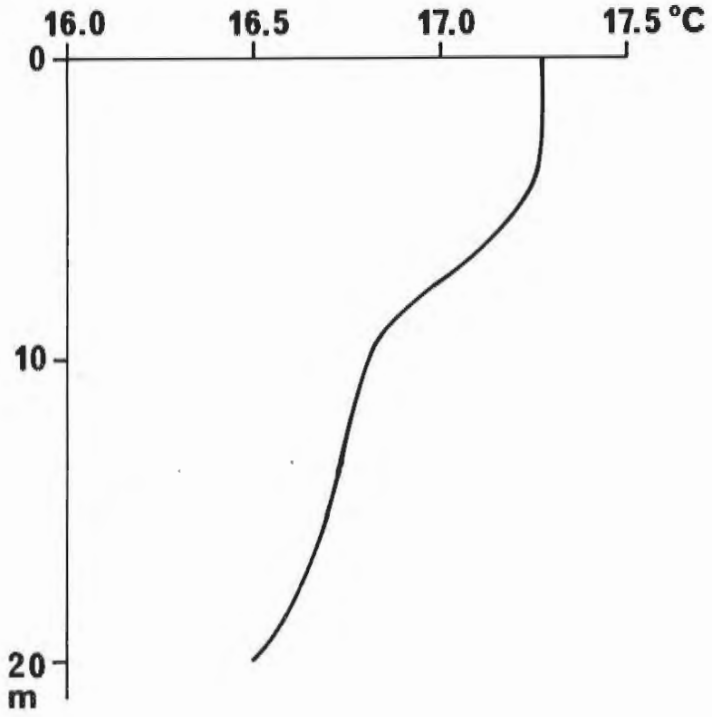

FIGURE 26 Background temperature on 2 September, 1974

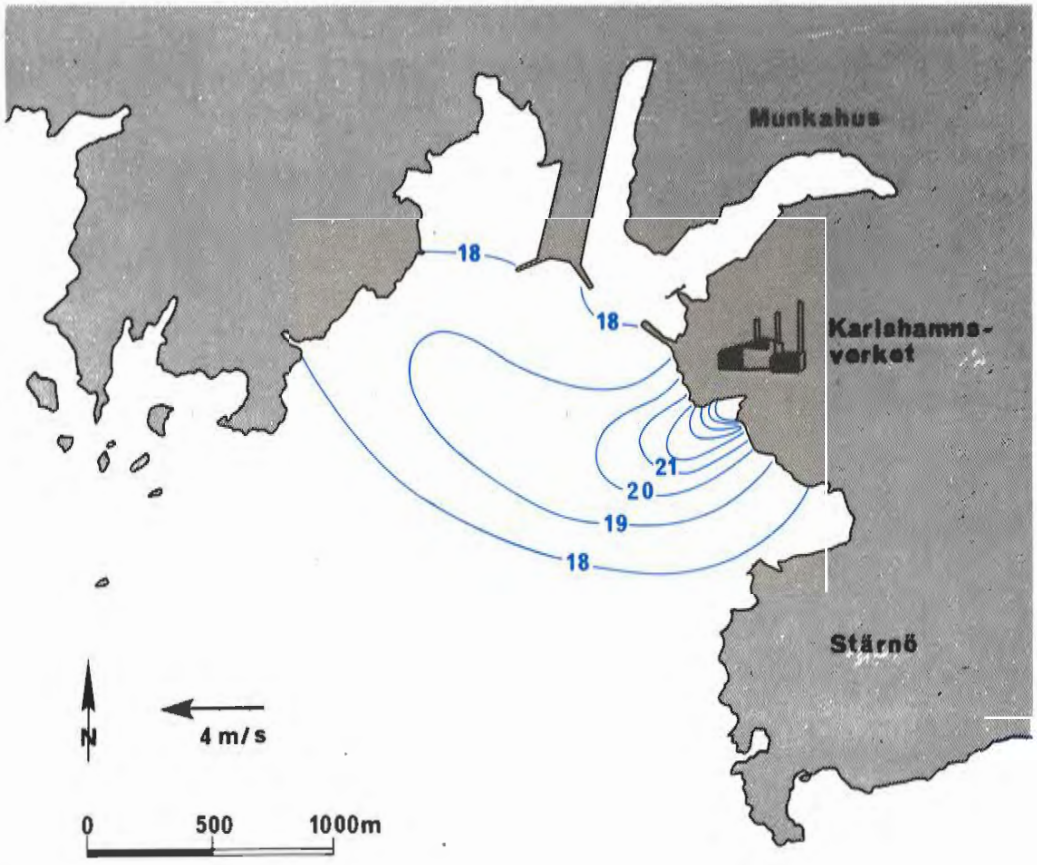

FIGURE 27 Calculated temperature at the surface at 0000, 2 September, 1974. Used as input data to the verification study.

Figure 28 shows the wind conditions measured at the power plant and the values used in the calculations. The observed wind was recorded at 25 m above sealevel and may thus be slightly too great, as the formula used for the windstress was based on wind conditions at 10 m. However, simultaneous observations have shown that the difference was rather small particulary at low wind speeds, why no corrections have been applied.

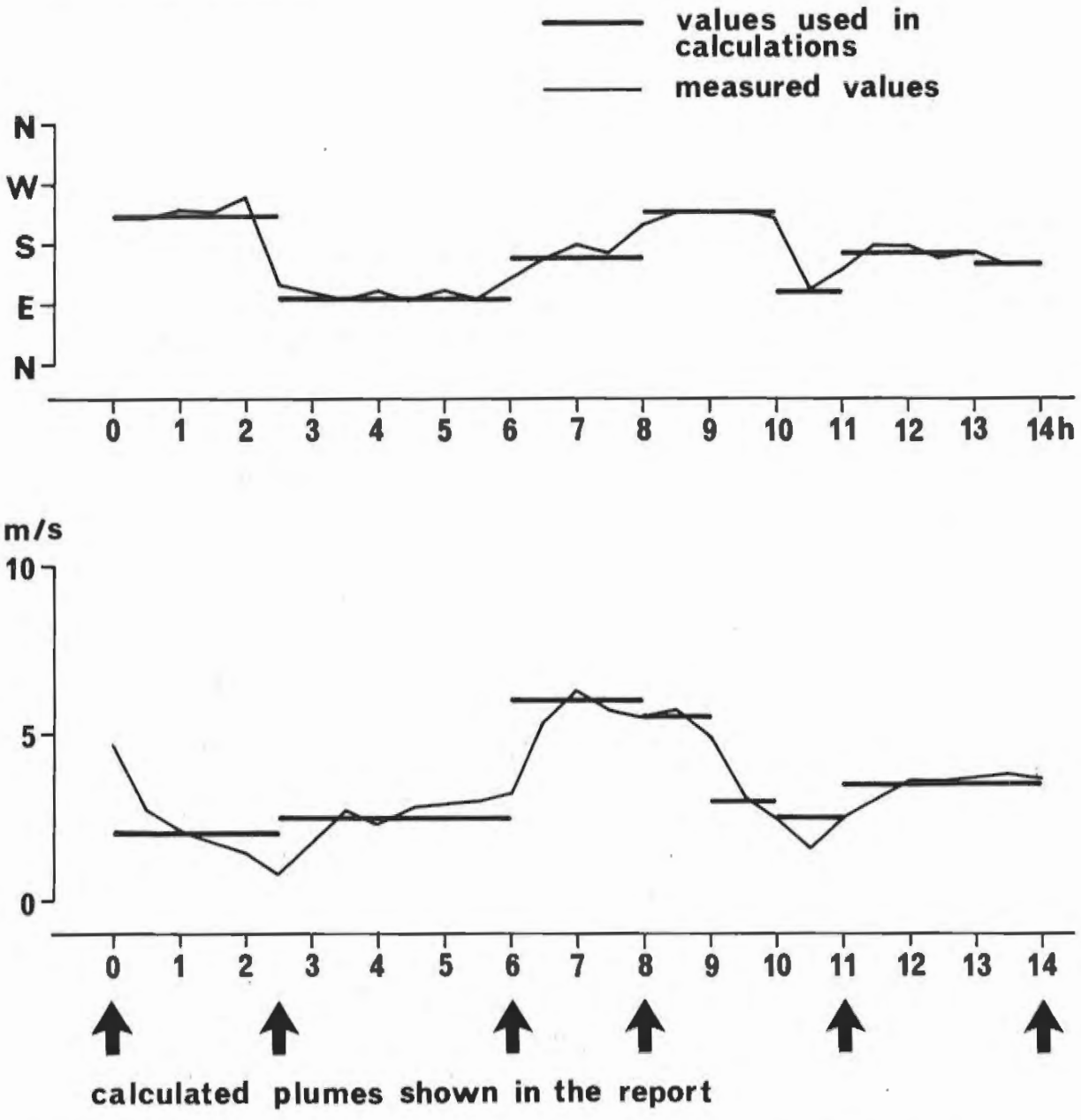

Figure 28. Wind on 2 September, 1974. Measured values and values used in the calculations.

As is evident in Figure 28, constant values for both the wind speed and the direction have been used as representing the wind conditions at periods in the range of 1 - 3.5 hours. It should be noticed that it is possible to change wind speed and direction at each time step in the model in order to obtain a more precise description. In these verifications we did not think this was necessary, as we believed this would only give marginal effects.

At the beginning of 2 September the wind direction was just opposite the direction of the discharged water. Even though the wind speed was rather low the plume was forced into the bay. As the wind stress works against the jet momentum and thus acts to neutralize it, the distribution of the surface temperature was almost concentrical, as if the Froude number was near 1 and the buoyancy was the dominating mechanism.

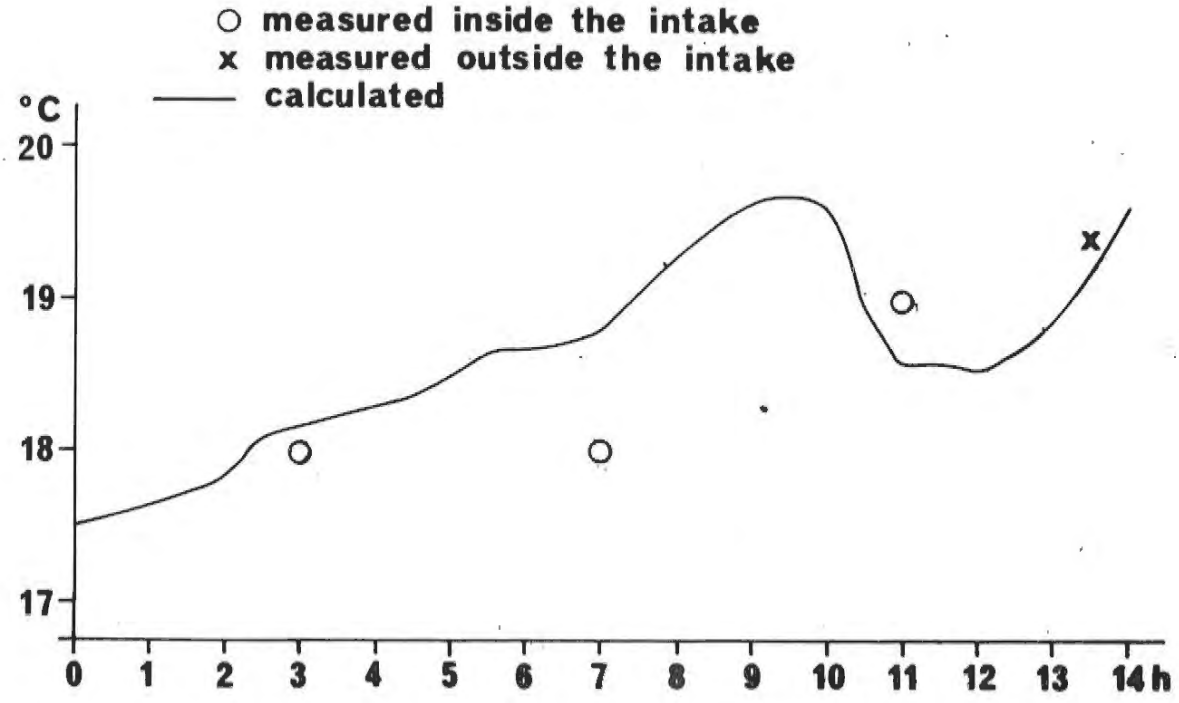

FIGURE 29 Temperature of the intake water, measured and calculated, on 2 September, 1974

Winds with directions between ESE and SW will press the plume inwards the bay. The intake is situated at the innermost part of the bay, and those wind conditions will therefore create a recirculation of the cooling water. This is seen in Figure 30 and also in Figure 29, which describes the calculated development of the water temperature at the intake. These calculations are compared with the available measurements. Unfortunately, the data marked with circles in the figure are very crude and give only an indication of the temperatures.

All measurements, perhaps with one exception, verified that the computed intake temperature was of the right magnitude. Based on experience, this temperature behaviour was what one could expect during the prevailing wind conditions.

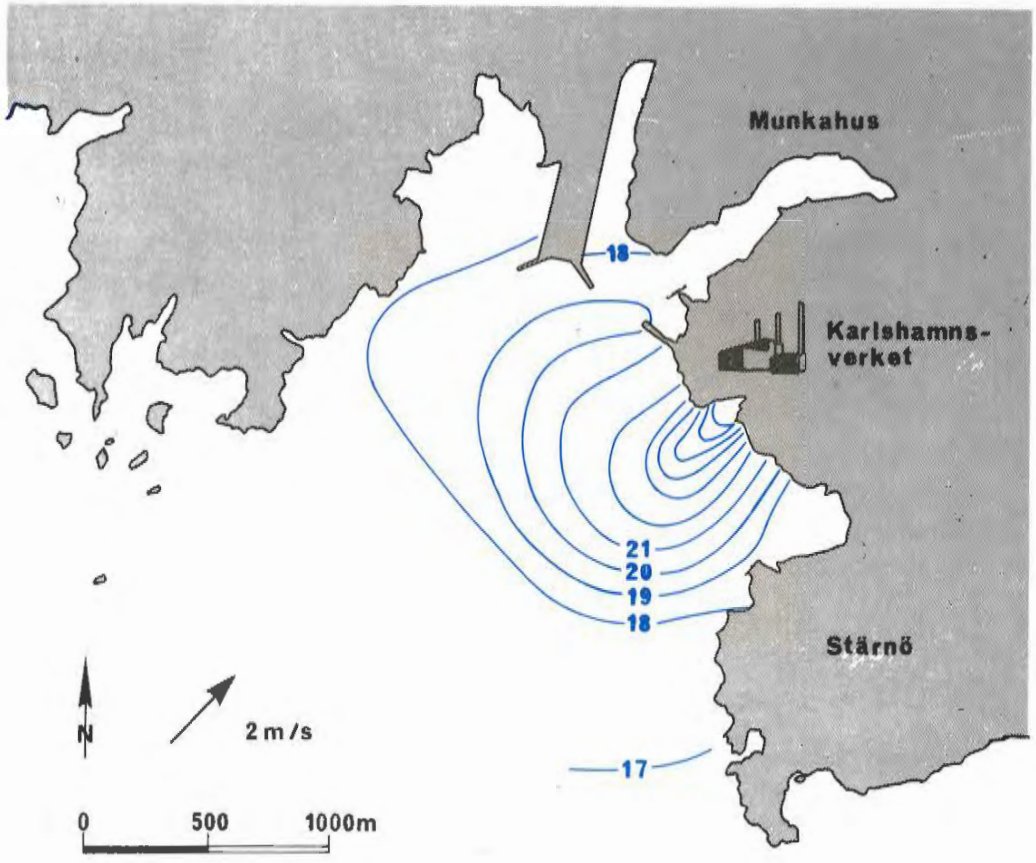

FIGURE 30 Calculated temperature at the surface at 0230, 2 September, 1974

When the wind changed into an easterly direction, it also altered the direction of the plume and dragged it across the bay. The bay was cut off by the plume, and so the withdrawal of cooling water towards the intake assured that the recirculation was maintained.

Figure 31 shows that the areas with temperatures of 20 °C and less had increased and the plume covered almost the whole bay.

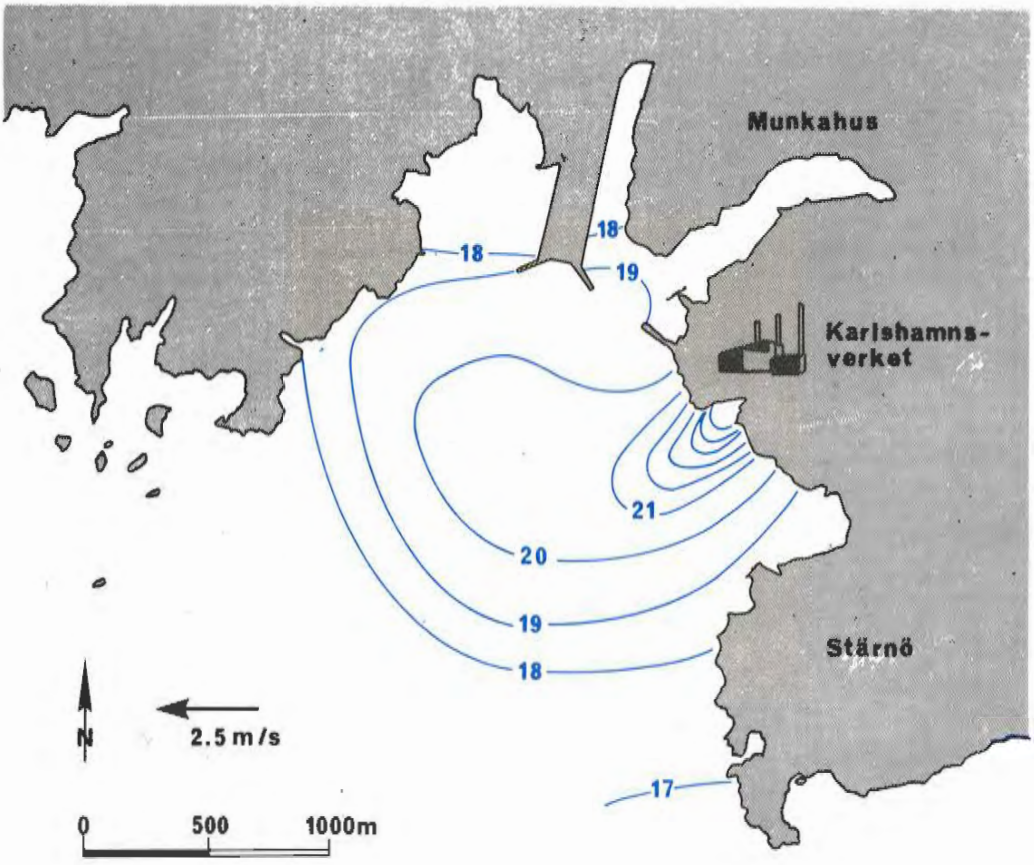

FIGURE 31 Calculated temperature at the surface at 0600, 2 September, 1974

Two hours later the plume had drawn back into the bay forced by a moderate wind from the south-east. The recirculation increased further and the temperature was about 2 °C above the background value. Not only the surface drag was increased by the wind. It also increased the

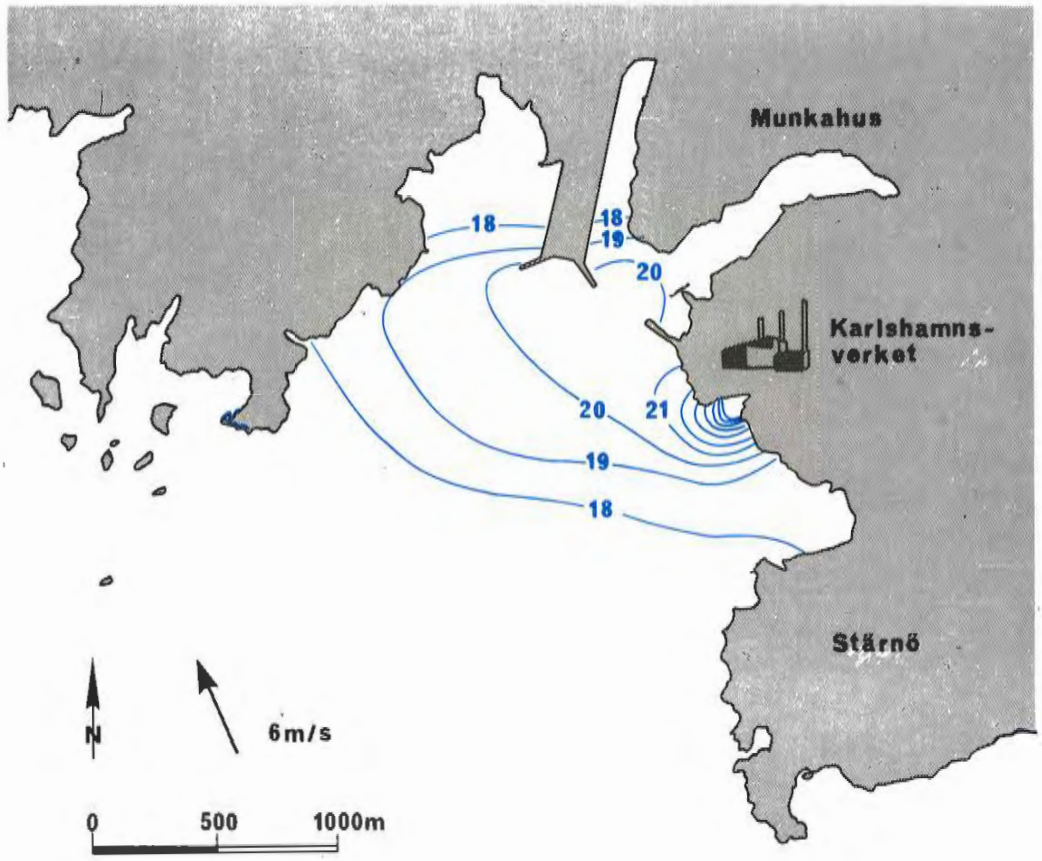

FIGURE 32 Calculated temperature at the surface at 0800, 2 September, 1974

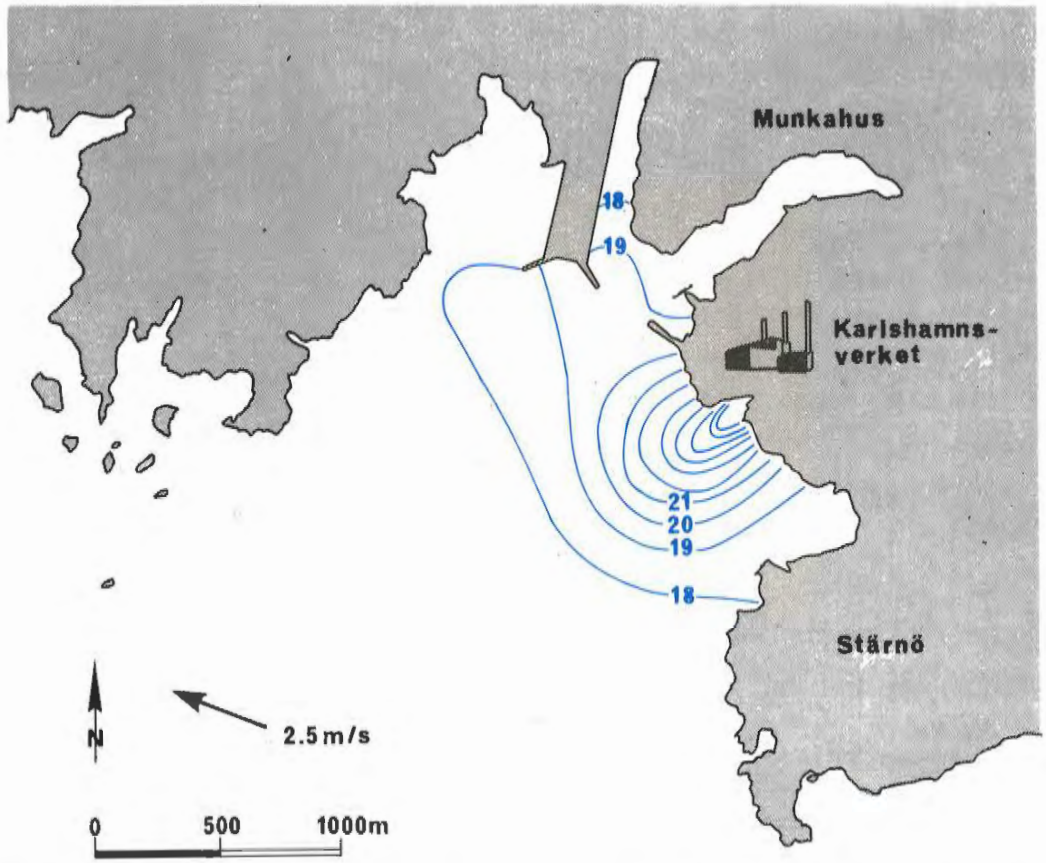

FIGURE 33 Calculated temperature at the surface at 1100, 2 September, 1974

turbulence, and therefore the cooling water was both forced and mixed deeper down. In Figure 32 the temperature areas are thus smaller than before. In the meantime the diffuse heat transport to the deeper layers increased. This is seen in Figure 35 at 10.5 m both in the measured and in the calculated values. As the observations were far out from the outlet, this temperature increase was delayed and started at about 0830.

The wind continued to blow one more hour with unchanged magnitude but turned to the south-west. The result was an even more suppressed plume, and the intake temperature reached its highest value by that time.

Figure 33 shows the calculated surface temperatures two hours later when the wind has fallen. The heavy turbulence and the great windstress created by the former strong winds had reduced the plume area considerably, but as lighter winds started to blow, the plume began to spread again in a thinner layer with the outlet as starting-point.

During the last hours before and at the temperature mapping the wind was rather stable, SE 3 - 4 m/sec. The altered wind direction increased the recirculation over again, as seen in Figure 29. The plume was not held back very effectively, and it covered most of the bay (see Figure 34).

The measured plume showed the same general behaviour. However, there were some smaller differences. The measured plume was somewhat further out. This is probably due to the fact that it was difficult to describe the local winds correctly. Another distinction was that the areas for temperatures between 21 and 24 ^{o}C were greater than in the prediction. Most likely this could be remedied by a better description of the turbulence and the near-field.

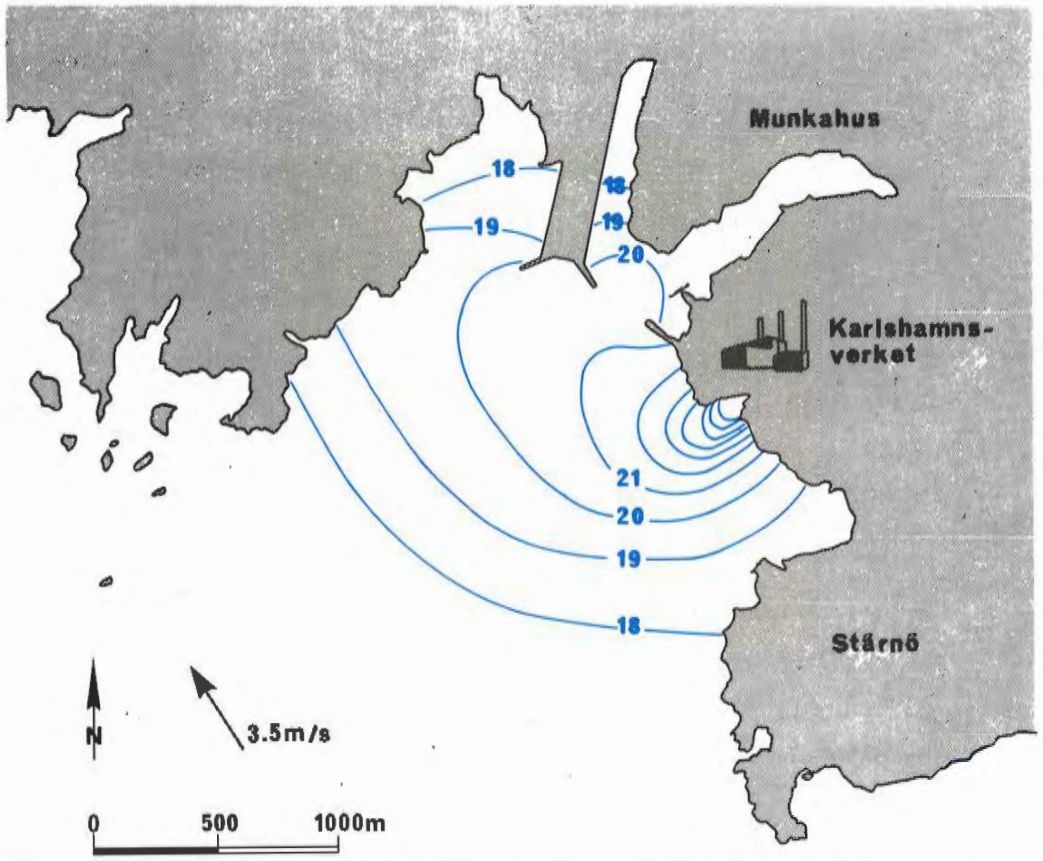

FIGURE 34 A Calculated temperature at the surface at 1400, 2 September, 1974

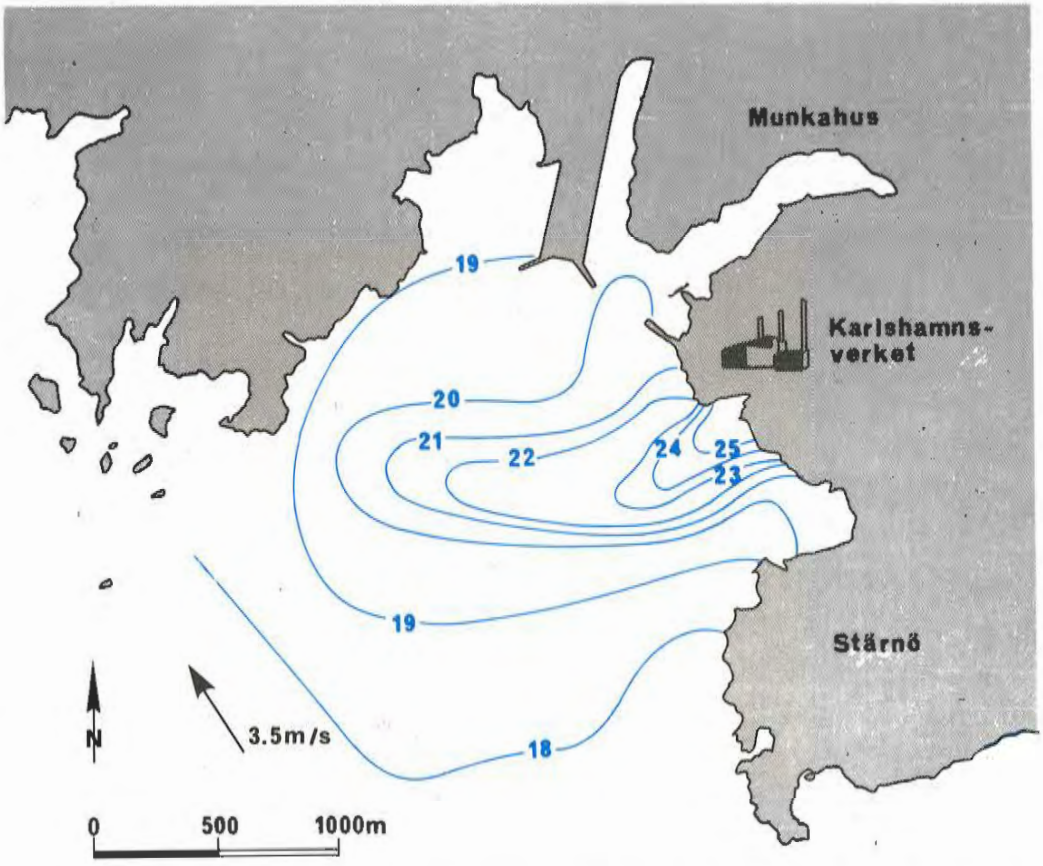

FIGURE 34 B Measured temperature at the surface at 1300 - - 1620, 2 September, 1974

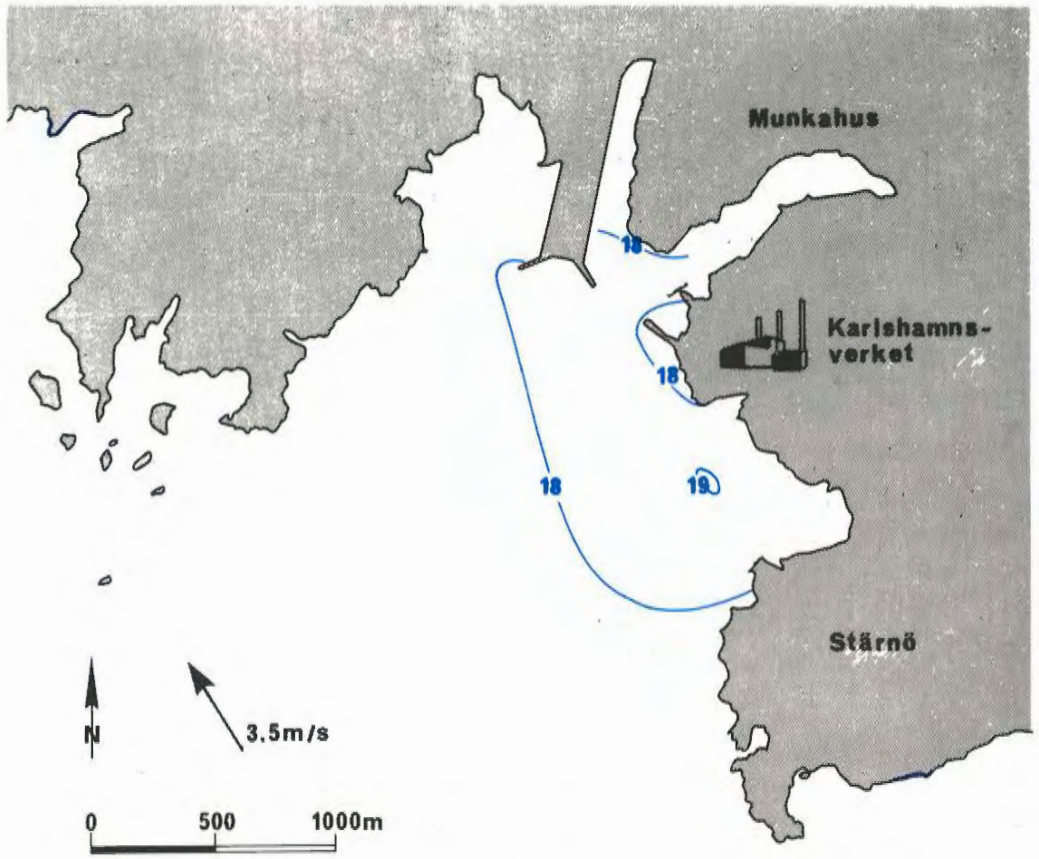

FIGURE 34 C Calculated temperature at 3 m at 1400, 2 September, 1974

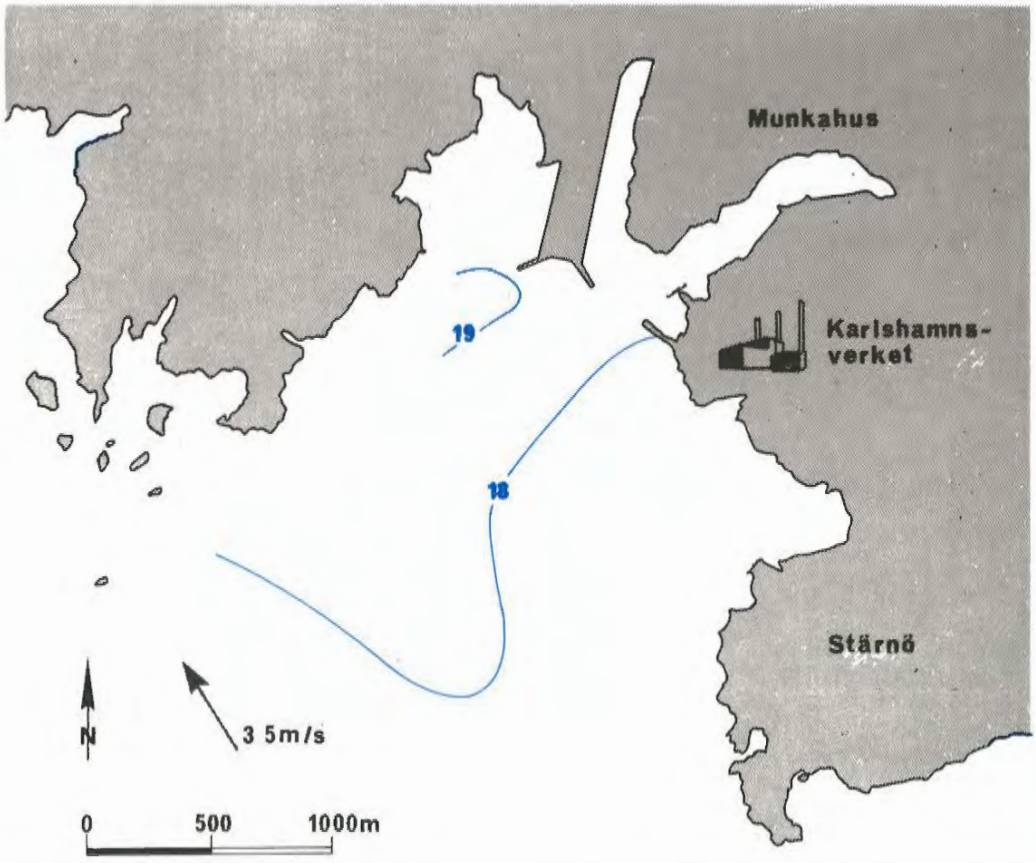

FIGURE 34 D Measured temperature at 3 m at 1300 - 1620, 2 September, 1974

In this verification study the near-field was treated very crude due to lack of time. The original intention was to use an integral model in order to make a more sophisticated description of the near-field and to use this as input to the far-field study. Instead of this technique the grid points were put closer to each other just outside the outlet in order ot be able to handle the great gradients. However, as the computer resources were limited, the grid could not be dense enough. Besides the numerical dispersion that was rather harmless, this course grid made the plume dive too much.

The depth increased rapidly just outside the outlet, and so the difference in depth between two grid points was great. So the plume was forced along the slope of the grid lines far down before the next grid point was reached and the buoyancy could have been felt again. This effect could have been avoided with a denser grid.

A comparison between Figure 34 C and D shows that too much heat was transported downwards in the near-field and the transition zone in the prediction. This is also shown in the diagram in Figure 35 for the temperature at 10.5 m depth at T 2, where the exaggerated diving and a somewhat overestimated turbulence in the lower layer caused a too high calculated temperature compared to the measurements. In reality the heated water was instead transported in the uppermost surface layer to the opposite shore where it was forced to dive.

Apart from this slightly overestimated diffusive transport of heat underneath the plume, the diagrams in Figure 35 show a good agreement between the measured and calculated temperature variations. At the beginning of the verification the plume was evidently not enough developed and/or

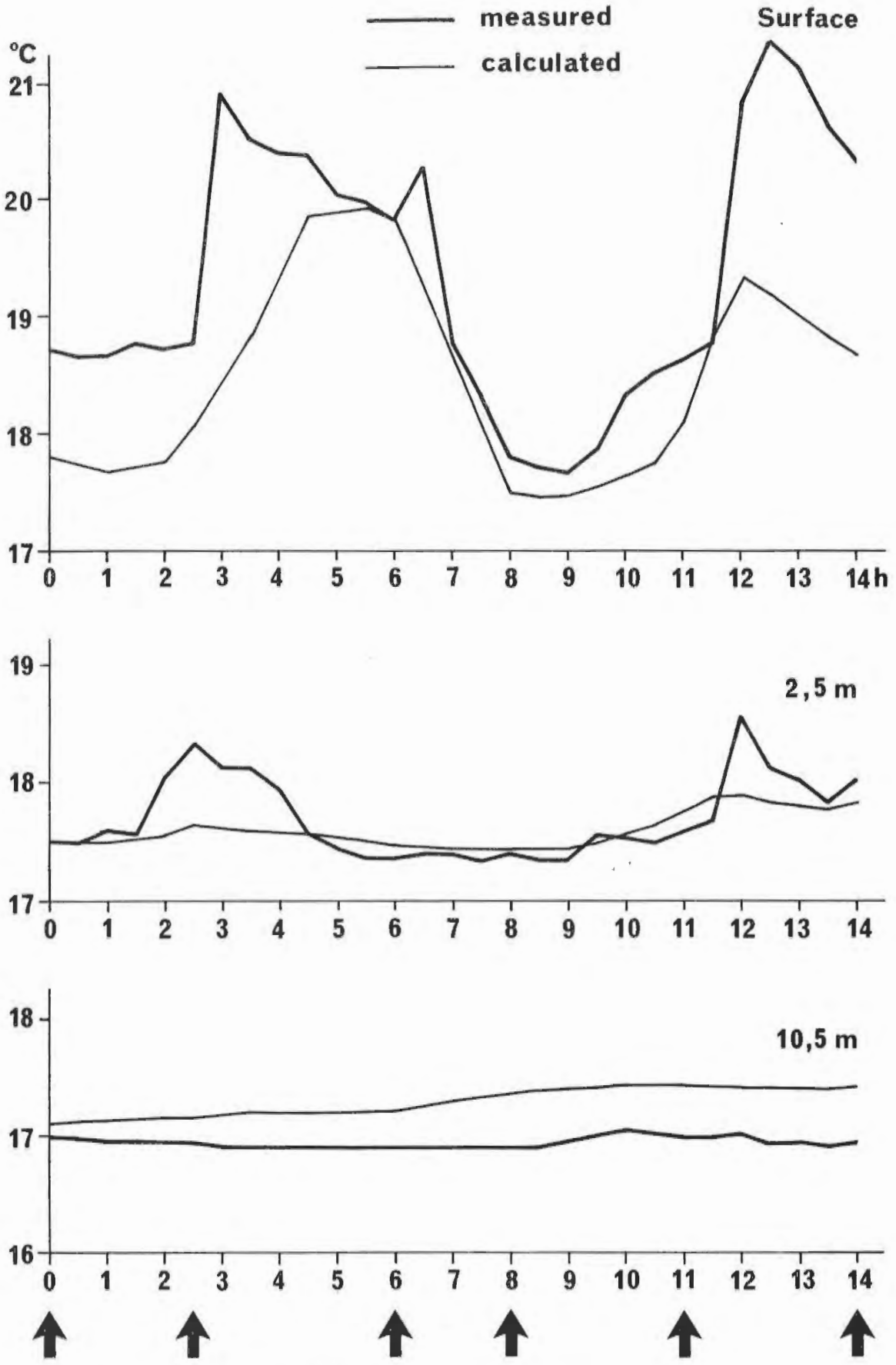

calculated plumes shown in the report

FIGURE 35 Temperature at T 2 on 2 September, 1974

had a slightly wrong direction, as the calculated temperature at the surface in T 2 was about 1 ^{o}C below the measured value. Disregarding this, the diagram shows that the temperature increase started at the right moment.

Two hours later this divergence had disappeared. The excellent agreement between the calculated and the measured temperature decrease afterwards indicated that the calculated plume behaviour, as the wind turned to the south-east and forced the plume back into the bay, was correctly modelled. This agreement continued during the rest of the verification, perhaps with a reservation for the last two hours when the calculated values were too low but had the right development. However, this difference could partially have been due to a marginal dislocalization of the computed plume caused by an uncorrectly wind description, as mentioned above. One can notice that the model reacted simultaneously and in accordance with the natural situation in the bay at T 2.

Figures 29 and 36 compare the development of the calculated and the measured temperature at the intake and at "Fisket" respectively. These diagrams indicates that the prediction was excellent in the whole bay during the verification period.

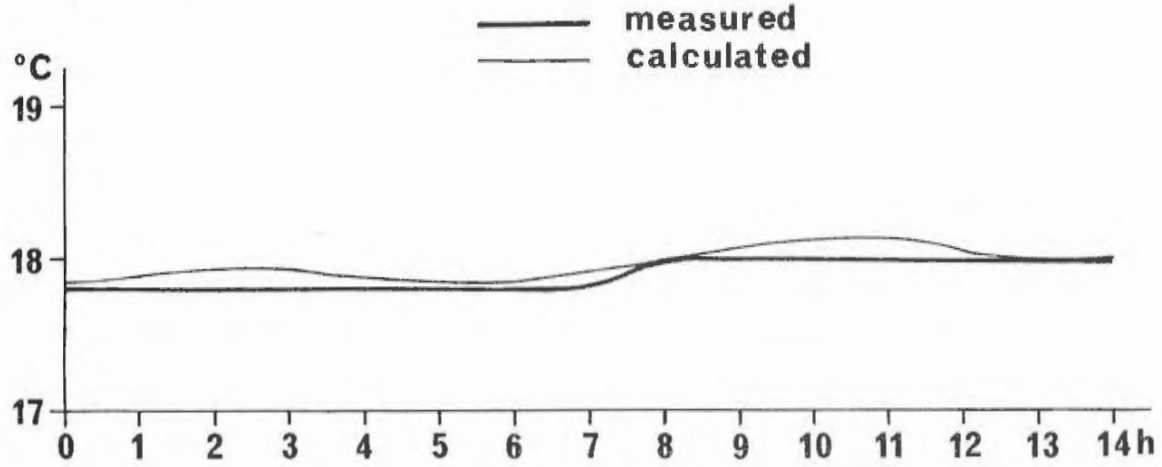

FIGURE 36 Temperature at "Fisket", 4 m, on 2 September, 1974. Calculated and measured values.

In order to get another fine structured comparison between predicted and measured values, the temperature mappings on 3 September were used as verification objects too. The wind conditions during the forenoon on that day are shown in Figure 37. The prediction started when the wind increased at five o'clock. In order to get an acceptable temperature field to start with, the predicted plume in the verification study for 2 September was used after two more calculated hours with an easterly wind.

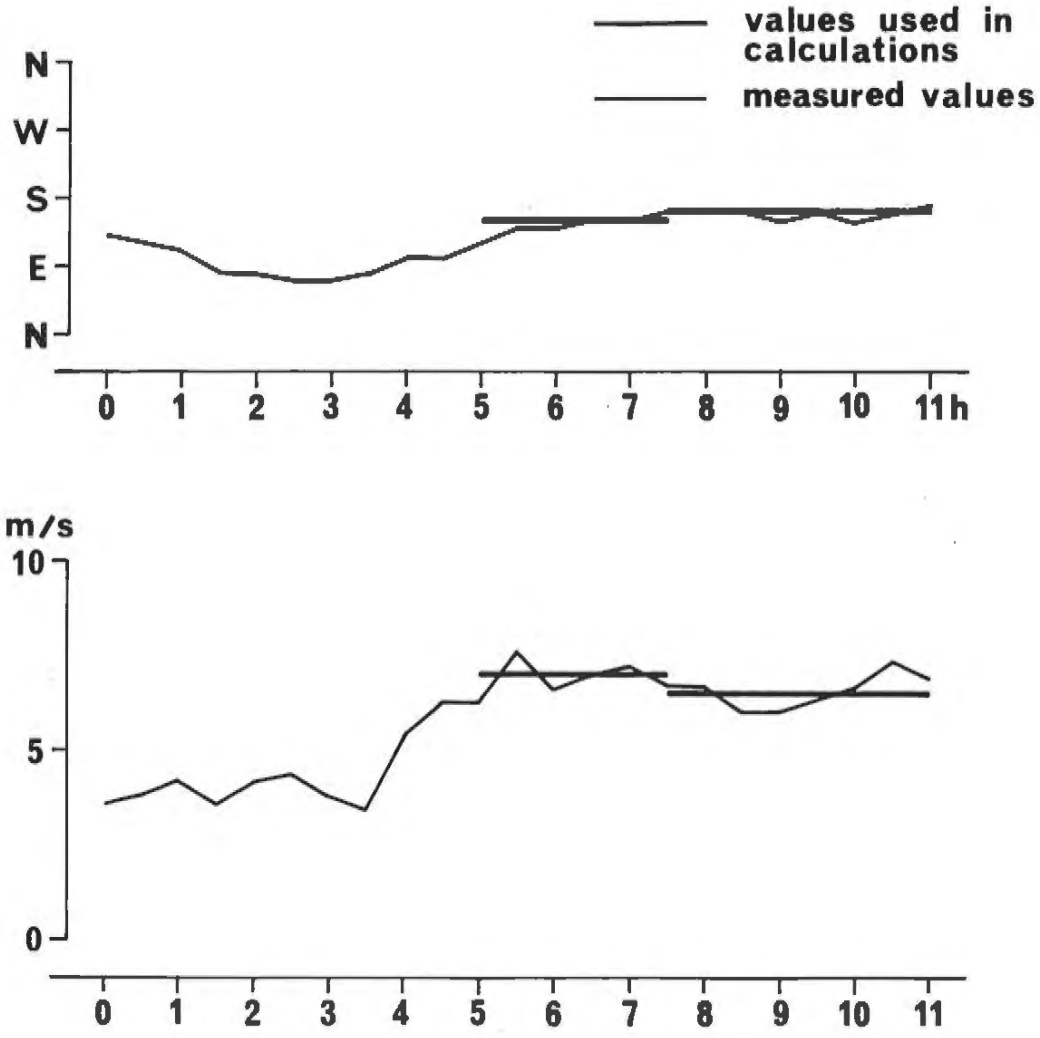

FIGURE 37 Wind on 3 September, 1974. Measured values and values used in the calculations.

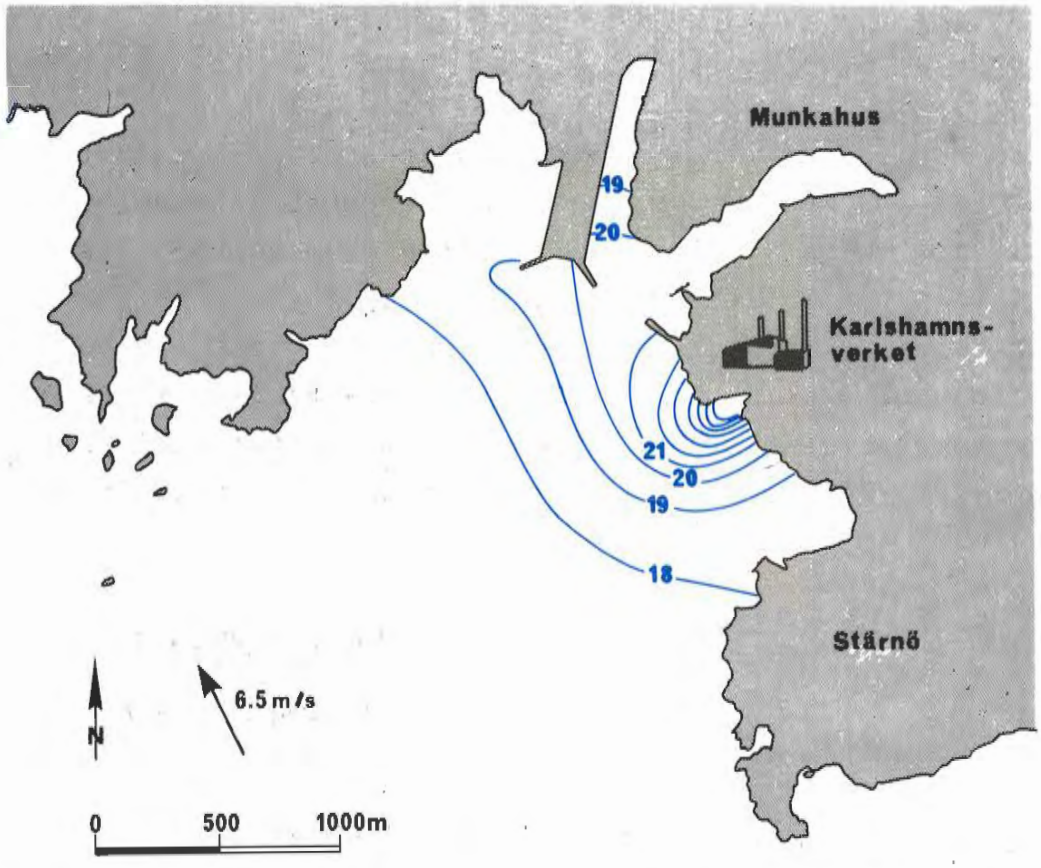

FIGURE 38 A Calculated temperature at the surface at 1000, 3 September, 1974

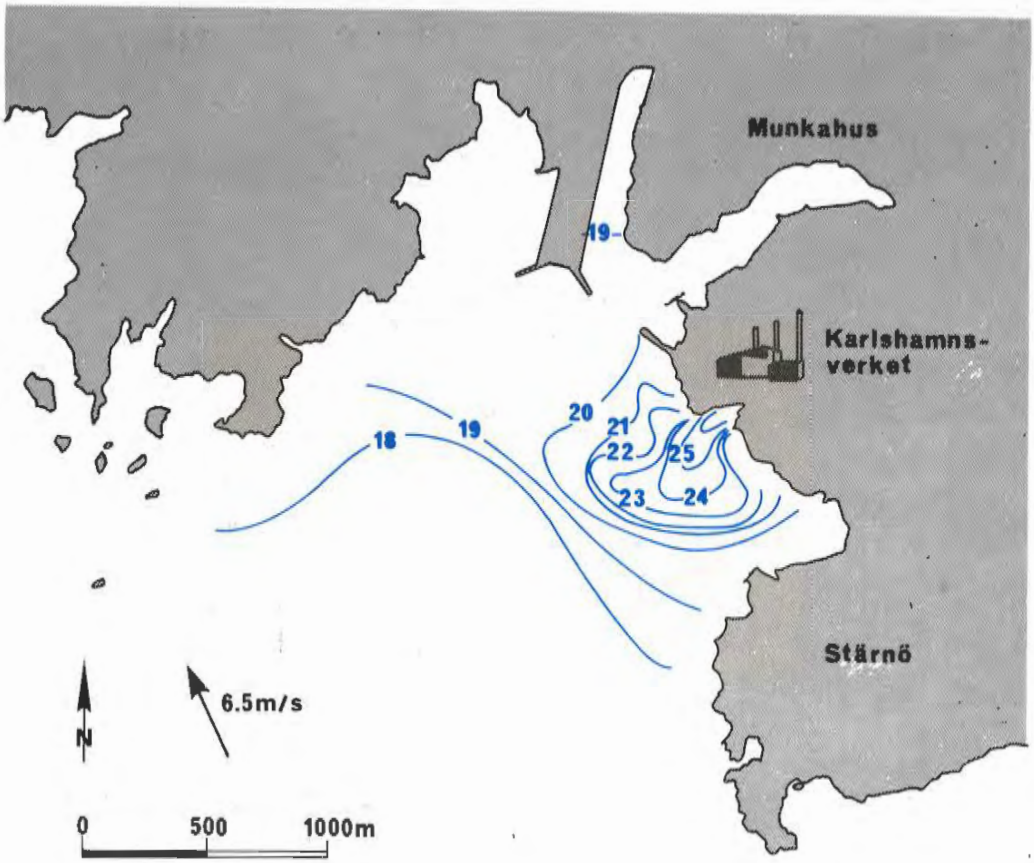

FIGURE 38 B Measured temperature at the surface at 0930 - 1235, 3 September, 1974

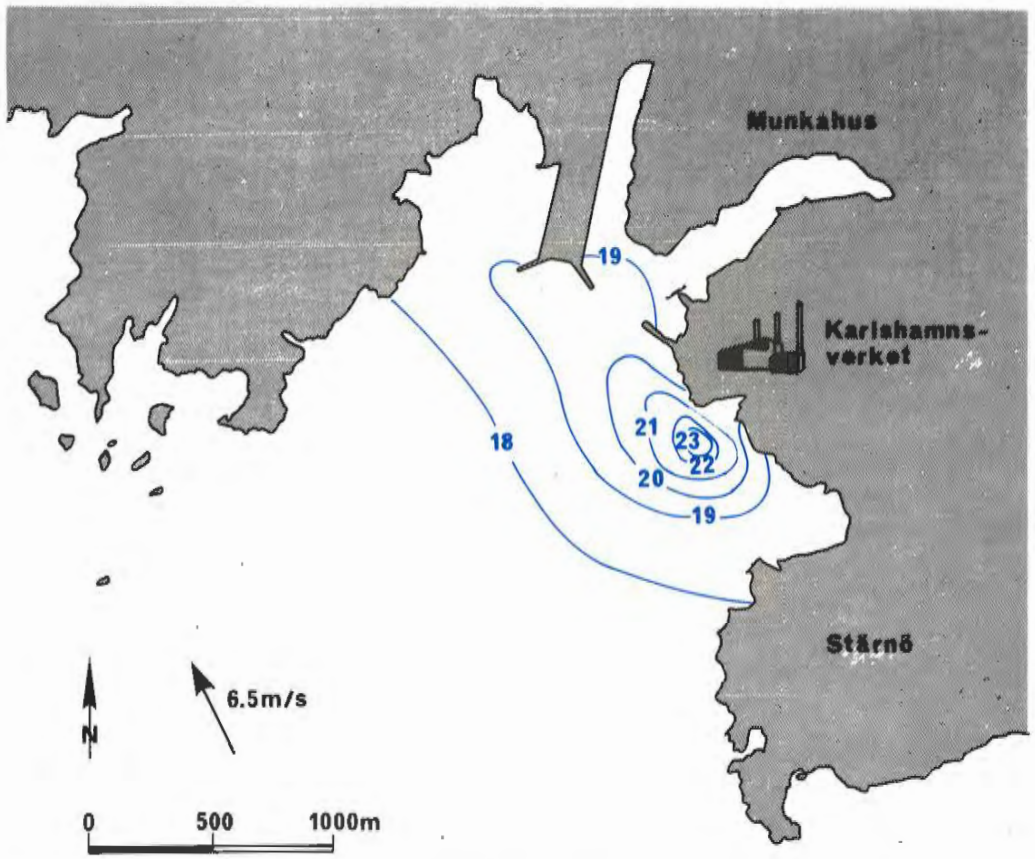

FIGURE 38 C Calculated temperature at 1.5 m at 1000, 3 September, 1974

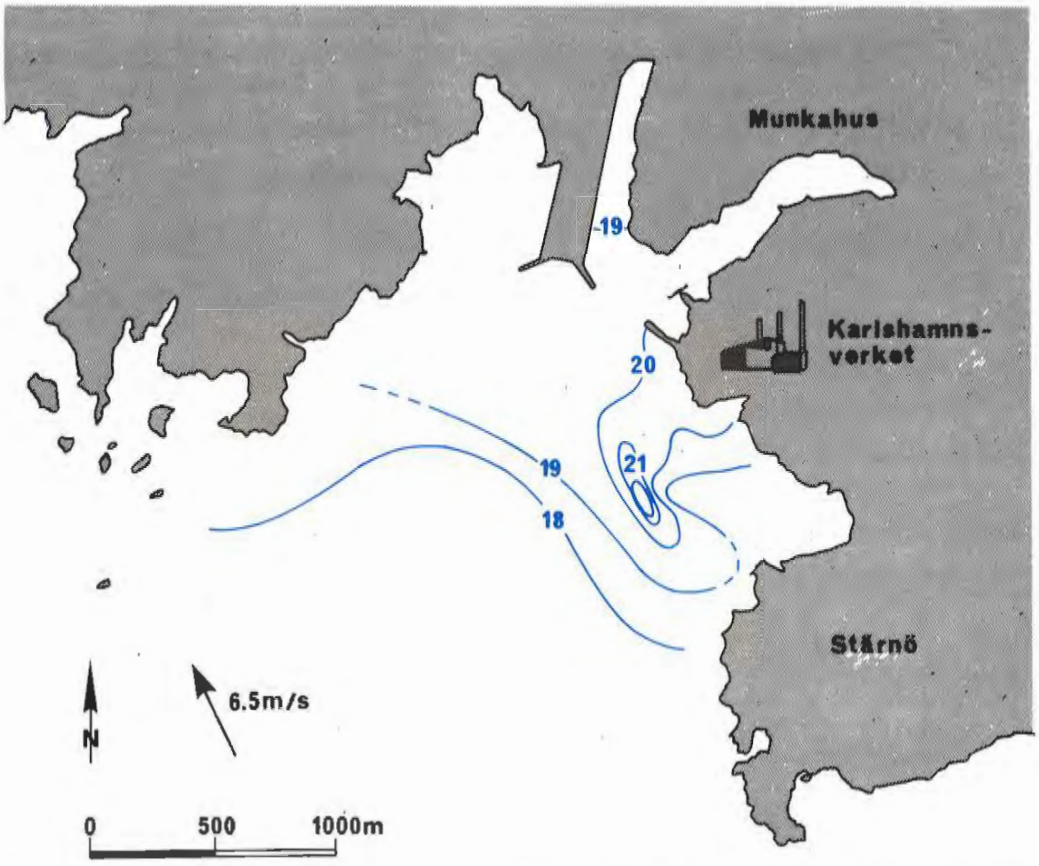

FIGURE 38 D Measured temperature at 1.5 m at 0930 - 1235, 3 September, 1974

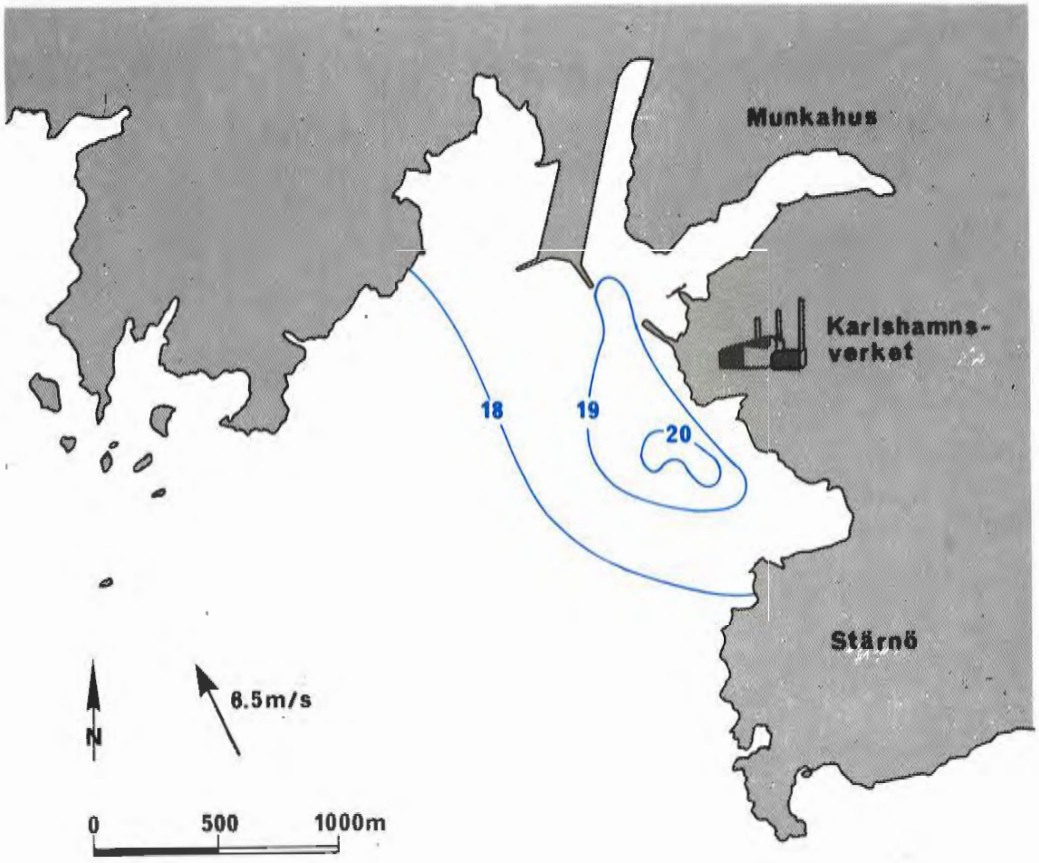

FIGURE 38 E Calculated temperature at 3 m at 1000, 3 September, 1974

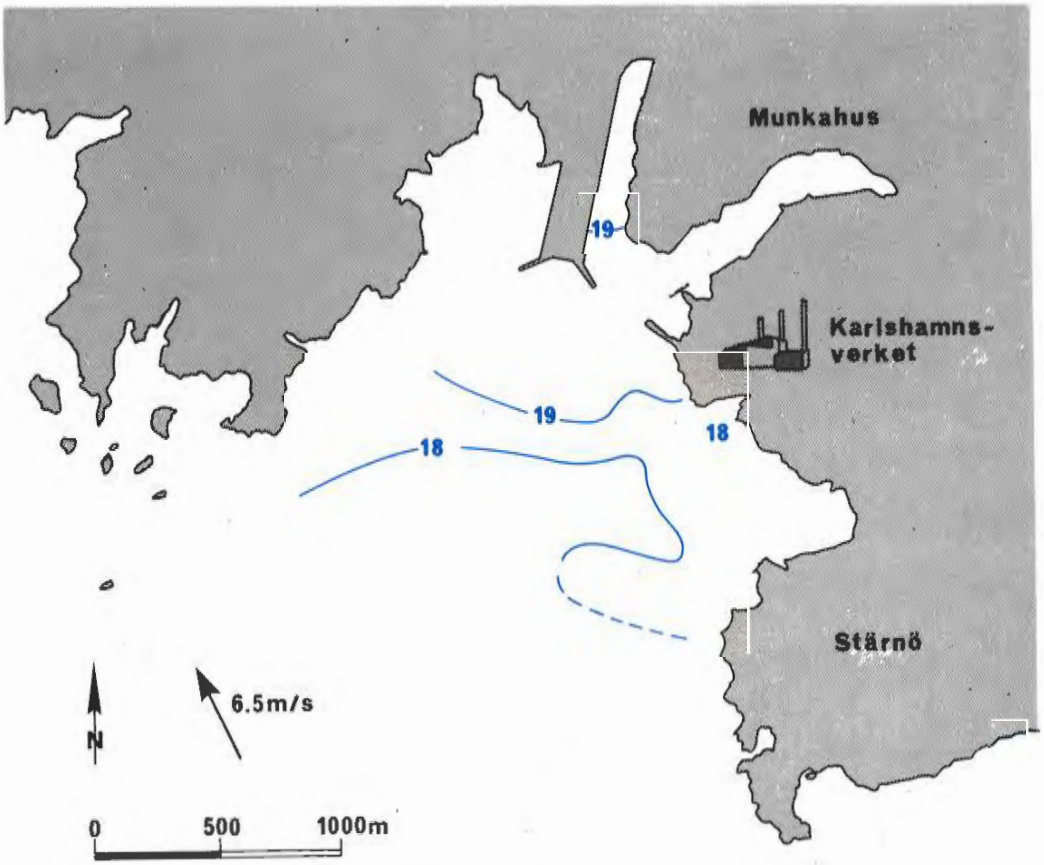

FIGURE 38 F Measured temperature at 3 m at 0930 - 1235, 3 September, 1974

Figure 38 compares the calculated and the measured temperature distributions at the surface, 1.5 m and 3 m depth. The agreement was evident at the surface except in the west, where the measurements showed somewhat higher temperatures. This was also true at 1.5 m depth, but at 3 m depth the calculated temperature was too high outside the outlet which meant a slightly exaggerated diving of the plume as before. The recirculation was well described.

Figure 39 shows that the agreement was very good in the plume at "Fisket". The comparision between measured and calculated temperature further out in the bay at T 2 gives the same indications as before: good time dependent temperature variations but too high values at 10.5 m (see Figure 40). As the whole water column at T 2 was mixed at the end of the verification period and as the calculated temperatures were too high in the lower layers, even the calculated temperature at the surface became slightly too high compared to the measurements. However, this had not been the case if the temperature beneath the plume would have had more realistic values from the beginning of the calculations.

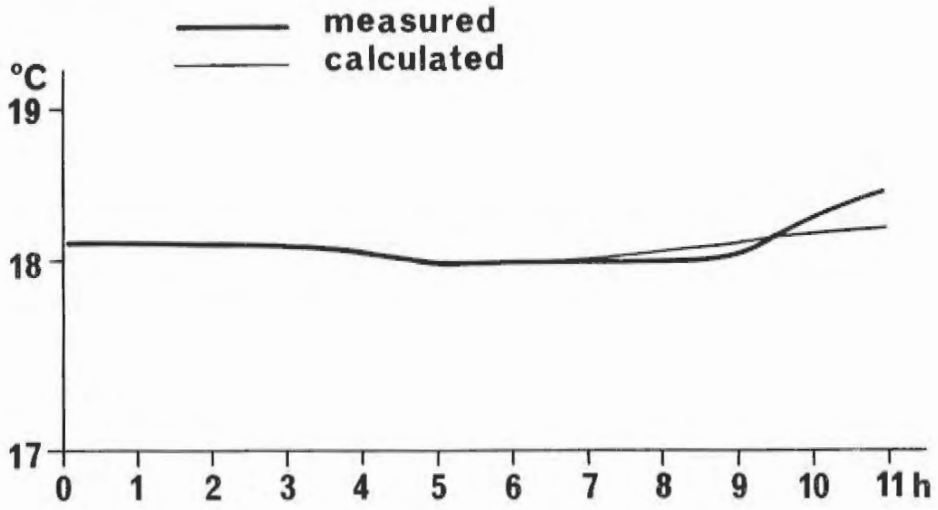

FIGURE 39 Temperature at "Fisket", 4 m, on 3 September, 1974. Measured and calculated values.

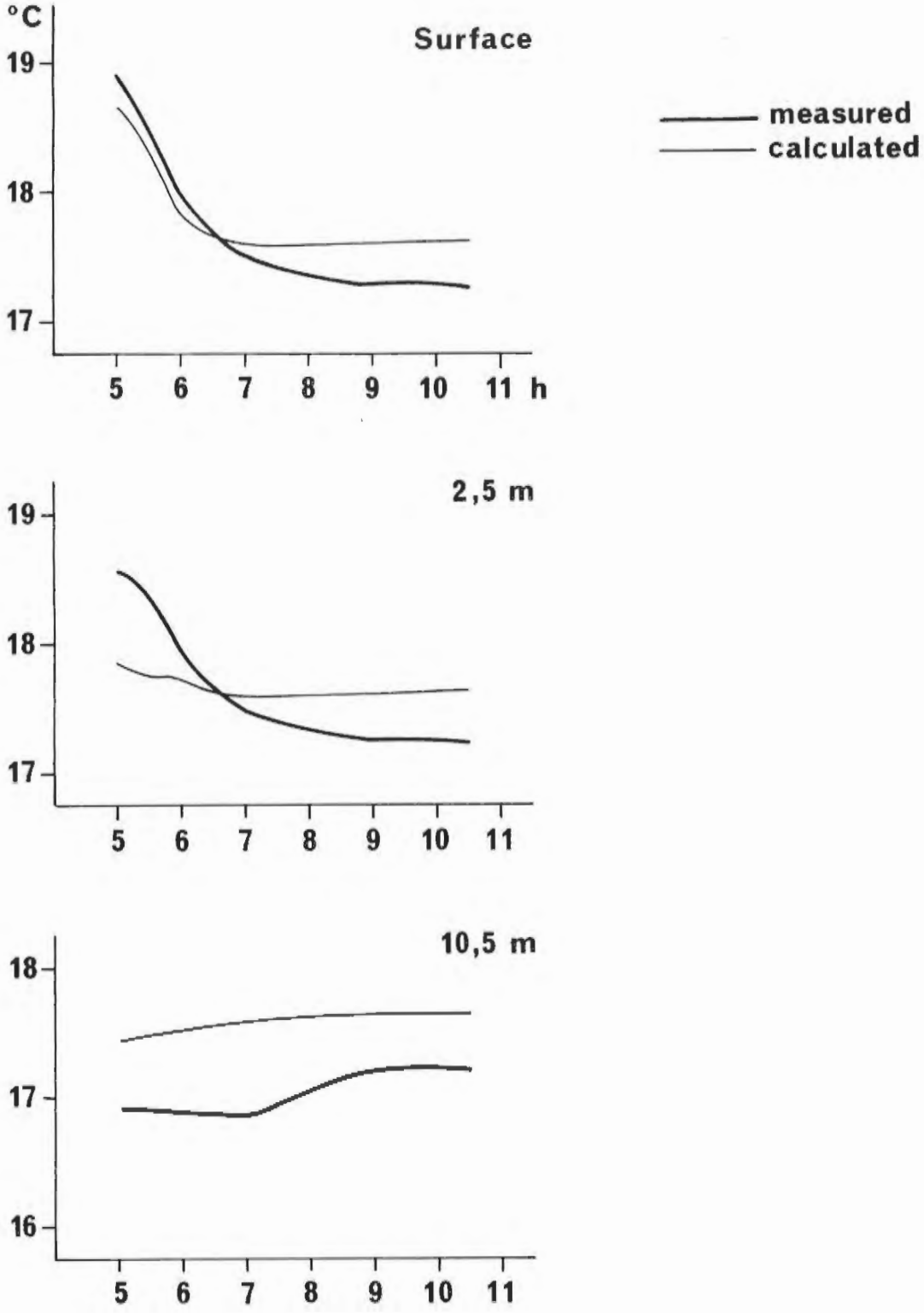

FIGURE 40 Temperature at T 2 on 3 September, 1974.
Calculated and measured values.

In order to illustrate what a calculated current field could look like, Figure 41 shows the current field at the surface predicted for the verification test for 3 September. It is evident how the rather moderate wind controlled the circulation in the bay and how small the near-field was. The velocities are in general about 10 cm/sec, as one should expect with this wind speed.

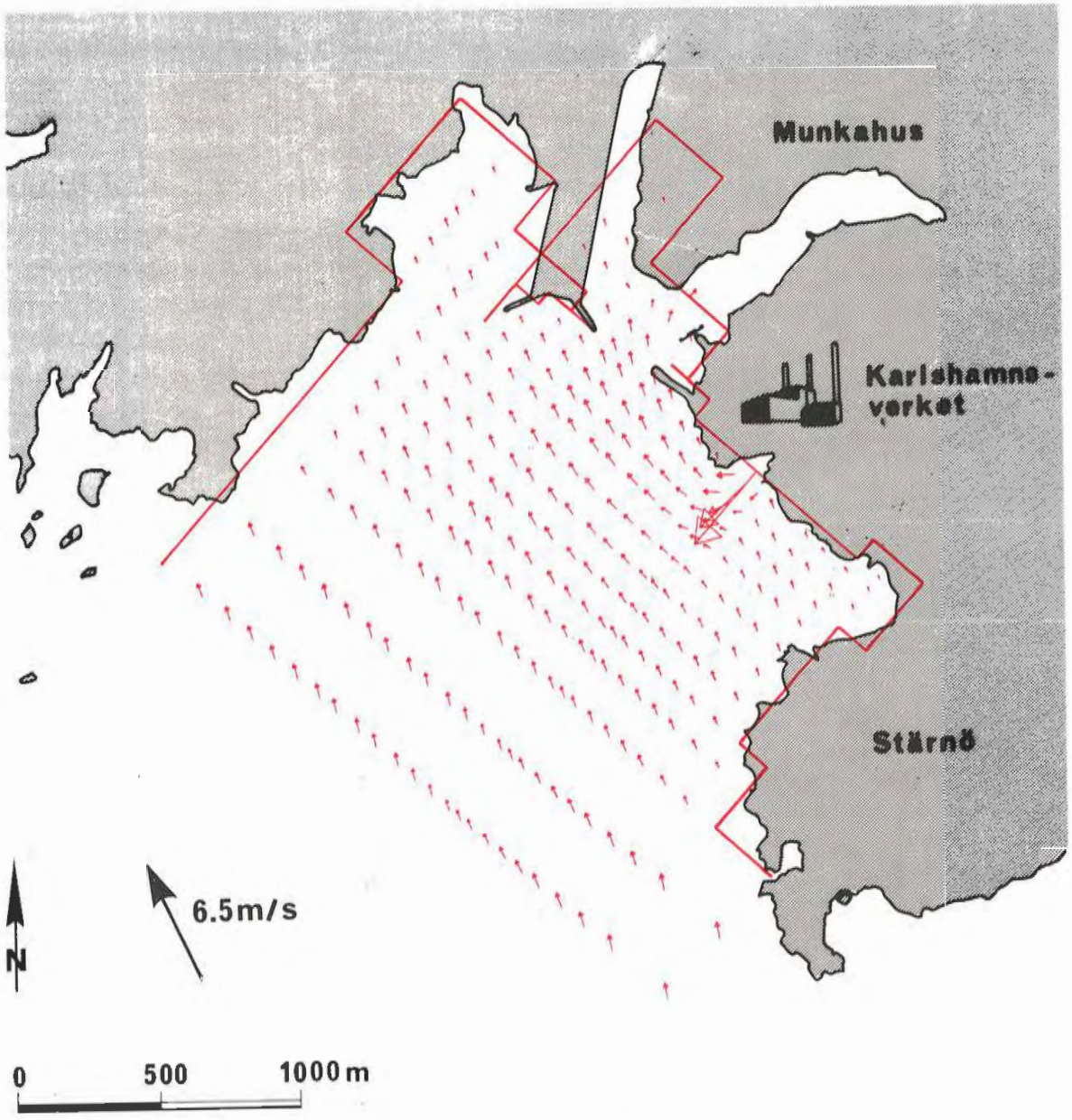

FIGURE 41 Calculated currents at the surface at 1000, 3 September, 1974

A test was made to elucidate the influence of reduced eddy coefficients below the thermocline on the vertical temperature distribution. For convenience, the number of gridpoints were reduced and the topography were simplified, but its results can, in spite of this, be used in the discussion of the verification study.

Two calculations were made. They were started with a natural background temperature (see Figure 26), but without any discharged cooling water and with the velocities equal to zero. In one of the calculations the eddy coefficients were chosen as in the verification study, but in the other case the eddy coefficients were not allowed to increase below the thermocline. Figure 42 shows the vertical temperature distribution in a

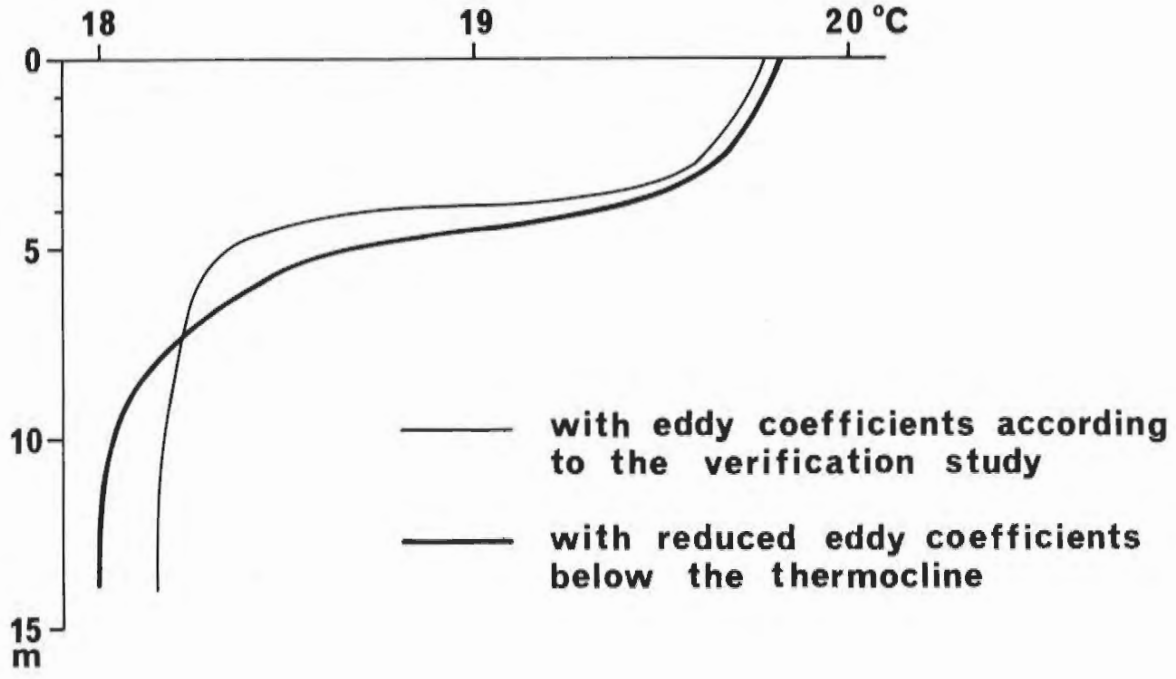

FIGURE 42 A test of different turbulent simulations. The vertical temperature distributions 800 m from the outlet after twelve simulated hours.

gridpoint 800 m from the outlet after twelve simulated hours for the two cases. The distributions illustrate that more heat is transported below the thermocline in the first case. Thus the temperature will be higher in the plume, and its depth will particularly increase, if reduced eddy coefficients are used. Furthermore, the temperature below the plume will be lower in accordance with the measurements.

BARSEBÄCK

Introduction

To simulate the spreading of cooling water outside the Barsebäck power plant, a situation with a north-going plume has been chosen. As mentioned in the part describing the physical background a north-going plume is the most common type. It also contains the largest area of heated surface water.

The history of the plume to be modelled is described by two plume mappings, made with a time difference of about 16 hours. At the time of the first mapping (Figure 43 a) the general current in Öresund is turning from the south to the north. The plume is restricted to a relatively small area right west of the outlet. When the current has turned to the north, it also increases and elongates the plume (Figure 43 b).

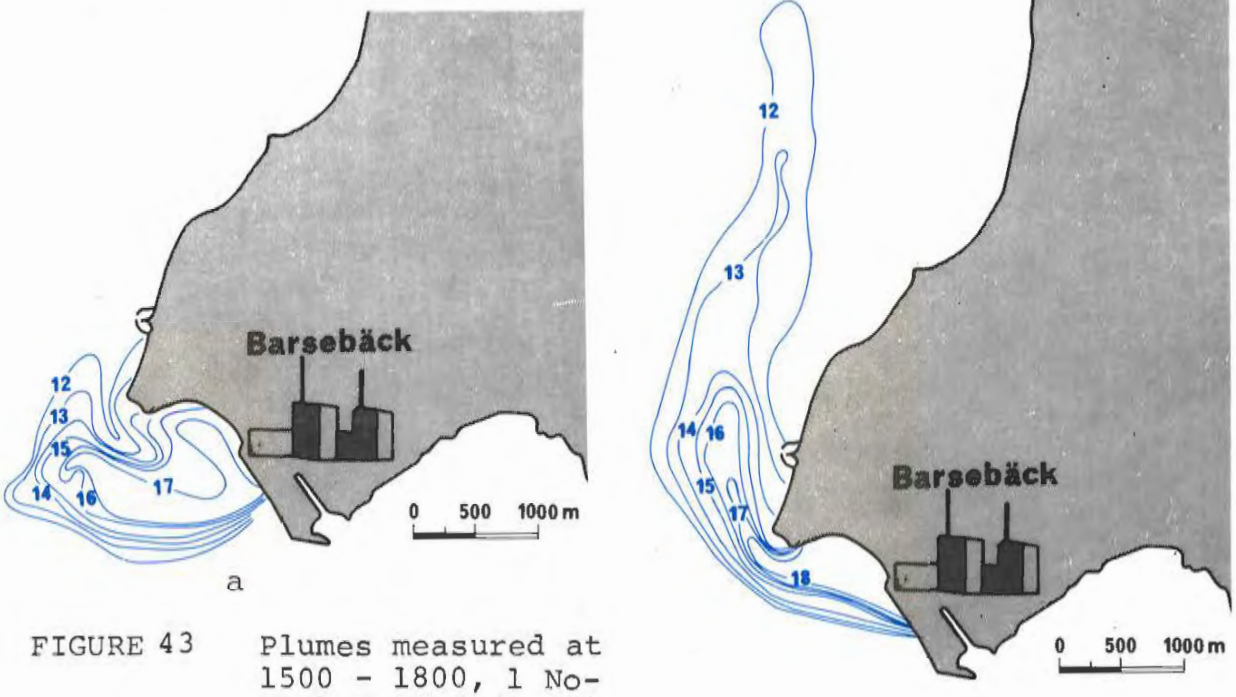

FIGURE 43 Plumes measured at 1500 - 1800, 1 November, 1977 (left) and at 0900 - 1200, 2 November, 1977 (right)

Grid construction

In constructing the grid (Figure 44) several factors have to be considered. In choosing a grid with open boundaries, the values of current and temperature used at these boundaries have to fulfil special conditions as mentioned in "Boundary conditions". Accordingly, the offshore boundary has been located far enough from shore to make sure that variations in the flow at the boundary will not influence the flow in the inner part. Another possibility had been to model the whole Öresund with a coarser grid and use a finer mesh for the plume-affected area. Computed values from the coarser grid then could be used as boundary values for the finer grid. This technique was tested in the beginning and was found not to be necessary. Furthermore, without letting the computational work increase to an unacceptable level, the proposed improvement of the boundary values in the finer grid was unsignificant.

As the eddies in the bay north of the plant have a big influence on the spreading of the plume and are difficult to treat as boundary values, the grid covers the whole bay north of the plant. The whole eddy-creating effect is then accounted for by processes inside the grid. The location of the upstream boundary with the inflowing plume is about 1.5 km from the outlet. This assures that, when prescribing the boundary conditions, the only jet-created effect to be considered is an increased temperature, and the predicted part of the plumes are in the far-field zone.

The grid-spacing is chosen to obtain a good resolution of the area of heated water, but is of course restricted by available computer resources. The variable grid-spacing is

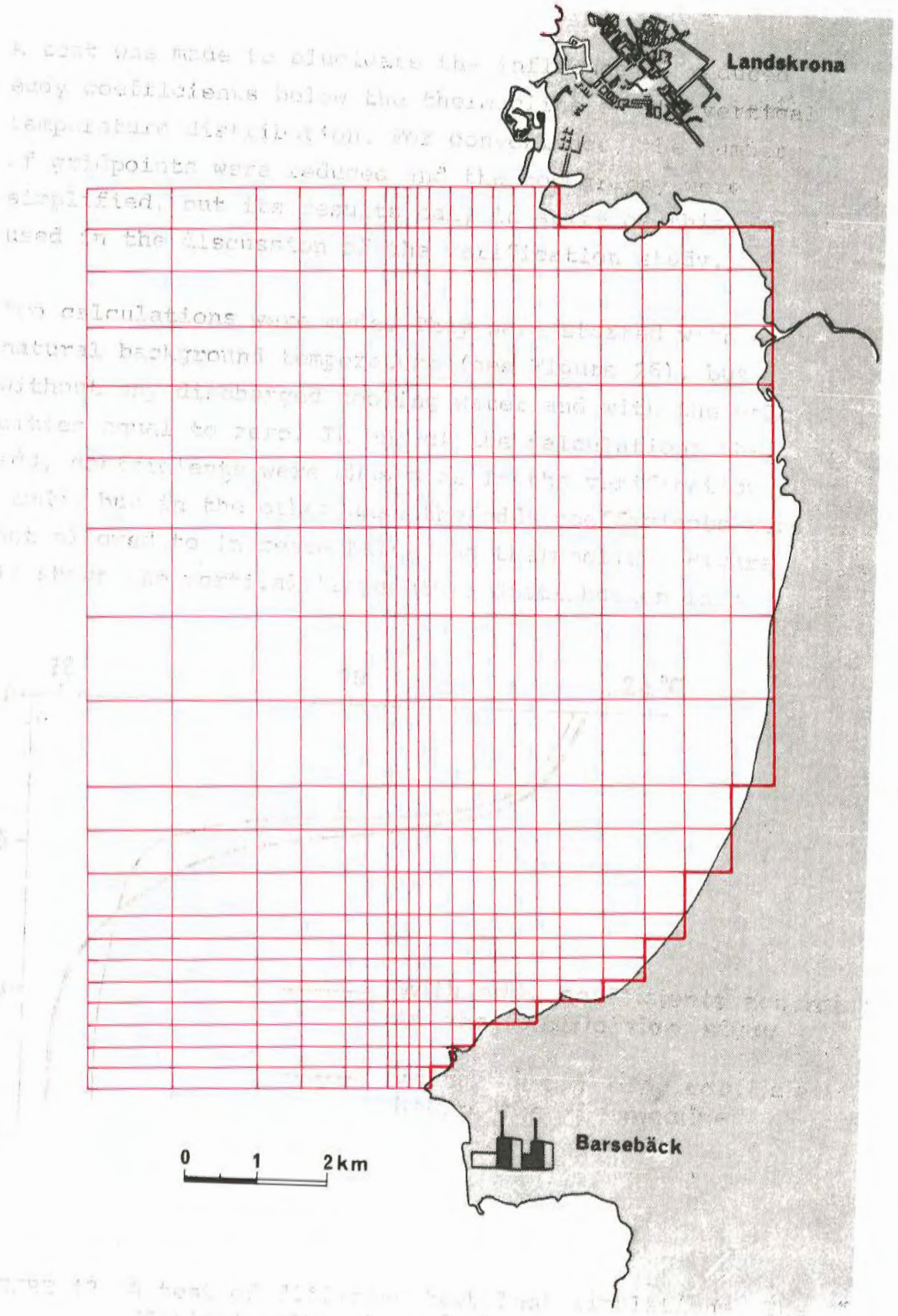

FIGURE 44 Computational grid for the plume predictions. Minimum and maximum gridsize are 150 m resp. 1200 m.

useful to reduce the computational work, but needs a careful treatment because the numerical stability and the horizontal diffusion parameters are to a high degree related to the grid size.

Horizontal extents	12.6 km	y-direction
	9.6 km	x-direction
Minimum depth	1.2 m	
Maximum depth	12 m	
Number of grid points	21	y-direction
	22	x-direction
	8	z-direction

Table 5 Dimensions of the Barsebäck model

Boundary values and input parameters

Both current and temperature values are held constant at the outer boundary. Their vertical variation is seen in Figure 45. At the downstream boundary it is assumed that variations of current and temperature normal to the boundary are negligible. The normal derivative of these variables then could be set to zero. The inflow takes place at the southern boundary. The currents at the inflow are interpolated from current measurements made during the plume mappings. In the beginning of the simulation the current profile shown in Figure 46 a is used for boundary values.

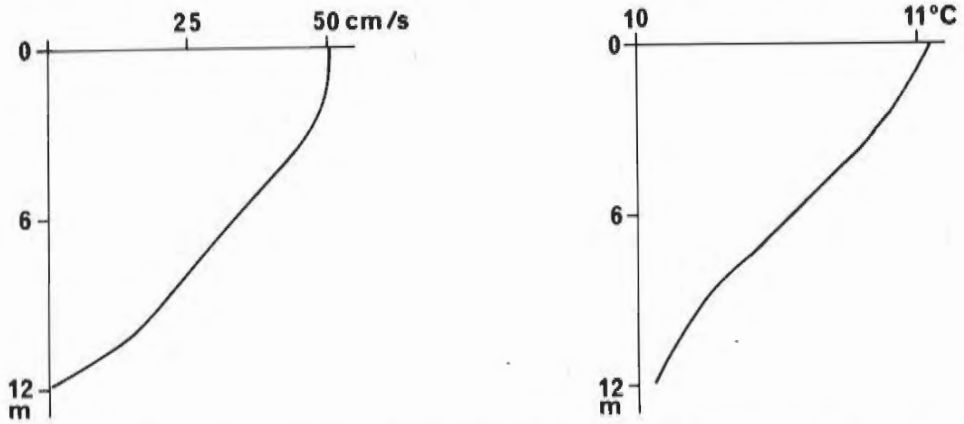

FIGURE 45 Vertical variations of current and temperature at outer boundary

After two hours the current is supposed to have increased to values in Figure 46 b.

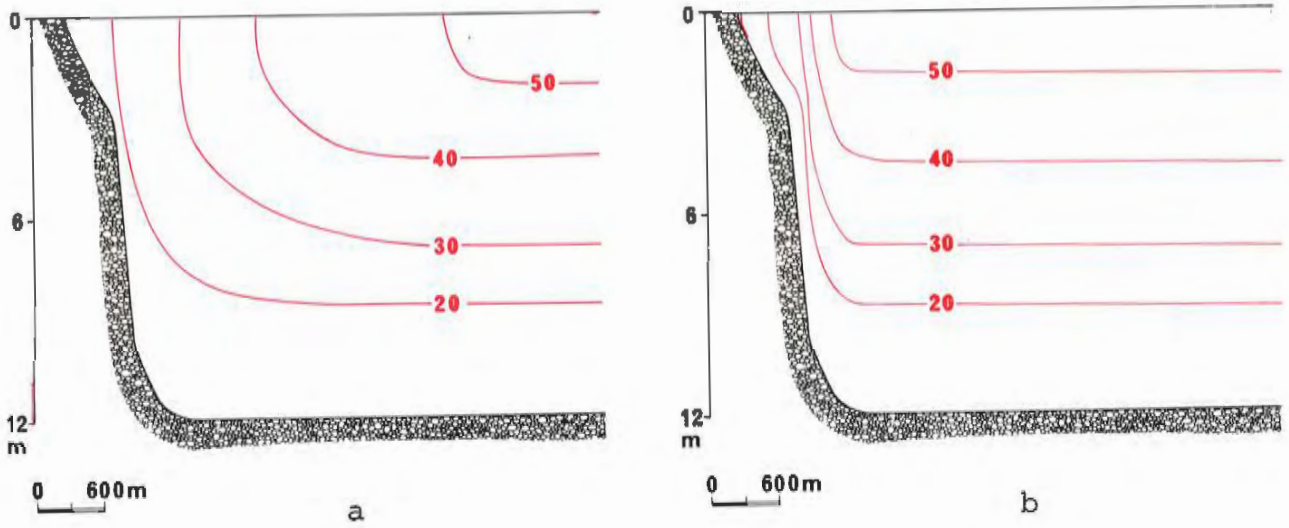

FIGURE 46 Current profiles at the upstream boundary

The latter values are used in the rest of the simulation. Guided by the plume mappings (Figure 43) the temperature of the inflowing water also is increased step by step in the plume-affected part of the boundary (Figure 47). Along the rest of the boundary the temperature is the same as at the offshore boundary.

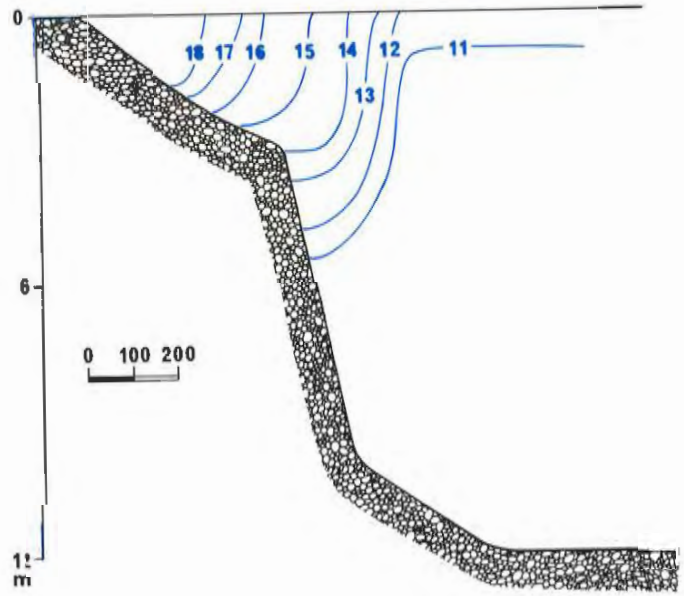

FIGURE 47 Temperature profile at the upstream boundary used at the end of the simulation

The salinity was observed to be fairly constant during the simulated event with the halocline staying at approximately 12 m depth. The halocline was rather sharp, acting as an effective barrier for exchange processes. It then seemed justified to use the halocline as bottom in the model and a constant salinity for the water mass above. The salinity only enters in the equation of state and computer work is saved by not having to add a separate equation for salinity. Heat loss to the atmosphere is accounted for by the kind of heat flux condition described in "Boundary conditions". Computational tests have shown that it has a very limited influence on processes with the time-scales used in this application.

The wind stress imposed on the surface varies in time and is computed from data from nearby meteorological stations. At the start of the simulation the whole water mass, except at the inflow boundary, has the temperature stratification shown in Figure 45. The specified currents at the outer boundary are used to compute the current field inside the boundary and at the downstream boundary. A simple interpolating procedure using the continuity equation is used.

Equilibrium temperature	11.0 ^{o}C
Salinity	11.0 $^{o}/oo$
Maximum velocity	50 cm/sec
Coriolis parameter	$1.21 \cdot 10^{-4}$ sec^{-1}
Surface heat transfer coefficient	30 - 60 $W/m^2 \cdot {}^{o}C$
Horizontal eddy viscosity	1 000 000 cm^2/sec
Vertical eddy viscosity	AVO $(1 + 4 \frac{\partial \Delta T}{\partial z})$ cm^2/sec
with AVO = 10 - 50	depending on the wind speed
Horizontal eddy diffusivity	33 000 cm^2/sec
Vertical eddy diffusivity	BVO $(1 + 0.5 \frac{\partial \Delta T}{\partial z})$ cm^2/sec
with BVO = 10 - 50	depending on the wind speed

TABLE 6 Input parameters

Computed plume

Figure 48 shows the computed plume after 8 hours' simulation. Nothing unexpected has happened and the plume has spread along the direction of the currents. A minor contribution has been given by the relatively weak (2 m/s) wind from the south-west. The currents at the inflow have not yet increased to their definite strength, and so the diffusive part of the transport is relatively effective.

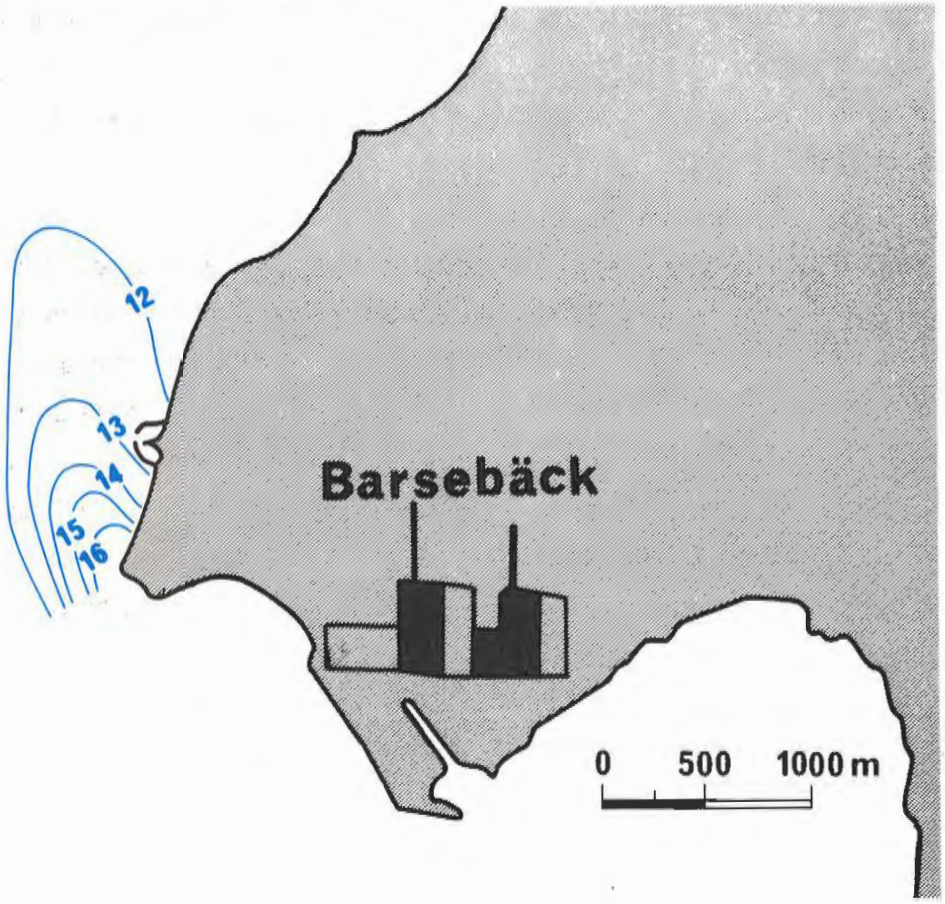

FIGURE 48 Predicted plume after 8 hours at 0100, 1 November, 1977

As the simulation proceeds, a more pronounced spreading of the plume in the longshore direction is noticed (Figure 49). The result after 16 hours' simulation is comparable in time to the plume mapping shown in Fig.50.The agreement between the computed and the observed plume is remarkable. Both the longitudinal and the lateral distribution seem to be correct-

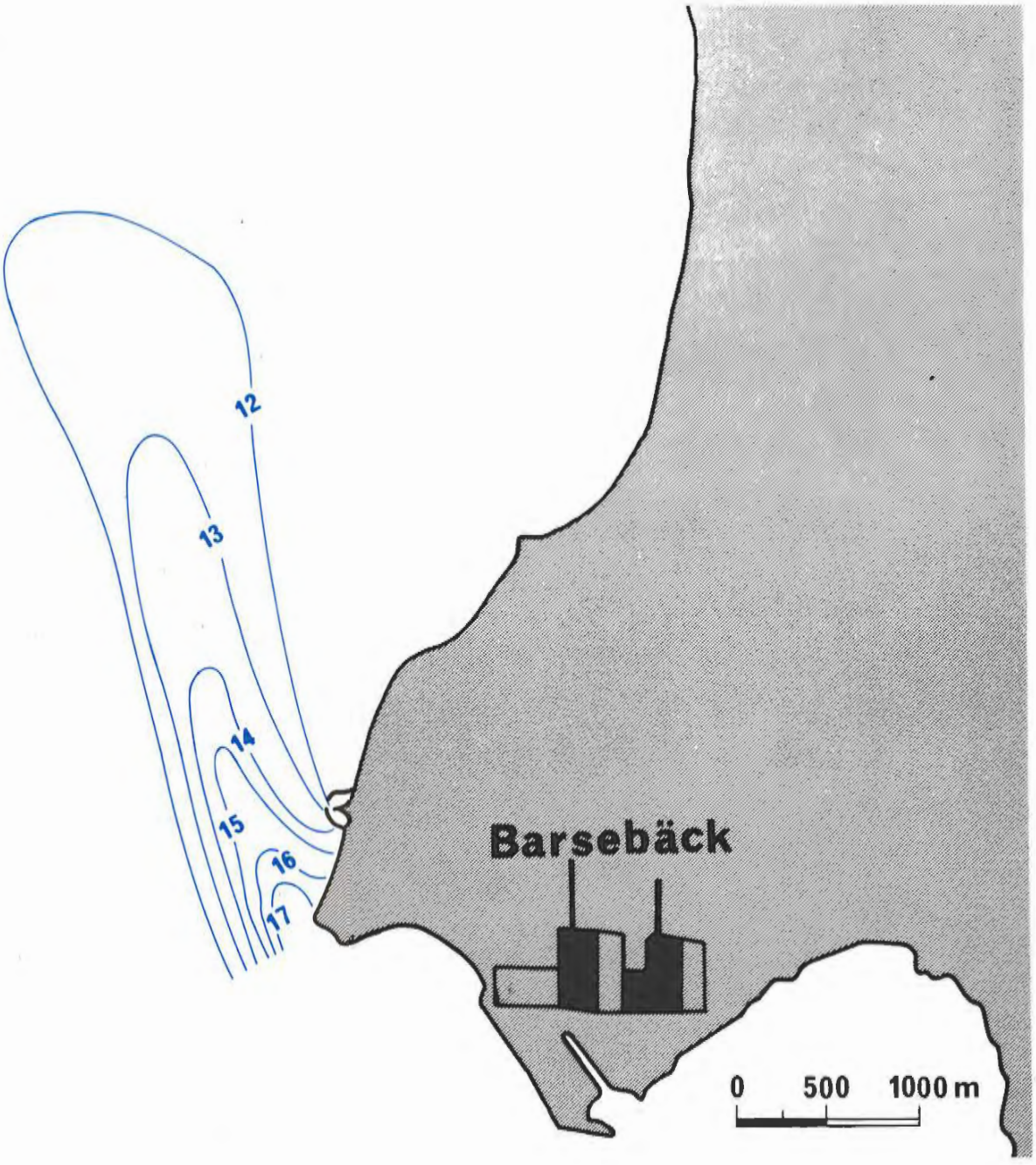

FIGURE 49 Predicted plume at 0900, 1 November, 1977

ly modelled. This indicates that the coefficient for the horizontal diffusion of temperature has a realistic value (33 000 cm^2/sec). The width of the plume is sensitive to changes of the horizontal diffusion coefficient, which has been shown by experimental runs of the model.

On the other hand, the same coefficient can't be further reduced because of problems to get stable solutions in the model. Connected to the stability is also the grid-spacing. Therefore it is an elaborate task to match the desired range of the diffusion parameter - based on physical arguments - against the grid-spacing.

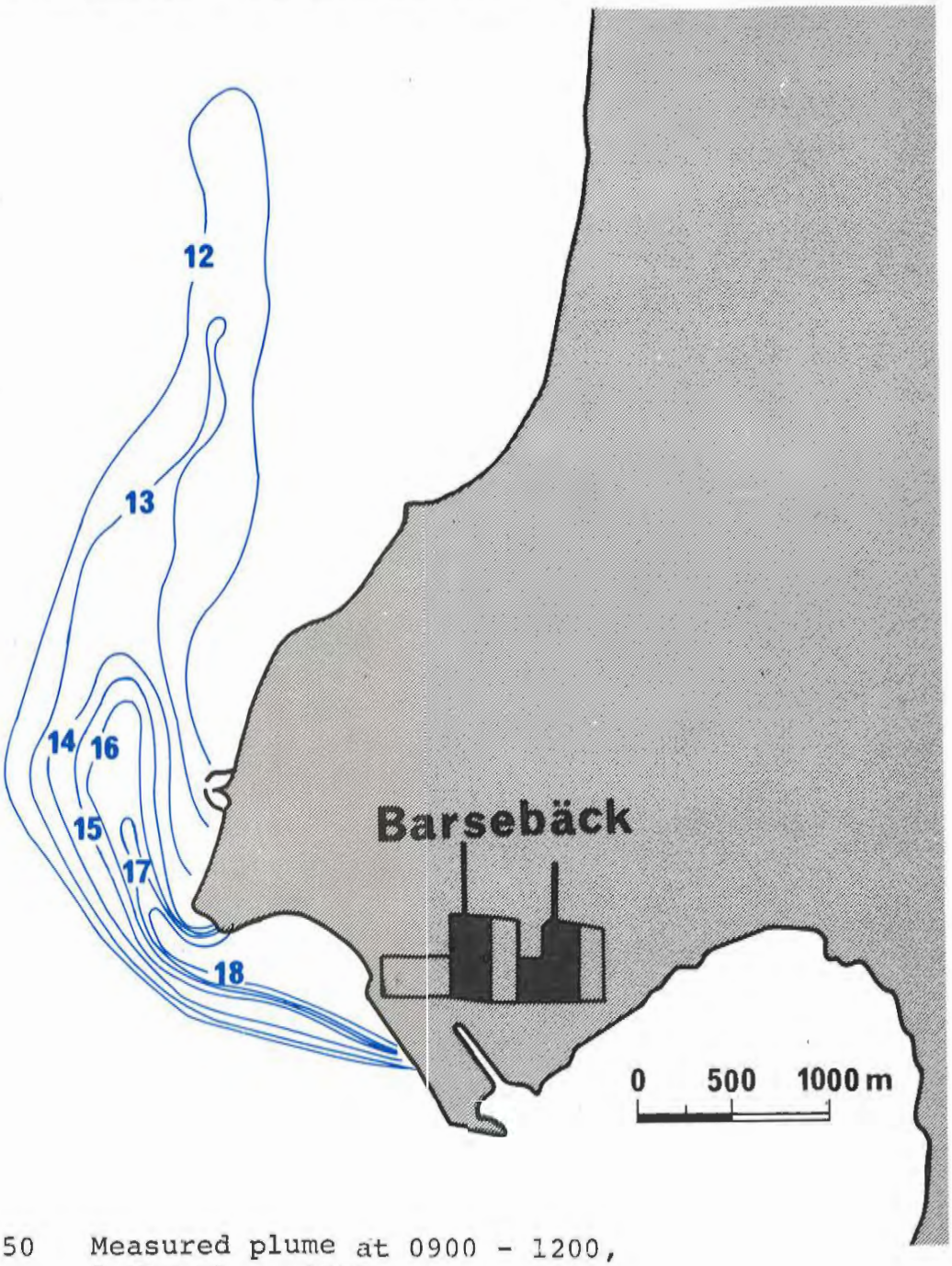

FIGURE 50 Measured plume at 0900 - 1200, 1 November, 1977

It is only at the end of the plume that the computed diffusive transport seems to be over-estimated. Here the predicted currents are of less magnitude than at the inflow and the dominance of the advective part of the transport is reduced. However, the measured plume suggests a more jet-like character of the currents. This means that the magnitude of the currents does not decrease enough along the plume to reduce the dominance of the advective transport. The character of the temperature distribution in the plume may also be the result of developing large eddies. Much of the detailed structure of these eddies is filtered out in the mapping procedure which lasts for about three hours. As no verification of the currents has been done due to lack of representative field data, it is difficult to decide the quality of the predicted currents.

The observed plume follows the depth contours while the computed one stays further offshore. The model only permits a perpendicular inflow at the boundary, and so this discrepancy could be removed or reduced if the grid was adjusted to fit the direction of the inflow better.

Even the computed vertical distributions are in good accordance with the measured ones (Figure 51). An implicit scheme for the vertical diffusion of temperature is used in the model. This greatly facilitates the choice of a reasonable physical value on the coefficient for the vertical diffusion of temperature without the necessity of paying attention to stability problems.

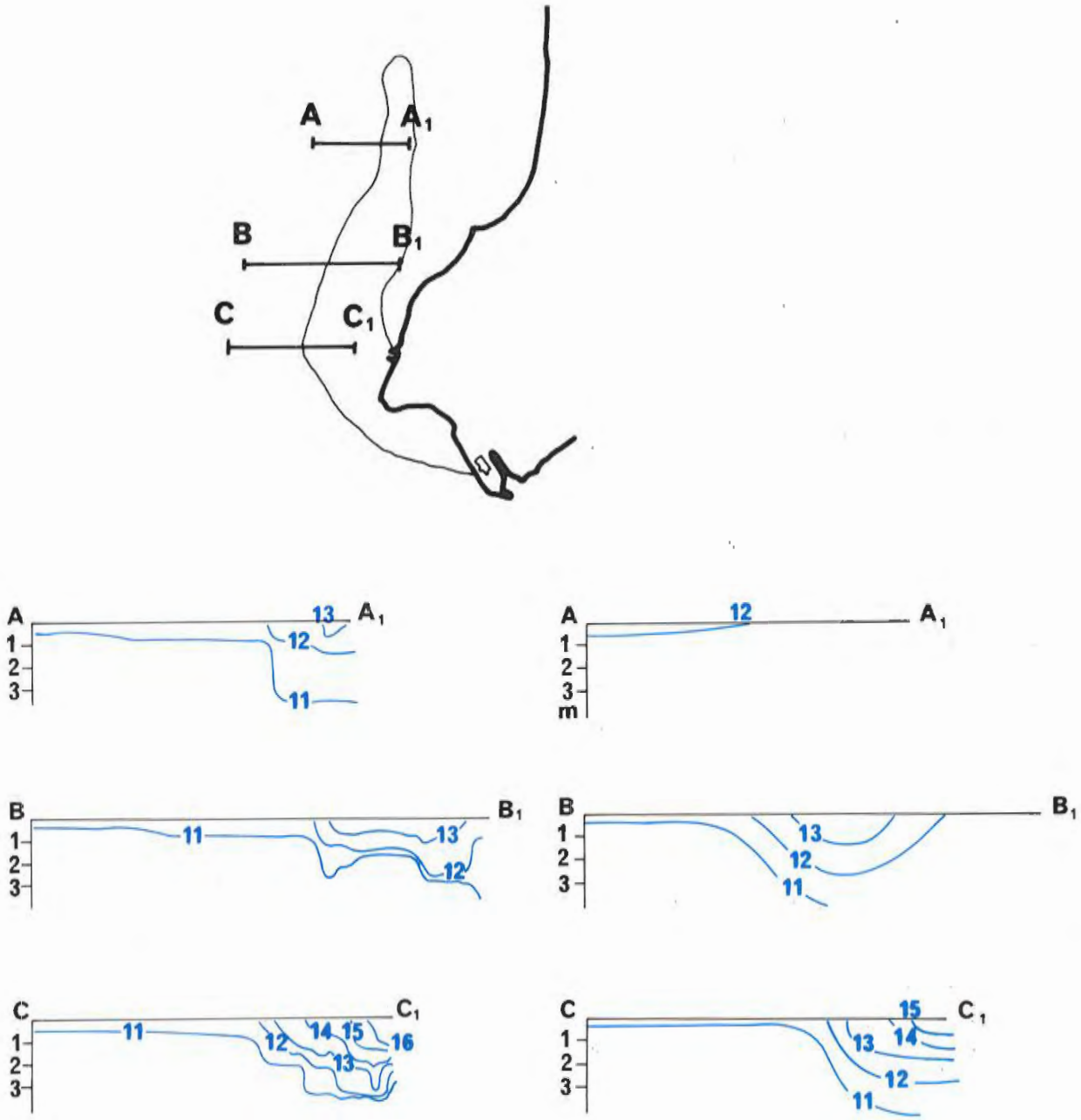

FIGURE 51 Observed (left) and computed (right) vertical profiles of temperature at three intersections. The locations of the intersections are shown at the top of the figure.

At the cross section A - A_1 the measured plume is narrower, and the 12°- and 13°-isotherms reach somewhat deeper than what the model predicts. This is connected with the earlier mentioned overestimation of the horizontal diffusion. Too much of the available heat is spread horizontally, and therefore the vertical extent is reduced.
At the cross sections B - B_1 and C - C_1 the horizontal spreading as well as the currents seem to be cor-

rectly modelled. There the vertical mixing also agrees with the measured one. It is then reasonable to believe that, if more work was spent on improvement of the description of the currents, the result would be an even more satisfactory answer on both the horizontal and the vertical extent of the whole plume-affected area.

To summarize, important plume characteristics like the vertical and horizontal extent and the centerline temperature decay have been predicted with an acceptable accuracy.

DISCUSSION

WAYS TO IMPROVE THE MODEL

The most important improvement is to include a better turbulence model. The vertical eddy coefficients used in our applications were, for instance, only dependent on the vertical stability that will decrease the turbulence, and not on the vertical current shear that will create turbulence. Thus, some kind of a Richardson number dependence may be the solution. However, the empirical relations suggested by Munk and Anderson (1948) or by Kullenberg (1974) are found for turbulence created by pure wind-driven shear. Their relations could therefore only be used in the far-field, where the initial jet momentum has no importance to the mixing.

One more problem with Kullenberg's formula is that it is derived for stratified water masses. If it were used for a homogeneous water mass and thus the Richardson number were zero, then the eddy diffusivity would be infinite. To get rid of this peculiarity one has to introduce an arbitrary upper limit for the eddy coefficients.

For winds less than 4 m/sec Kullenberg suggested that the turbulence was mainly "old" turbulence created in an earlier stage. His data relates, however, from measurements in rather open areas. This must be remembered both when one considers the influence of "old" turbulence for a certain wind speed and also when one uses the empirical relations he got. His formula for lighter winds is a doubtful tool in a model, as it depends on the horizontal current fluctuations. As the input data do not take all, if any, perturbations into account and every value in a grid point represents an average value, the current fluctuations in the model will only be a small fraction of those in nature.

The rest of the current fluctuations will be thought of as horizontal turbulence and parametrized by the horizontal eddy coefficients.

Sometimes the stratification outside a power plant can be unstable, i.e., when the cooling-water is saltier than the receiving water or at cooling-water discharges in lakes or in the Baltic Sea in wintertime when the surface temperature is less than the value for maximum density. If so, neither Munk and Anderson's relation nor Kullenberg's will be of any help. Mamayev's (1958) relation was constructed to take care of these phenomena, but it is to our knowledge not tested enough.

None of these empirical models can be used with accuracy below the pycnocline. Here the turbulence will be a mixture of wind-induced turbulence, turbulence created by internal waves, current shear or bottom shear, and of "old" turbulence. However, it will not generally reach the same intensity as above the pycnocline even if the Richardson numbers are the same. In consequence of this Murthy and Okubo (1977) suggested the use of Kullenberg's relation obtained for weak winds below the pycnocline.

The model is purposely built so that different kinds of turbulence models easily can be used. Unfortunately, as we have seen, most of the turbulence models are designed or derived for a certain turbulence-creating mechanism and they are therefore of limited values. To be able to calculate the near-field and the transition zone correctly one should for instance need a model for the shear-induced turbulence between the jet and the receiving water. Most of the models are also verified only by laboratory experiments with mainly one turbulence-creating mechanism in a controlled simple form, and not for the more complex situations that occure in nature.

A dependence of the grid size in a varying mesh to the horizontal eddy coefficients could be useful if the numerical stability criteria can be met. Murthy and Okubo (1977) suggest that the design of a variable grid similar to the scale dependence of the horizontal eddy diffusivity could be applicable in plume modelling.

When a wind starts to blow over the modelled area it takes some time to build up a fully developed wave-field. During this process the proportions of the energy input used to develope the waves, the currents and the turbulence will vary considerably. For instance the energy input to the turbulence will increase and when the wave-field is fully developed more turbulence will be created by breaking waves.

A certain fetch is also needed to get this fully developed wave-field. The length of this fetch increases rapidly with the wind-speed. If the wind comes from land, turbulence near the shore could thus be weaker than further out. In the Karlshamn case, for example, this is the case for the whole bay at wind-speeds higher than 3 m/sec. This indicates that a space- and time-dependent model could be necessary.

The model already got the possibility of using a space-varying wind-field. The amplitude of the wind-stresses can be changed each time step, but the relations of the wind-stresses between all the grid points are constant in time. However, to be able to incorporate all the phenomena mentioned above, these relations must be time-dependent. In order to make these manipulations meaningful, a more complicated wind-stress model must be developed.

To be able to calculate the near-field with a satisfactory accuracy it must be covered by a large number of grid points. This is not necessary if the near-field is calculated by an integral model and is used as input data for the transition zone. However, integral models should not be used, if the area just outside the outlet is very shallow. In this case one can run Paul's model with a finer mesh for a smaller area to get better input data. As the near-field is mainly dependent of the nature of the jet, this calculation is only needed once, if temperature and velocity in the discharged water do not vary much.

Another way to reduce the cost of a model prediction for thermal plumes is to start with a realistic temperature-field that includes a plume. This could be done by qualified guesses, by an integral model calculation or by using a measured plume. By doing so the time to build up a realistic start situation is reduced a lot.

The bottom boundary conditions in the model are no-slip but this can rather easily be changed to a slip boundary. This could improve the model results for certain cases when the influence from the bottom is estimated to be important.

A self-evident improvement for a proper use of the model in the Baltic Sea is to include salinity calculations. The equation system will thus be increased by an equation for conservation of salinity. One version of the model has already been used in an application for the Sea of Azov (Paul, Richardson, Gorstko and Matveyev, 1979) where salinity calculations were included.

APPLICABILITY OF THE MODEL

The verification results show that the model is a useful tool for calculating the transition zone and the far-field of a thermal plume. Verification studies for the Point Beach power plant demonstrate that calculations of the near-field are successful as well (Paul and Lick, 1974).

In order to study the ecological effects of thermal discharges it is necessary to have a good description of both the conditions in the vicinity of the outlet and the temperature distribution and variations in wider surroundings. Therefore, this model ought to be an important tool in such studies. Of a special interest is to predict how discharged cooling water from more than one power station interacts.

The decision of how a power plant should be constructed can be facilitated by the use of the model. The effects of, e.g., pier constructions and the dimensions of the inlet and outlet on the plume behaviour can be analysed. Furthermore, the locations of the inlet in relation to the outlet could be investigated in order to minimize the recirculation of cooling water.

As the model is based on a very general set of equations and rather few simplifications have been done, it can be used for other problems of different nature. The model has already been used to calculate the circulation in both rather shallow and very deep basins with and without partial ice-cover (Paul, Richardson, Gorstko and Matveyev, 1979), the mixing of water from a river when it enters a lake, how large constructions in lakes as harbours and jetport islands will change the circulation pattern and how contaminants are spread (Paul and Lick, 1975, and Lick, Paul and Sheng, 1976).

Most of pollution outlets are situated at the coast. The model has therefore a special advantage as it is able to have a good vertical resolution in the calculations in shallow areas due to the variable transformation. Particularly as good predictions of pollution concentrations along the coast are mostly of great interest.

The model can also be used as a tool for more general ecological studies. Here, the distribution and transport of nutrients can be calculated to get realistic input data for a biological model.

Furthermore, a free-surface version of the model has been developed. With this model sedimentation studies can be done particularly in shallow areas where influence of waves is important.

REFERENCES

Amsden, A A, and F H Harlow. 1970. The SMAC method: A numerical technique for calculating incompressible fluid flows. LA-4370, Los Alamos Scientific Laboratory, Los Alamos, N.M.

Bennett, J R. 1971. Thermally driven lake currents during the spring and fall transition periods. Proc. 14th Conf. Great Lakes Res., IAGLR, pp 535-544

Bennett, J R. 1977. A three-dimensional model of Lake Ontario's summer circulation. I. Comparison with observations. J. Phys. Ocean. 7:591-601

Bradshaw, P. 1971. An introduction to turbulence and its measurements. Pergamon Press

Bryan, K. 1969. A numerical method for the study of the circulation of the world ocean, J. Comp. Phys. 4:347-376

Cederwall, K, and A Sjöberg. 1969. Kylvattenutsläpp från värmekraftverk. Chalmers tekniska högskola. Inst. för vattenbyggnad. Medd. 45

Crowley, W P. 1968. A global numerical ocean model. Part I. J. Comp. Phys., 3:111-147

DHI. 1977. Helsingør-Helsingborg tunnel. Delrapport 7: Hydrauliske undersøgelser af aendringer i dybvandsindstrømningen ved alternative tunnelkonstruktioner

Dietrich, G. 1957. Allgemeine Meereskunde. Gebrüder Borntraeger, Berlin

Dunn, W E, A J Policastro and R A Paddock. 1975. Surface thermal plumes: evaluation of mathematical models for the near and complete field. ANL/WR - 75 - 3, Argonne National Laboratory, Argonne, Illinois

Ellison, T H. 1957. Turbulent transport of heat and momentum from an infinite rough plane. J. Fluid Mech. 2:456-466

Ellison, T H, and J S Turner. 1959. Turbulent entrainment in stratified flows. J. Fluid Mech., 6:423-448

Fredrich, H, and S Levitus. 1972. An approximation to the equation of state for sea water, suitable for numerical ocean models. J. Phys. Ocean., 2:514-517

Freeman, N G, A M Hale and M B Danard. 1972. A modified sigma equations' approach to the numerical modeling of Great Lakes hydrodynamics. J. Geoph. Res., 77:1050-1060

Haq, A, W Lick and Y P Sheng. 1974. The time-dependent flow in large lakes with applications to Lake Erie. Dept. of Earth Sciences, Case Western Reserve Univ., Cleveland, Ohio

Hinze, J O. 1959. Turbulence. Mc Graw-Hill

Hirt, C W, and F W Harlow. 1967. A general corrective procedure for the numerical solution of initial-value problems. J. Comp. Phys., 2:114-119

Holzman, B. 1942. The influence of stability on evaporation. Annals New York Acad. Sci., 44:13-18

Huanq, J C K. 1977. A general circulation model for lakes. NOAA Tech. Mem. ERL GLERL-16

Kullenberg, G. 1969. Measurements of horizontal and vertical diffusion in coastal waters. Kungl. Vetenskaps- och Vitterhets-Samhället, Göteborg

Kullenberg, G. 1971. Vertical diffusion in shallow waters. Tellus, 23:129-135.

Kullenberg, G. 1974. An experimental and theoretical investigation of the turbulent diffusion in the upper layer of the sea. Københavns universitet, Inst. for fysisk oc. Report No. 25

Kullenberg, G, C R Murthy and H Westerberg. 1973. An experimental study of diffusion characteristics in the thermocline and hypolimnion regions of Lake Ontario. Proc. 16th Conf. Great Lakes Res., IAGLR, pp 774-790.

Kullenberg, G, C R Murthy and H Westerberg. 1974. Vertical mixing characteristics in the thermocline and hypolimnion regions of Lake Ontario (IFYGL). Proc. 17th Conf. Great Lakes Res., IAGLR, pp 425-434.

Launder, B E, and D B Spalding. 1974. The numerical computation of turbulent flows. Comp. Methods in Appl. Mech. and Eng. 3

Lick, W J, J Paul and Y P Sheng. 1976. The dispersion of contaminants in the near-shore region. In: Modeling biochemical processes in aquatic ecosystems (R P Canale, ed.) Ann Arbor Science Publishers, Inc. pp 93-112

Mamayev, O I. 1958. The influence of stratification on vertical mixing in the sea. Izv. Acad. Sci. USSR Geoph. Ser., pp 870-875

McGuirk, J J, and W Rodi. 1976. Calculation of three-dimensional heated surface jets. In: Turbulent buoyant convection (ed. D B Spalding), Hemisphere Publ. Corp., Washington

Milanov, T. 1969. Avkylningsproblem i recipienter vid utsläpp av kylvatten. Ser. Hydr. Rep. Nr 6, Swedish Meteorological and Hydrological Institute, Norrköping

Munk, W H, and E R Anderson. 1948. Notes on a theory of the thermocline. J. Mar. Res., 7:276-295.

Murthy, C R, and A Okubo. 1977. Interpretation of diffusion characteristics of oceans and lakes appropriate for numerical modeling. In: Symposium on modeling of transport mechanisms in oceans and lakes. Manuscript report series No. 43, Marine Sciences Directorate Department of Fisheries and the Environment, Ottawa

Nihoul, J C J. 1975. Modelling of marine systems. Elsevier Scientific Publ. Co., Amsterdam

Okubo, A. 1971. Oceanic diffusion diagrams. Deep-Sea Res. 18:789-802

Okubo, A. 1974. Some speculations on oceanic diffusion diagrams. Rapp. P.-v.Reun. Cons. int. Explor. Mer, 167:77-85

Okubo, A. 1976. Remarks on the use of 'diffusion diagrams' in modeling scale-dependent diffusion. Deep-Sea Res. 23:1213-1214

Ozmidov, R V. 1965. Some features of the energy spectrum of oceanic turbulence. Doklady Acad. Nauk, SSSR, 160:11-14

Paul, J F, and W J Lick. 1973. A numerical model for a three-dimensional, variable-density jet. Proc. 16th Conf. Great Lakes Res., IAGLR, pp 818-830.

Paul, J F, and W J Lick. 1974. A numerical model for thermal plumes and river discharges. Proc. 17th Conf. Great Lakes Res., IAGLR, pp 445-455

Paul, J F, and W J Lick. 1975. Report to Argonne National Laboratory of the application of the Paul-Lick model to Point Beach Unit 1 outfall. Appears in appendix of Surface thermal plumes: Evaluation of mathematical models for the near and complete field (W E Dunn, A J Policastro and R A Paddock), ANL/WR-75-3, pp 484-511

Paul, J F, and W J Lick. 1976. Application of three-dimensional hydrodynamic model to study effects of proposed jetport island on thermocline structure in Lake Erie. Report 17-6 of Lake Erie International Jetport Model Feasibility Investigation. U.S. Army Engineer Waterways Experimental Station Contract Report H-75-1.

Paul, J F, and W J Lick. 1979. An efficient, implicit method for calculating time-dependent, free-surface hydrodynamic flows. Presented at the 22nd Conf. on Great Lakes Research, Rochester, New York

Paul, J F, and W J Lick. 1980. Numerical model for three-dimensional, variable-density, rigid-lid hydrodynamic flows: Volume 1. Details of the numerical model. U.S. EPA Ecological Report Series, in press

Paul, J F, W L Richardson, A B Gorstko and A A Matmeyev. 1979. Results of a joint USA/USSR hydrodynamic and transport modeling project. Report No. EPA-600/3-79--015, Env. Res. Lab., EPA, Duluth, Minnesota

Phillips, N A. 1957. A coordinate system having some special advantages for numerical forecasting. J. Meteorol., Vol. 14, pp 184-185

Prych, E A. 1972. A warm water effluent analyzed as a buoyant surface jet. Ser. Hydr. Rep. Nr 21, Swedish Meteorological and Hydrological Institute, Norrköping

Roache, P J. 1972. Computational fluid dynamics, Hermosa Publishers, Albuquerque, N.M.

Rossby, C G, and R B Montgomery. 1935. The layer of frictional influence in wind and ocean currents. Papers Phys. Oc. Meth. III (3)

Schmidt, W. 1941. Turbulente Ausbreitung eines Stromes erhitzter Luft. Zeitschr. Angew. Math. und Mech., 21:265-278

Sheng, Y.P. 1975. The wind-driven currents and containment dispersion in the near-shore of large lakes. Report 17-5 of Lake Erie International Jetport Model Feasibility Investigation. U.S. Army Engineer Waterways Experimental Station Contract Report H-75-1.

Sheng, Y P, W J Lick, R T Gedney and F B Molls. 1978. Numerical computation of three-dimensional circulation in Lake Erie: a comparison of a free-surface model and a rigid-lid model. J. Phys. Ocean. 8:713-727

Simons, T J. 1971. Development of numerical models of Lake Ontario. Proc. 14th Conf. Great Lakes Res., IAGLR, pp 654-669

Simons, T J. 1972. Development of numerical models of Lake Ontario: Part 2. Proc. 15th Conf. Great Lakes Res., IAGLR, pp 655-672

Simons, T J. 1974. Verification of numerical models of Lake Ontario: Part I. Circulation in spring and early summer. J. Phys. Ocean., 4:507-523

Smagorinsky, J, S Manabe and J L Holloway. 1965. Numerical results from a nine-level general circulation model of the atmosphere. Monthly Weather Review, 93:727-768

SMHI. 1965. Utlåtande ang. vattenförhållanden vid Karlshamnsverket

SMHI. 1967. Rapport rörande hydrologiska bas- och kontrollundersökningar utanför Karlshamnsverket mars 1965 - juni 1967

SMHI. 1968. Hydrografiska observationer i Pukaviksbukten vid Karlshamnsverket

SMHI. 1969 a. Rapport rörande hydrologiska bas- och kontrollundersökningar utanför Karlshamnsverket juni 1967 - april 1968

SMHI. 1969 b. Preliminärt yttrande angående inverkan på de hydrografiska förhållandena av det planerade kärnkraftverket vid Barsebäck

SMHI. 1969 c. Komplettering av preliminärt yttrande angående inverkan på de hydrografiska förhållandena av det planerade kärnkraftverket vid Barsebäck

SMHI. 1971. Preliminär rapport rörande hydrologiska bas- och kontrollundersökningar utanför Karlshamnsverket 1969 - 1970

SMHI. 1972. Rapport över hydrologiska kontrollundersökningar utanför Karlshamnsverket 1971

SMHI. 1974 a. Rapport över oceanografiska kontrollundersökningar utanför Karlshamnsverket 1972

SMHI. 1974 b. Rapport rörande vattentemperaturmätning under 1967, 1968 och 1972 vid det planerade Barsebäcksverket

SMHI. 1977 a. Rapport över oceanografiska kontrollundersökningar utanför Karlshamnsverket 1973 - 1974

SMHI. 1977 b. Rapport över oceanografiska kontrollundersökningar utanför Karlshamnsverket 1975 - april 1976

SMHI. 1977 c. Oceanografiska kontrollundersökningar utanför Barsebäcks kärnkraftverk 1976

SMHI. 1978. Oceanografiska kontrollundersökningar utanför Barsebäcks kärnkraftverk 1977

SMHI. 1979. Oceanografiska kontrollundersökningar utanför Barsebäcks kärnkraftverk 1978

Spalding, D B, and U Svensson. 1976. The development and erosion of the thermocline. In: Turbulent buoyant convection (ed. D B Spalding), Hemisphere Publ. Corp., Washington

Sundaram, T R, C C Easterbrook, K R Piech and G Rudinger. 1969. An investigation of the physical effects of the thermal discharge into Cayuga Lake (analytical study). Report No. VT-2626-0-2. Cornell Aeronaut. Lab., Buffalo, New York

Sundaram, T R, R G Rehm, G Rudinger and G E Merritt. 1970. A study of some problems on the physical aspects of thermal pollution. Report No. VT-2790-A-1, Cornell Aeronaut. Lab., Buffalo. New York

Svensson, J. 1980. Sinking cooling water plumes in a numerical model. Ser. RHO Nr 23, Swedish Meteorological and Hydrological Institute, Norrköping

Svensson, J, and W Wilmot. 1978. A numerical model of the circulation in Öresund. Evaluation of the effect of a tunnel between Helsingör and Helsingborg. Ser. RHO Nr 15, Swedish Meteorological and Hydrological Institute, Norrköping

Sverdrup, H U, M V Johnson and R H Fleming. 1942. The Oceans. Prentice-Hall, Inc., Englewood Cliffs, New Jersey

Taylor, G I. 1945. Dynamics of a mass of hot gas rising in air. U.S. Atomic Energy Commission, MDDC 919, LADC 276

Tennekes, H, and J L Lumley. 1972. A first course in turbulence. MIT Press

Varga, R S. 1962. Matrix iterative analysis. Prentice-Hall. Inc., Englewood Cliffs. New Jersey

Vasseur, B. 1979. Modifying a jet model for cooling water outlets. Ser. RHO Nr 17, Swedish Meteorological and Hydrological Institute, Norrköping

Waldrop, W, and R Farmer. 1973. Three-dimensional flow and sediment transport at river mouths. Tech. Rep. No. 150, Coastal Studies Institute, Louisiana State Univ., Baton Rouge

Waldrop, W, and R Farmer. 1974. Three-dimensional computation of buoyant plumes. J Geoph. Res., 79:1269-1276

Wilmot, W. 1976. A numerical model of the effects of reactor cooling water on fjord circulation. Ser. RHO Nr 6, Swedish Meteorological and Hydrological Institute, Norrköping

Wilson, B W. 1960. Note on surface wind stress over water at low and high wind speeds. J. Geoph. Res., 65:3377-3382

Rapporter i SMHIs publikationsserier med anknytning till oceanografiska avdelningens verksamhet

Notiser och Preliminära Rapporter, serie Hydrologi

Nr 3 Karström, U

Infrarödteknik i hydrologisk tillämpning
Stockholm 1966

Nr 5 Ehlin, U & Nyberg, L

Hydrografiska undersökningar i Nordmalingsfjärden
Stockholm 1968

Nr 6 Milanov, T

Avkylningsproblem i recipienter vid utsläpp av kylvatten
Stockholm 1969

Nr 7 Ehlin, U & Zachrisson, G

Spridningen i Vänerns nordvästra del av suspenderat material från skredet i Norsälven i april 1969
Stockholm 1969

Nr 9 Ehlin, U & Carlsson, B

Hydrologiska observationer i Vänern 1959-1968 jämte sammanfattande synpunkter
Stockholm 1970

Nr 10 Ehlin, U & Carlsson, B

Hydrologiska observationer i Vänern 17-21 mars 1969
Stockholm 1970

Nr 11 Milanov, T

Termisk spridning av kylvattenutsläpp från Karlshamnsverket
Stockholm 1971

Nr 19 Holmström, H

Test of two automatic water quality monitors under field conditions
Stockholm 1972

Nr 20 Wennerberg, G

Yttemperaturkartering med strålningstermometer från flygplan över Vänern under 1971
Stockholm 1972

Nr 21 Prych, E

A Warm water effluent analyzed as a buoyant surface jet
Stockholm 1972

Nr 27 Wändahl, T & Bergstrand, E

Oceanografiska förhållanden i svenska kustvatten
Stockholm 1973

Nr 28 Ehlin, U

Kylvattenutsläpp i sjöar och hav
Stockholm 1973

Nr 36 Ehlin, U & Juhlin, B

Oceanografiska observationer runt svenska kusten med kustbevakningens fartyg 1979.
Norrköping 1980

Nr 38 Juhlin, B & Carlsson, B

Resultat och erfarenheter från försöksverksamhet med utökad vattenprovtagning från kustbevakningens båtar
Norrköping 1980

SMHI Rapporter

HYDROLOGI OCH OCEANOGRAFI

Nr RHO 1 Weil, J G
Verification of heated water jet numerical model, Stockholm 1974

Nr RHO 2 Svensson, J
Calculation of poison concentrations from a hypothetical accident off the Swedish coast, Stockholm 1974

Nr RHO 3 Vasseur, B
Temperaturförhållanden i svenska kustvatten, Stockholm 1975

Nr RHO 4 Svensson, J
Beräkning av effektiv vattentransport genom Sunninge sund, Stockholm 1975

Nr RHO 5 Bergström, S och Jönsson, S
The application of the HBV runoff model to the Filefjell research basin, Norrköping 1976

Nr RHO 6 Wilmot, W
A numerical model of the effects of reactor cooling water on fjord circulation, Norrköping 1976

Nr RHO 7 Bergström, S
Development and application of a conceptual runoff model, Norrköping 1976

Nr RHO 8 Svensson, J
Seminars at SMHI 1976-03-29--04-01 on numerical models of the spreading of cooling water, Norrköping 1976

Nr RHO 9 Simons, J, Funkquist, L och Svensson, J
Application of a numerical model to Lake Vänern, Norrköping 1977

Nr RHO 10 Svensson, S
A statistical study for automatic calibration of a conceptual runoff model, Norrköping 1977

Nr RHO 11 Bork, I
Model studies of dispersion of pollutants in Lake Vänern, Norrköping 1977

Nr RHO 12 Fremling, S
Sjöisars beroende av väder och vind, snö och vatten, Norrköping 1977

Nr RHO 13 Fremling, S
Sjöisars bärighet vid trafik, Norrköping 1977

Nr RHO 14 Bork, I
Preliminary model studies of sinking plumes, Norrköping 1978

Nr RHO 15 Svensson, J och Wilmot, W .
A numerical model of the circulation in Öresund. Evaluation of the effect of a tunnel between Helsingborg and Helsingör, Norrköping 1978

Nr RHO 16 Funkquist, L
En inledande studie i Vätterns dynamik, Norrköping 1978

Nr RHO 17 Vasseur, B
Modifying a jet model for cooling water outlets, Norrköping 1979

Nr RHO 18 Udin, I och Mattisson, I
Havsis- och snöinformation ur datorbearbetade satellitdata - en metodstudie, Norrköping 1979

Nr RHO 19 Ambjörn, C och Gidhagen, L
Vatten- och materieltransporter mellan Bottniska viken och Östersjön, Norrköping 1979

Nr RHO 20 Gottschalk, L och Jutman, T
Statistical analysis of snow survey data, Norrköping 1979

Nr RHO 21 Eriksson, B
Sveriges vattenbalans. Årsmedelvärde (1931-60) av nederbörd, avdunstning och avrinning

Nr RHO 22 Gottschalk, L and Krasovskaia, I
Synthesis, processing and display of comprehensive hydrologic information

Nr RHO 23 Svensson, J
Sinking cooling water plumes in a numerical model Norrköping 1980

Nr RHO 24 Vasseur, B, Funkquist, L och Paul, J F
Verification of a numerical model for thermal plumes Norrköping 1980

SMHI
SVERIGES METEOROLOGISKA OCH HYDROLOGISKA INSTITUT
Folkborgsvägen 1, Box 923, 601 19 Norrköping. Telefon 011-108000.